

**Numerical Modelling of the Effects of Bin Inserts
on
Stress Distribution in Storage Bins for
Cohesive Powder Material**

by

Neeraj Singh Visen

A thesis

Submitted to the Faculty of Graduate Studies
in Partial Fulfilment of the Requirements
for the Degree of

Master of Science

Department of Biosystems Engineering
University of Manitoba
Winnipeg, Manitoba

© August, 1998



**National Library
of Canada**

**Acquisitions and
Bibliographic Services**

**395 Wellington Street
Ottawa ON K1A 0N4
Canada**

**Bibliothèque nationale
du Canada**

**Acquisitions et
services bibliographiques**

**395, rue Wellington
Ottawa ON K1A 0N4
Canada**

Your file Votre référence

Our file Notre référence

The author has granted a non-exclusive licence allowing the National Library of Canada to reproduce, loan, distribute or sell copies of this thesis in microform, paper or electronic formats.

The author retains ownership of the copyright in this thesis. Neither the thesis nor substantial extracts from it may be printed or otherwise reproduced without the author's permission.

L'auteur a accordé une licence non exclusive permettant à la Bibliothèque nationale du Canada de reproduire, prêter, distribuer ou vendre des copies de cette thèse sous la forme de microfiche/film, de reproduction sur papier ou sur format électronique.

L'auteur conserve la propriété du droit d'auteur qui protège cette thèse. Ni la thèse ni des extraits substantiels de celle-ci ne doivent être imprimés ou autrement reproduits sans son autorisation.

0-612-32972-0

**THE UNIVERSITY OF MANITOBA
FACULTY OF GRADUATE STUDIES

COPYRIGHT PERMISSION PAGE**

**NUMERICAL MODELLING OF THE EFFECTS OF BIN INSERTS
ON STRESS DISTRIBUTION IN STORAGE BINS FOR
COHESIVE POWDER MATERIAL**

BY

NEERAJ SINGH VISEN

**A Thesis/Practicum submitted to the Faculty of Graduate Studies of The University
of Manitoba in partial fulfillment of the requirements of the degree
of
MASTER OF SCIENCE**

Neeraj Singh Visen ©1998

**Permission has been granted to the Library of The University of Manitoba to lend or sell
copies of this thesis/practicum, to the National Library of Canada to microfilm this thesis
and to lend or sell copies of the film, and to Dissertations Abstracts International to publish
an abstract of this thesis/practicum.**

**The author reserves other publication rights, and neither this thesis/practicum nor
extensive extracts from it may be printed or otherwise reproduced without the author's
written permission.**

ABSTRACT

A study was undertaken to demonstrate the applicability of modified Cam-clay model to the study stress distribution in storage bins. Effects of insert location, insert size, insert friction, hopper outlet size, hopper slope, and bin wall friction on stress distribution in ground feed inside storage bin were investigated using finite element models. Simulations were carried out for filling of the storage bin and initiating draw-down. Stress distribution were plotted after the bin was filled with ground feed and after draw-down was initiated. Results of simulation were compared to results of experiments on model size bins.

The modified Cam-clay model is an elastoplastic model that uses three critical state parameters in the constitutive equation: λ , κ , and Γ . The Cam-clay parameters for ground feed were determined by triaxial tests. The parameters λ , κ , Γ , and M were 0.045, 0.016, 2.003, and 1.977, respectively. SIGMA/W software was used to prepare models of storage bins and solve finite element equations. Stress distribution changed in the bin when any of the insert or bin parameters were changed. The region near the hopper outlet had low vertical and horizontal stresses in bins where high flowability was expected. It was observed that mounting method of insert resulted in change of flow behaviour. Flowability increased and then remained unchanged as the insert was mounted higher up in the bin. Flowability increased as insert size and friction was decreased. Flowability increased with increase in size of hopper outlet but decreased as the hopper slope was reduced. Chances of interrupted flow decreased with decrease in wall friction.

ACKNOWLEDGEMENTS

I take this opportunity to sincerely thank my advisor, Dr. Q. Zhang, whose guidance, encouragement, and affection has had a major influence throughout my research. His positive attitude and words of comfort always inspired me to go further. I don't have enough words to thank him.

I'm grateful to Dr. M. G. Britton for his words of encouragement and suggestions and for serving on my advisory committee. I wish to express my gratitude to Dr. R. K. N. D. Rajapakse for his precious time evaluating my thesis and helping me in my course work.

I also thank Dr. J Graham and Mr. James Blatz for letting me use the SIGMA/W software and help overcome the problems. Special thanks to Dr. Stephan Cenkowski and Dr. Sri Ranjan for their suggestions in conducting experiments. I would also like to thank Dr. Digvir Jayas and Dr. W. E. Muir for their support and constructive criticism.

I'm thankful to Messrs. Dale Bourns, Matt McDonald, and Jack Putnam who helped me with experiment ideas and saw the project through completion.

This project was funded by Natural Sciences and Engineering Research Council of Canada (NSERC). I wish to thank NSERC for the financial support.

I lack words of gratitude for my parents and my wife Preeti, whose love and affection has always been by my side. Their sacrifices are invaluable. The love and care of my sisters and their families has always been my strength. Finally, I would like to thank all my friends, especially Jitendra Paliwal for all the help.

TABLE OF CONTENTS

ABSTRACT	i
ACKNOWLEDGEMENTS	ii
TABLE OF CONTENTS	iii
LIST OF TABLES	vi
LIST OF FIGURES	viii
1. INTRODUCTION	1
2. LITERATURE REVIEW	4
2.1. Flow Patterns in Storage Bins	4
2.2. Factors Affecting Flow Behaviour	6
2.3. Pressure Profile in Storage Bins	7
2.4. Arch Formation	9
2.5. Flow Promoting Devices	12
2.6. Constitutive Equations for Cohesive Materials	14
2.7. Finite Element Modelling of Stored Material	15
2.8. Critical state and Cam-Clay Model	17
2.9. Previous Study and Direction of Research	18
3. OBJECTIVES	20
4. MATERIALS AND METHODS	21
4.1. Finite Element Simulation of Model Bins	21
4.1.1. <i>Lab bin</i>	21
4.1.2. <i>Half bin</i>	22
4.1.3. <i>Full bin</i>	22
4.1.4. <i>Farm bin</i>	22
4.2. Description of SIGMA/W	28
4.2.1. Units	29
4.2.2. Convergence criteria	29
4.2.3. Simulating filling	30
4.2.4. Simulating draw-down initiation	30
4.2.5. Viewing results	30
4.3. Insert	31
4.4. Ground Feed	33
4.5. Interface Between the Stored Material and the Structure	34
4.6. Constitutive Relationship for Ground Feed	36
4.7. Cam-clay Model Parameters	37
4.8. Determination of Parameters for Cam-clay Model	39

4.8.1. Triaxial apparatus	39
4.8.2. Preparation of triaxial sample	40
4.8.3. Parameters	41
4.8.4. Conventional triaxial compression (CTC) test	42
4.8.5. Undrained test	43
4.8.6. Isotropic compression test	44
4.9. Yield Function, Cam-clay Model	48
4.10. Constitutive Equations in Matrix Format	51
4.11. Modified Cam-clay Model	54
4.12. Model Parameters	58
4.13. Model Verification	59
5. RESULTS AND DISCUSSION	61
5.1. Finite Element Model	61
5.1.1. Property parameters of ground feed	61
5.1.2. Model verification	63
5.1.3. Stress contour patterns in model bins	64
5.2. Stress Distribution in <i>Half Bin</i>	65
5.2.1. Stress distribution after filling	65
5.2.2. Stress distribution after draw-down initiation	66
5.3. Stress Distribution in <i>Full Bin</i>	74
5.3.1. Stress distribution after filling	74
5.3.2. Stress distribution after draw-down initiation	74
5.4. Effect of Insert Location on Stress Distribution in <i>Farm Bin</i>	80
5.4.1. Stress distribution after filling	80
5.4.2. Stress distribution after draw-down initiation	80
5.5. Effect of Insert Size on Stress Distribution in <i>Farm Bin</i>	86
5.5.1. Stress distribution after filling	86
5.5.2. Stress distribution after draw-down initiation	86
5.6. Effect of Insert Friction on Stress Distribution in <i>Farm Bin</i>	92
5.6.1. Stress distribution after filling	92
5.6.2. Stress distribution after draw-down initiation	92
5.7. Effect of Size of Hopper outlet on Stress Distribution in <i>Farm Bin</i>	98
5.7.1. Stress distribution after filling	98
5.7.2. Stress distribution after draw-down initiation	98
5.8. Effect of Hopper Slope on Stress Distribution in <i>Farm Bin</i>	104
5.8.1. Stress distribution after filling	104
5.8.2. Stress distribution after draw-down initiation	104
5.9. Effect of Bin wall Friction on Stress Distribution in <i>Farm Bin</i>	110
5.9.1. Stress distribution after filling	110
5.9.2. Stress distribution after draw-down initiation	110
6. CONCLUSIONS	116
7. RECOMMENDATIONS FOR FUTURE WORK	118

8. REFERENCES	119
APPENDIX A - Formulation in SIGMA/W	125
A.1. Finite Element Equations	125
A.2. Strain-Displacement Matrix	127
A.3. Elastic Constitutive Relationship	129
A.4. Body Forces	130
A.5. Numerical Integration	131
A.6. Assemblage of Global Equations	134
A.7. Equation Solver	135
A.8. Element Stresses	135
A.9. Nonlinear Analysis	136
A.10. Convergence Criteria	140
A.11. Evaluation of the Plastic Matrix, Cam-clay Model	142
A.12. Slip Surface Element	146
APPENDIX B - Results of experiments	149
B.1. Triaxial Tests	149
B.1.1. Drained Tests	149
B.1.2. Undrained Tests	153
B.1.3. Isotropic Tests	157
APPENDIX C -Other Tests	161
APPENDIX D - Verification of modified Cam-clay model	163

LIST OF TABLES

Table 4.1. Parameter combinations used for <i>Farm bin</i> study	26
Table 4.2. R/W ratios for <i>Half bin</i> and <i>Full bin</i>	27
Table 4.3. Examples of consistent sets of units in SIGMA/W	29
Table 4.4. Composition of ground feed used in experiments of Hao (1998)	33
Table 4.5. Physical properties of ground feed used in experiments of Hao (1998)	34
Table 4.6. List of parameters used in finite element model in SIGMA/W	58
Table 4.7. Comparison of modified Cam-clay parameters as determined from simulation of triaxial tests and actual triaxial tests.	60
Table 5.1. Analysis of triaxial test data to determine parameters λ , κ , and Γ	63
Table 5.2. Effect of insert location on stresses near the hopper outlet for <i>Half bin</i>	67
Table 5.3. Effect of insert location on stresses near the hopper outlet for <i>Full bin</i>	75
Table 5.4. Effect of insert location on stresses near the hopper outlet with change in insert location	81
Table 5.5. Effect of insert size on stresses near the hopper outlet	87
Table 5.6. Effect of insert friction on stresses near the hopper outlet	93
Table 5.7. Effect of hopper outlet size on stresses near the hopper outlet	99
Table 5.8. Effect of hopper slope on stresses near the hopper outlet	105
Table 5.9. Effect of bin wall friction on stresses near the hopper outlet	111
Table A.1. Sample point locations and weightings for four point quadrilateral element	132
Table A.2. Sample point locations and weightings for nine point quadrilateral element	133

Table A.3. Sample point location and weighting for one point triangular element . . .	133
Table A.4. Sample point locations and weightings for three point triangular element	133
Table A.5. Acceptable element integration orders	134
Table C.1. Tests to determine particle density of ground feed	161
Table C.2. Tests to determine moisture content of ground feed	162
Table C.3. Tests to determine poisson's ratio for ground feed	162
Table D.1. Comparison of bin-hopper stresses during discharge	165
Table D.2. Comparison of bin-hopper stresses after filling	166

LIST OF FIGURES

Figure 4.1. Schematic of <i>Lab Bin</i>	23
Figure 4.2. Bin models (a) <i>Half Bin</i> , (b) <i>Full Bin</i> , and (c) <i>Farm Bin</i>	24
Figure 4.3. A typical stress contour plot with color legend	32
Figure 4.4. Schematic of insert (elevation and isometric view) used by Hao (1998) ...	32
Figure 4.5. Analogy between volume-pressure and stress-strain relationships	37
Figure 4.6. Definition of model parameters for Cam-clay	39
Figure 4.7. Triaxial test apparatus	40
Figure 4.8. Load curve for drained tests	45
Figure 4.9. Load curve for undrained tests	46
Figure 4.10. Three cycle isotropic test on ground feed	47
Figure 4.11. Yield curve for the Cam-clay model	49
Figure 4.12. Definition of Soil Parameters for Cam-clay Model	50
Figure 4.13. Yield function for modified Cam-clay	55
Figure 5.1. Critical state line determined for ground feed from regression analysis on drained and undrained test data	62
Figure 5.2.(a) Effect of insert location on stress distribution in <i>half bin</i> after filling but prior to draw-down initiation. Y-total stress (left column) and x-total stress (right column)	68
Figure 5.2.(b) Effect of insert location on stress distribution in <i>half bin</i> after draw-down initiation. Y-total stress (left column) and x-total stress (right column)	71

Figure 5.3.(a) Effect of insert mounting method on stress distribution in <i>full bin</i> after filling but prior to draw-down initiation. Y-total stress (left column) and x-total stress (right column)	76
Figure 5.3.(b) Effect of insert mounting method on stress distribution in <i>full bin</i> after draw down initiation. Y-total stress (left column) and x-total stress (right column)	78
Figure 5.4.(a) Effect of insert location on stress distribution in <i>farm bin</i> after filling but prior to draw-down initiation. Y-total stress (left column) and x-total stress (right column)	82
Figure 5.4.(b) Effect of insert location on stress distribution in <i>farm bin</i> after draw-down initiation. Y-total stress (left column) and x-total stress (right column)	84
Figure 5.5.(a) Effect of insert size on stress distribution in <i>farm bin</i> after filling but prior to draw-down initiation. Y-total stress (left column) and x-total stress (right column)	88
Figure 5.5.(b) Effect of insert size on stress distribution in <i>farm bin</i> after draw-down initiation. Y-total stress (left column) and x-total stress (right column)	90
Figure 5.6.(a) Effect of insert friction on stress distribution in <i>farm bin</i> after filling but prior to draw-down initiation. Y-total stress (left column) and x-total stress (right column)	94
Figure 5.6.(b) Effect of insert friction on stress distribution in <i>farm bin</i> after draw-down initiation. Y-total stress (left column) and x-total stress (right column)	96
Figure 5.7.(a) Effect of size of hopper outlet on stress distribution in <i>farm bin</i> after filling but prior to draw-down initiation. Y-total stress (left column) and x-total stress (right column)	100

Figure 5.7.(b) Effect of size of hopper outlet on stress distribution in <i>farm bin</i> after draw down initiation. Y-total stress (left column) and x-total stress (right column) .	102
Figure 5.8.(a) Effect of hopper slope on stress distribution in <i>farm bin</i> after filling but prior to draw-down initiation. Y-total stress (left column) and x-total stress (right column)	106
Figure 5.8.(b) Effect of hopper slope on stress distribution in <i>farm bin</i> after draw-down initiation. Y-total stress (left column) and x-total stress (right column)	108
Figure 5.9.(a) Effect of bin wall friction on stress distribution in <i>farm bin</i> after filling but prior to draw-down initiation. Y-total stress (left column) and x-total stress (right column)	112
Figure 5.9.(b) Effect of bin wall friction on stress distribution in <i>farm bin</i> after draw-down initiation. Y-total stress (left column) and x-total stress (right column)	114
Figure A.1. Storage scheme for global characteristic matrix	134
Figure A.2. Iteration schemes for non-linear analysis	139
Figure A.3. A typical slip surface element	147
Figure B.1.(a) Drained tests at 100 kPa	149
Figure B.1.(b) Drained tests at 75 kPa	150
Figure B.1.(c) Drained tests at 40 kPa	151
Figure B.1.(d) Drained tests at 20 kPa	152
Figure B.2.(a) Undrained tests at 100 kPa	153
Figure B.2.(b) Undrained tests at 75 kPa	154
Figure B.2.(c) Undrained tests at 40 kPa	155
Figure B.2.(d) Undrained tests at 20 kPa	156

Figure B.3.(a) Three cycle isotropic test	157
Figure B.3.(b) Three cycle isotropic test	158
Figure B.3.(c) Three cycle isotropic test	159
Figure B.3.(d) Three cycle isotropic test	160
Figure D.1. Typical effective stress path during triaxial simulation (at confining pressure = 100 kPa)	163
Figure D.2. Critical state line (Slope = M) determined by triaxial simulation	163
Figure D.3. Critical state line in $e-\ln(p')$ plot to determine the parameter I and G by triaxial test simulation	164
Figure D.4. Unloading-reloading cycle in triaxial test simulation to determine the parameter k	164
Figure D.5. Stress conditions at bin-hopper wall calculated by Janssen's equations	165

1. INTRODUCTION

In any operation involving particulate solids, successful handling, storage, and flow of the bulk material is a major and essential part of the overall plant design (Shamlou 1988). The proper design of bulk solid storage and handling equipment requires knowledge of particle and bulk properties of the particulate material in static and dynamic conditions. Bulk materials are composed of individual particles and pores filled with air. Bulk properties, therefore, depend on both individual particles and inter-particle interactions. Particle size, shape, and surface area are fundamental characteristics of bulk solids and are of paramount importance in most unit operations involving such materials. They determine, to a large extent, the degree of interactions of particles with the surrounding material and with each other. These interactions critically influence the behavior of the bulk material, e.g., its flowability, fluidizability, and compressibility (Shamlou 1988). Throughout the process industries, deep bins and silos are used extensively for the storage and transfer of bulk solids such as chemicals, foodstuffs, pharmaceuticals, cement, coal, polymers, and powdered metals. In most cases it is important to ensure an even mass discharge of the material between process stages, with a minimum of alteration in the quality of the stored product. Flowability of a material, however, may change depending on the condition of the stored material and type of storage structure. Pariseau and Nicholson (1979) showed that flow-no flow condition in a grain bin depends on the extent of the plasticity zone near the hopper outlet. Depending upon the bin structure and construction material, stored material properties, and size of outlet, the flow can be mass flow or funnel flow (Shamlou 1988). The terminologies used in this study to describe the flow of ground feed are those defined in the ASAE Engineering Practice dealing with loads exerted by free flowing grains on bins (ASAE 1993). Funnel flow is

defined as “flow from a bin in which all grain movement occurs through a central core with no movement occurring along the bin wall.” Mass flow is described as “flow from a bin in a manner such that movement occurs along all or part of the bin wall” (ASAE 1993). The common problems associated with funnel flow in bins are that of segregation of material and formation of rathole and arches in the proximity of the discharge opening. The tendency of material to bridge over the outlet and stop the flow is greater when funnel flow occurs than during mass flow. The arches are formed at arbitrary intervals and have various forms and durations. They can be formed locally or over the whole area of the aperture. The formation of an arch may or may not cause the flow to fall to zero. Each time an arch is formed, the flow is partially interrupted and the arch carries all the dynamic pressure of the material flowing above the arch(Peschl 1969). The unstable arch formed for a short duration is also called dynamic arch. Unfavourable circumstances can cause an arch to become stable and the bin to be clogged. The chance of arch formation increases as the ratio of aperture diameter to particle size decreases and as the cohesion and interlocking of particles increases. When a stable arch collapses by itself or is caused to collapse, the material flows again for a duration which depends on bin-particle interactions. An arch can be collapsed by mechanically breaking the arch with a rod, hammering the hopper, vibrating the bin and material, designing bins with adjustable hopper aperture, or by using flow corrective inserts. Flow aid devices such as vibrators and air blasters are also used to break arches. These devices, however become unsuitable for cohesive materials as they are sensitive to the over-compaction caused by these devices. Alternatively, bin inserts can be placed within a bin, usually within its hopper section, to increase the size of the active flow channel in a funnel flow bin and to relieve pressures at the outlet region thereby decreasing chances of arch formation and improving the

flow. Inverted cones and pyramids have been used for years in this regard but with limited success. Work by Johanson (1966) suggest that inserts of an appropriately chosen shape when placed at a certain height above the silo outlet considerably reduce the size of stagnant zones observed in a funnel flow bunker and thus enhances uniform flow behaviour. Despite all the research done, the exact mechanism that causes the insert to work effectively is not known. Jenike (1964) indicated that an insert could also be employed to redistribute the stresses in the flow channel. He suggested that self-perpetuated over-consolidation of flowing materials could not develop due to the influences of inserts hence stable arch or dome formation near a hopper outlet would not occur. It may be noted that most of the research has been done on granular material (Johanson 1966, Jenike and Johanson 1969, Tuzun and Nedderman 1983, and Zhang *et al.* 1987). Though several models have been developed to study the behavior dry powders, very few have been applied to simulate the material behavior in storage bins. In this research, finite element method was used to determine the effect of insert on the stress distribution in stored material inside storage bins. Models were also developed to study the influence of bin-hopper parameters on stress distribution. Study of stress distribution becomes imperative as it largely influences the formation and stability of arches at the outlet which in turns effects the flowability of the material. In this regard it is worth noting that for cohesive materials, cohesion of a few tenths of a psi (700 Pa) or less may mean the difference between flow and no flow.

2. LITERATURE REVIEW

2.1. Flow Patterns in Storage Bins

The material flow pattern in a storage bin depends on various factors such as the shape of bin, roughness of interior surfaces, and properties of stored materials. Mass flow occurs when the entire volume of stored material is in motion while funnel flow occurs when the material flows towards the outlet in a channel that forms within the stored material. Jenike and Leser (1964) indicated that the conditions of mass flow depended on wall friction, internal friction, and hopper half angle. Any factor which affected one of these three parameters could have an effect on the flow mode. Gaylord and Gaylord (1984) concluded that for mass flow to occur, the hopper walls would need to be sufficiently steep and smooth to assure sliding of the solid along the wall. Jenike and Johanson (1969) indicated that for mass flow to occur, it is also necessary that the flow controlling device permit flow through the whole cross section of the outlet.

Photographic techniques were used by O'Callaghan (1960) to study flow patterns of grains (wheat and barley) in rectangular model bins. He observed that the failure lines between the stationary and moving grain were not straight lines, as were generally assumed, when grain was discharged through a central outlet. Based on the principles of soil mechanics he concluded that the rupture lines between the stationary and moving grain were best described by logarithmic spirals. Giunta (1969) determined flow patterns of granular material in flat bottom bins. He found that boundaries of flow patterns were a function of the effective angle of friction of the material, the diameter of the outlet, and the head of material in the storage bin. The flow expanded outward from the edge of the opening and became almost vertical near the top of the bin. Bernache (1969) opposed the common notion that a smooth

wall finish, such as stainless-steel mill finish as opposed to carbon steel would produce mass flow in less steep cone. He presented case studies of how the kinematic angle of friction between dry solids and bin walls affected the design of mass flow hoppers and how it varied for different materials. The kinematic angle of friction was determined on a flow-factor tester and wall yield locus was plotted. The wall yield locus for earth Celite 545 was same for carbon steel and cold-rolled stainless steel. This meant that though carbon steel had high surface friction, it could be used instead of stainless steel for bin fabrication and yet there would be no effect of surface roughness of bin wall on flow of earth Celite 545. Moriyama (1983) investigated the effects of filling methods (central and peripheral) on flow patterns in a half cylindrical bin with a glass board in the front. The results showed that when bulk solids were poured into the central part of the bin, perfect mass flow could be attained during discharge. Inversely, when bulk solids were peripherally filled to the central part of the bin, funnel flow occurred during the discharge. The effects of depth of grain on flow patterns were studied by Schwab *et al.* (1989). They carried out tests by discharging wheat from the central outlet of a full scale steel bin which was 4.08 m in diameter and with a maximum possible H/D ratio (the depth of grain in the bin to the diameter of the bin cross-section) of 5.0. They found that funnel flow occurred when the ratio of H/D was less than 1.55, and mass flow occurred when the ratio of H/D was greater than 2.6. Bucklin *et al.* (1991) conducted similar studies. They observed flow patterns of corn and wheat during discharge from four clear plastic flat bottom model bins. When the ratio of H/S (the grain depth to the distance across the bin) was less than 1.25, wheat and corn always discharged in funnel flow. For $1.25 \leq H/S < 2.5$, wheat discharged in a transition state between funnel flow and mass flow, called intermediate flow. For $2.5 \leq H/S < 3.5$, wheat discharged in either intermediate or mass

flow. Wheat always discharged in mass flow for $H/S=3.5$. For $1.25 \leq H/S < 3.5$, corn discharged in uncertain flow patterns.

2.2. Factors Affecting Flow Behaviour

Knowledge of bulk properties of particulate materials is essential to predict the flow pattern that would exist in the storage bin when the material is discharged. The important properties include the effective angle of the internal friction, the angle of the wall friction, the flow factor, and the flow function.

For an arch to occur in a flow channel, the solid had to be consolidated to such a degree that it developed sufficient strength to support the weight of the arch (Jenike 1964). Jenike (1964) proposed that since there were no stresses on the exposed surface of arch, the stresses parallel to it was the principal stress whose maximum value was equal to the unconfined yield strength f_c when the arch was broken. Hence, the higher the value of f_c for a material at a given consolidating pressure in a channel, the lower the flowability of the material in the channel. Jenike expressed the flow function (FF) as the ratio of major consolidating pressure to f_c . He also prepared charts for flow factor (ff), which was function of the effective angle of friction, the angle of friction of solid on hopper wall, the slope of the wall, and the type of flow. If for any storage condition, $ff > FF$, uninterrupted flow occurred in bin.

Schweds (1983) studied the effect of the effective angle of friction on flow patterns. He concluded that the distinction between mass flow and funnel flow was determined by the bin geometry and flow properties, and the governing parameter was the angle of the friction between solids and wall material. Ooms and Roberts (1984) also indicated that the angle of the wall friction had influence on flow patterns both in conical and plane-flow bins. For a

given geometry, a small increase in the wall friction angle would change a mass flow hopper into a funnel flow hopper. Roberts (1991) concluded that of the various parameters affecting the performance of a hopper, friction at the boundary surface had major influence. Carson and Marinelli (1994) stated that the effective angle of the internal friction and the angle of the wall friction were important parameters characterizing the flow properties of a solid. They concluded that the lower the angle of the wall friction, the less steep the hopper walls needed to be to get mass flow. This conclusion was in agreement with that drawn by Ooms and Roberts (1984). Typically as the consolidation pressure increased, the effective angle of the internal friction increased.

2.3. Pressure Profile in Storage Bins

Knowledge of the pressures acting in the stored material and on the walls of the silo is essential not only for the structural design, but also for determining the critical storage bin dimensions in order to ensure unobstructed discharge. The geometry of the storage bin and the characteristic properties of the stored material ultimately decide the flow patterns and the pressure profiles developed within the storage (Shamlou 1988). Johanson (1964) presented a mathematical theory of stress and velocity fields for steady gravity flow of bulk solids in converging channels. The equations were based on the principles of soil mechanics and the theory of plasticity. A simplified stress field, also referred as radial stress field was calculated and supported with experiment evidence. He concluded that stress fields in the plain strain and in axial symmetry conditions converge to the radial stress field as the vertex of the channel was approached, i.e. $r \rightarrow 0$. This convergence was of fundamental importance in the derivation of flow-no-flow criteria for particulate solids because most of the obstructions to the flow originated at the outlets of channels. Since, in real channels, convergence to a radial

stress field is very rapid, the stresses in the region of an outlet are well represented by the radial stress field. Jenike and Johanson (1969) proposed that three loading conditions should be considered in the analysis of loads acting on a bin : initial loading which occurred when bulk solid was filled in the storage bin without any of it being withdrawn, flow loading which occurred after the flow had been established, and switch loading which occurred during the switch from initial to flow loading. Switch loading is transient and exerts large concentrated forces on bin wall. Under the initial loading condition, the active state of pressure exists. The direction of principal stresses is vertically down. During the flow, the passive state of pressure sets in, while the material in the hopper expands in a vertical direction and contracts in horizontal. Flow loading developed only within the boundaries of flow channel. At the beginning of flow a reorientation of stress fields occurs in the hopper area. Pariseau (1969) presented experimental evidence to show that the plasticity theory was a suitable framework for analysing the flow of bulk materials in bins and hoppers. He proposed a plasticity theory viewing the effects of deviatoric and direct stresses on the strain rates as separate but related phenomenon using a yield function based on the Mohr-Coulomb yield criterion. Pariseau and Nicholson (1979) studied the influence of hopper wall slope, wall friction angle, and outlet width on the stress and displacement fields that evolved for a layer by layer filling sequence of a V-shaped gravity flow hopper. The results were based on the elastic-plastic material idealisation and all the computation were made using finite element method. Practical design information in the form of hopper wall and bottom loads and growth of the plasticity zone in the vicinity of the outlet during draw-down initiation was obtained. They found that increasing wall friction enhanced shear failure at the outlet, but also retarded the material movement. Increasing outlet width increased displacement, however increasing slope did not increase displacement as the effect of wall friction dominated over the effect of slope.

2.4. Arch Formation

The two basic causes for the formation of a stable arch at the outlet are the mechanical interlocking of large (diameter $> 3000 \mu\text{m}$) free-flowing particles and the cohesive strength of fine grains (Shamlou 1988). The concept of flowability of a bulk solid is based on the observation that, in order to support an obstruction to a flow, a solid has to have compressive strength. A solid which develops no strength, like dry sand, is free flowing. Flowability of cohesive materials is measured primarily by the flow function (Shamlou 1988) which is determined by consolidating a sample of solid under a given pressure and measuring the generated compressive strength; the higher the strength, the more the capability of the solid to support obstruction to flow and, the lower its flowability. When the unconfined yield strength of the powder exceeds the force tending to break it, a stable cohesive arch is formed. Mechanical arching may be avoided by having an outlet size that is several times larger than the particle size. In order to determine the minimum dimension of the outlet to prevent an arch or a dome from forming. An arch or a dome is defined by the flow channels in which blockages formed. An arch formation takes place if the channel is wedged-shaped and a dome is formed if it is a conical channel. In the worst case scenario, the only force acting on the thin uniform layer over the arch, which tends to break it, is its own weight. The arch is a self-supporting structure such that the upper and lower boundaries were free surfaces. The minor principal stress (normal to the free surfaces) was zero at any section, and the corresponding major principal stress was tangential to the arch. Since the maximum shear stress in principal stress space is at 45° with the principal direction and is equal to one-half of the major principal stress (since minor principal stress = 0), the maximum span of an arch which could be self-supporting under this stress state would be attained when the shear stresses on the vertical

sections at the abutments were equal to unconfined yield strength. Jenike (1964) postulated that this condition was realized when the major principal stress at the abutments reached the unconfined yield strength of the solid and acted at 45° with the horizontal. Based on this criterion, the following equations were derived to predict the minimum dimension of the bin opening for avoiding arch formation:

- 1) For a wedge-shaped bin, the rectangular opening width was:

$$b = \frac{f_c}{g\gamma} \quad (2-1)$$

- 2) For a conical bin, the diameter of a circular opening was:

$$d = \frac{2f_c}{g\gamma} \quad (2-2)$$

where:

b = minimum width of a rectangular opening (m),

g = gravitational acceleration (m/s²),

f_c = unconfined yield strength of solid (Pa),

γ = bulk density of solid (kg/m³), and

d = minimum diameter of a circular opening (m).

Equations (2-1) and (2-2) were correct only for hopper angle $\theta=0$. Jenike (1964) asserted that the required outlet diameter was also a function of the hopper half angle θ , and thus, his solution gave values of b for wedge hoppers varying essentially linearly from $\frac{2f_c}{g\gamma}$ at $\theta=0$ to $\frac{1.3f_c}{g\gamma}$ at $\theta=60^\circ$, and values of d for conical hoppers ranged from $\frac{2f_c}{g\gamma}$ at $\theta=0$ to $\frac{2.6f_c}{g\gamma}$ at $\theta=40^\circ$.

Laforge and Boruff (1964) carried out a study of formation of arches by observing the movements of particles in a model bin during draw-down. They described converging particle flow paths as turbulence in which particles collided and rebounded, resulting in erratic movements in all directions, and thus the periodic breaking of temporary arches was observed. They suggested that the formation of an arch over the hopper outlet was a result of compaction of cohesive material into solid mass. The material was compacted by the internal pressures. They pointed out that these pressures were not uniform throughout the mass, and were not equal in all directions as in case of liquids. Brown and Richards (1970) explained the mechanism of arching through a series of experiments. They assumed the motion of the particles to be governed by Bernoulli's equation. They derived theoretical expressions for discharge through plane and axisymmetric flow geometries by considering the changes in the potential and kinetic energies of the moving grains and observed that the flow field immediately above the arch was purely radial. They found that there was an empty space adjacent to the edge of the aperture within which practically no flow could take place. Peschl (1969) propounded that an arch was made up of one or more layers of grains arranged in such a way as to be in equilibrium under contact stress of grains, so the theory of arches needed to be applied and not soil mechanics. By building up mechanical model of the arch, fields were found in the 'bin curve' in which a stable arch and a dynamical arch formed. Bin curve was plotted for arch load versus displacement and fields were defined on the plot where dynamical or stable arches could be expected. When an arch is formed, the stress suddenly increase and the material of which the arch is made up reacts by deforming. The deformation causes the radius of the arch to increase and this lead to increased stress in arch. The interaction process is repeated until either equilibrium is reached or the arch collapses. He suggested that stable

arches could be prevented from forming by designing the hoppers side wall at the outlet with a spring mechanism in such a way that if the stress increased, the wall would expand sufficiently to cause the required collapse.

2.5. Flow Promoting Devices

In case where it is impractical to design a bin or hopper that would be self-emptying, various devices can be used to promote flow. One possible way is to blow air into the material via the perforated pipe located in the material close to the outlet of the hopper. Williams *et al* (1983) reported that the best position for air entry in this method of injecting was about four times the orifice diameter above the hopper outlet. An improvement to this method was suggested by Rappen and Wright (1983). They reported a number of successful case studies involving the application of air cannons to initiate flow in bunkers. Sledgehammer is also used to mechanically dislodge any kind of blockage (Gaylord and Gaylord 1984). In some cases, hoppers are provided with holes through which rods can be inserted to loosen the material in case of arching or funnelling. Vibrators have also been reported to be in use to induce flow in storage bins (Gaylord and Gaylord 1984). Vibrators were designed as units either suspended inside hopper or mounted on the side wall. Alternatively, entire hopper have also been designed to vibrate to promote flow.

In case where the conical bin is not steep enough to have flow along the walls, an insert may be used to achieve the desired flow. The insert forms an annular slot opening, which in effect forms a wedge-shaped hopper resulting in flow at the walls only in the region influenced by the insert. Johanson (1966) predicted theoretically the region influenced by the insert. The equations describing a flowing granular solid were hyperbolic, partial differential equations. Johanson (1966) also developed procedures based on the theory of gravity flow

of granular solids to predict the proper placement of conical inserts in conical hoppers to create a mass flow in bins. Johanson (1966) suggested that an insert of an appropriately chosen shape when placed at a certain critical height above the outlet considerably reduced the size of stagnant zones observed in funnel flow bunker and thus enhanced uniform flow pattern. He also studied the effect of fixed inserts on arch formation near hopper outlet and suggested that inserts redistribute the stresses that develop due to over consolidation of the flowing material. Experiments and practical investigation by Kvapil and Tanaka (1965) showed that for free flowing bulk materials the use of horizontal baffles as inserts over the outlet produced a larger active flow zone. He suggested that a large insert placed near the transition of the bin and hopper developed a mass flow pattern and an insert placed near the outlet was useful in eliminating piping and arching of bulk solids. He also calculated the minimum baffle dimensions to improve flow. Ersov and Lisin (1964) found in test models that the flow diminished or even stopped if the distance between the outlet and the bottom of the conical insert became too small, but if the distance was too great, segregation occurred below the insert. The Bituminous Coal Research Inc. (Lee 1964) developed a method of placing a double-cone which was fitted in a tube below the bunker outlet. This arrangement was found to be superior to the single cone placed within the bunker, especially when handling coal at high moisture content and where the bunker was not operated for several days (Lee 1964). Compacting pressures in the double cone attachment were low, and thus a low cohesive strength was maintained in the material. Tüzün and Nedderman (1983) investigated the effects of obstacles in a bunker on the formation of arches. They observed that obstacles increased the wall stresses during filling, but decreased them during flow. They concluded that stable arches, once formed, resulted in sporadic discharge behaviour or in some cases, completely

stopped the discharge. Formation of arches was prevented by allowing the material to flow in a cascading manner onto successive stress-breaking inserts placed at different heights along the bunker.

2.6. Constitutive Equations for Cohesive Materials

This research aimed at applying elastic-plastic finite element method to study the constitutive behavior of ground feed which is a cohesive powder material. This was decided by observations of the physical behavior of the material. Finite element methods can be applied to study the bulk solids as the material stored in the storage bin can be treated as a continuum. Several models available in the literature were investigated as to their application to cohesive materials. The concept of plasticity was first introduced as early as later half of 18th century by Coulomb who proposed a yield criterion for solids such as soils (Desai and Siriwardane 1984). Later on, Rankine(1857) applied Coulomb's concept to problems of calculation of earth pressure on retaining wall. However, Tresca (1864) is regarded as the first one to perform a scientific study of plasticity and formulated his yield criterion of maximum shear stresses.

A generalisation to account for the effects of all principal stresses on yielding of the material was suggested by Drucker and Prager (1952) by using the invariants of the stress tensor. When the state of stress reaches the yield surface, the material undergoes plastic deformations. According to the criterion, a state of stress outside the surface is not stable. The material can undergo plastic deformation while the stress point was moving on the yield surface. Rendulic (1936) and later Hvorslev (1969) observed that the constant void ratio contours on the triaxial plane for cohesive soils were the same under undrained and drained conditions. The findings of Rendulic and Hvorslev were investigated by Roscoe *et al.* (1963)

who proposed models for the yielding of the soils based on the theory of plasticity. Many models have hence been developed to describe the yielding during compaction (Thompson 1981, Doraivelu *et al.* 1984, Nagoa *et al.* 1988, Brown & Weber 1988, Weber *et al.* 1989, Trassoras *et al.* 1989).

Stainforth and Ashley (1973) presented a comprehensive model for determining the flow function for cohesive powders using an empirical equation. This model was an extension of equations developed by Ashton *et al.* (1965) which related the tensile strength to normal stress. The calculated flow function was compared to the flow function determined using Jenike shear tests. The results compared reasonably well to data obtained using Jenike shear tests. Molerus (1975, 1978) constructed yield loci of cohesive powders by noting that shear and normal stresses were functions of the particle coordination number, material porosity, average particle spherical diameter, and the force components between particles. The parameters involved were determined by using shear test data. A detailed review has also been presented by Tripodi (1994) concerning key models in the literature that are applicable to cohesive materials.

2.7. Finite Element Modelling of Stored Material

There are numerous theories to relate the applied load to resulting deformation behaviour in powders. Constitutive modelling can be approached by either microscopic (discrete element) models or macroscopic (finite element) models. Microscopic models consider each particle as distinct entity and then predict stress-strain behaviour based on distribution of inter-particle forces whereas macroscopic models treat the bulk solid as a continuum and describe load deformation characteristics of the material as a whole. Due to a large number of particles in a given volume and complexity of the behavioural equations,

no microscopic model is available that can be readily applied. On the other hand, macroscopic models are easier to implement. They satisfy the mass, momentum, and energy equations, and can be quite accurate if the model assumptions are reasonable. A number of studies have been carried out to investigate the behaviour of stored material using the finite element models. Pariseau and Nicholson (1979) carried out a parametric study of the influence of hopper wall slope, wall friction angle and outlet width. The stress and displacement fields were determined for a layer by layer filling sequence of a V-shaped gravity flow hopper of fixed storage capacity and fitted with a slot outlet. The main objective of the study was to demonstrate the applicability of the finite element technique to the solution of bin-hopper mechanics problems such as calculation of stress fields during bin filling and draw-down initiation. An existing elastic-plastic finite element program was used and the yield function was based on the extended form of von Mises yield criterion. Bock (1989) and Bock *et al.* (1989) utilized a viscoplastic model to predict the stress relaxation of wheat *en masse*. Zhang *et al.* (1987, 1988, 1989) used an elastoplastic constitutive model developed by Lade (1977) for soils to predict the response of wheat *en masse* to thermally induced loads in grain bins. This model was subsequently expanded (Li 1989; Li *et al.* 1990, 1991) to incorporate the elasto-viscoplastic equations of Youngs (1982). The finite element method has also been used to predict loads in a powder during uniaxial compressive loading (Messing *et al.* 1982). Haussler and Eibl (1984) described the stress and velocity fields in discharging bins using the finite element method. The bin and hopper geometry were discretized into triangular elements, varying in size from smallest at the hopper outlet to largest at the top. The constitutive equations were based on a model proposed by Lade (1977) and stresses had both static and dynamic components. The velocity fields were calculated using kinematic boundary conditions

and equations of equilibrium. Askari and Elwi (1988) predicted stresses in a grain bin at the incipient flow condition using Drucker-Prager's elastoplastic constitutive theory. Link and Elwi (1990) also predicted bin pressures at the incipient flow condition using Drucker-Prager theory. The bin and hopper were discretized into 8-noded grain elements and interface elements were introduced between the grain and the wall material.

2.8. Critical state and Cam-Clay Model

The critical state concept was used by Roscoe *et al.* (1963) in an attempt to describe the yielding of soils during triaxial tests. The critical states concept stated that a particulate material reaches a critical volume after which additional loading does not produce a change in volume. In other words, when a particulate material is loaded, particles rearrange, agglomerate, and fracture, causing the volume to either decrease or increase. The material then reaches a point at which additional load changes the shape of the given mass but not the volume. This state point is termed the critical state. Before reaching the critical state, the material undergoes successive yield states depending upon the material's response to loading conditions and the stress history of consolidation.

The most common critical state models were those patterned after the Cam-clay model. The Cam-clay model which was proposed by Roscoe *et al.* (1963) used three critical state parameters: M (slope of critical state line); λ (slope of loading path); and κ (slope of unloading path). Parameters e_0 (initial void ratio), p_c (hardening parameter), and Γ (specific volume at the critical state when natural log on mean effective stress ($\ln(p')$) is 0) were also used in the elastoplastic constitutive equations. All parameters were determined from the conventional triaxial tests. The prominence of the model can be established from the fact that its concepts were, and still are, utilized by several researchers. Nova and Wood (1979)

developed a load-deformation model for sand based on the Cam-clay model. Seven material parameters, determined by triaxial compression tests, described the plastic potential and yield functions. This cohesionless model was modified by Nova (1981) to include cyclic loading on clays. Carter *et al.* (1982) modified the Cam-clay model by introducing a degradation parameter to take into account cyclic and hysteretic behaviour. Akai and Yano (1985) incorporated deviatoric strain into Cam-clay model by defining a yield function which considered flow to be non associative and was described as both a consolidation function and shear function. Herai (1989) modified the Cam-clay model to consider anisotropic consolidation, non-associative flow rule and cyclic loading. Ten material parameters were determined using undrained triaxial tests. Tripodi *et al.* (1995) applied modified Cam-clay elastoplastic model for predicting the stress strain behaviour of wheat flour compacted in an aluminium cylinder. The model was also used to predict the response of wheat flour under compaction loading. Wheat flour responded anisotropically to the applied loading, resulting in unequal wall strains hence unequal stress distribution in the compressed flour.

2.9. Previous Study and Direction of Research

In a recent study done at Department of Biosystems Engineering, University of Manitoba by Hao (1998) experiments were performed to investigate the effects of inserts on flow behaviour of cohesive materials stored in two-dimensional wedge shaped model bin. The bin was 2400 mm high, and was rectangular in cross section with a width of 1000 mm and side of 400 mm. The hopper made a 30 degrees angle with horizontal and had an opening of 38 mm. Flow patterns were recorded using a video camera and a computer image processing tool was used to analyse the acquired image to determine the influence of inserts on flow patterns and velocity profiles.

The tests were performed without inserts, with fixed inserts, and with rotating inserts installed in the bin. The tests with the fixed insert were done at heights of 83, 174, 261, and 450 mm from the bin outlet to the bottom of the insert, and tests with rotating inserts were done at heights of 53 and 174 mm from the bin outlet to the bottom of the insert.

Placing a fixed insert at a height of 261 mm and a rotating insert at a height of 174 mm improved the flow quality to the point where the bin was emptied without human intervention. Flow was improved as the insert location was increased from 83 to 261 mm and from 53 to 174 mm for the fixed insert and for the rotating insert, respectively. No further improvement in flow was observed by increasing the mounting height of the fixed insert after 261 mm. The rotating insert performed better than the fixed inserts did in improving material flow.

The present research was an effort to apply finite element technique to simulate conditions similar to that of the previous study and extend the result to larger size bins. Modified Cam-clay model was used to predict stress distribution in ground feed (cohesive material) inside storage bins of size used by Hao (1998) and farm size bins (4 m high, 2 m diameter). Finite element calculation was done using an existing software SIGMA/W (GEO-SLOPE International Limited), which also provided CAD interface to draw shapes of bins, inserts, interface elements, quadrilateral and triangular material elements, boundary conditions and specify parameters such as type of analysis (axisymmetric or two dimensional), body weight of material, number of iterations, convergence criteria, Cam-clay parameters, and time-steps for fill. Contours were plotted for Y-total stress and X-total stress after step-by-step fill and after draw-down initiation.

3. OBJECTIVES

The literature review cited in the above accentuates that the study of bin-hopper is a complex subject. Problems such as arching and rat-holing have always been associated with storage bins especially when dealing with cohesive materials. Placing inserts of an appropriate size at an appropriate location enhances the flow behaviour in storage bins. Although inserts have been in use for many years now, more work is still needed to investigate the exact mechanism which makes them effective. This research started with the hypothesis that placing an insert in a storage bin redistributes stresses in stored material which results in an unobstructed flow.

The objectives of the research were :

1. to demonstrate the applicability of a finite element model to the study of the effects of inserts on stress distribution in cohesive materials inside storage bins during filling and draw-down initiation;
2. to carry out parametric study to examine the effect of :
 - i. insert location,
 - ii. insert size,
 - iii. insert surface friction,
 - iv. size of hopper outlet,
 - v. hopper slope,
 - vi. bin wall friction, and
 - vii. mounting method of inserton stress distribution in cohesive materials inside storage bin; and
3. to compare the theoretical results with experimental data from a model bin from previous research.

4. MATERIALS AND METHODS

4.1. Finite Element Simulation of Model Bins

The finite element simulation was carried out using an existing software, SIGMA/W (GEO-SLOPE International Limited). The CAD interface was used to make the bin models.

The discretized system consisted of following components:

- (i) the stored material (ground feed),
- (ii) the structure (bin wall) surrounding the material,
- (iii) the interface between the wall and stored material,
- (iv) the insert inside the ground feed, and
- (v) the interface between the ground feed and the insert.

Before proceeding any further, it is important to specify the nomenclature used to refer to the model bin used by Hao (1998) and model bins used in the finite element analysis:

Lab bin - Physical storage bin used by Hao(1998)

Half bin - Finite element model used in axisymmetric analysis of *Lab bin*

Full bin - Finite element model used in two dimensional analysis of *Lab bin*

Farm bin - Finite element model used in axisymmetric analysis of farm size storage bins

A finite element analysis consisted of two steps: (1) to model the problem and (2) to formulate and solve the associated finite element equations. Modelling involved designing the mesh, defining the material properties, and defining the boundary conditions. The modelling was done using 'Define' option of SIGMA/W for each type of bin for different conditions.

4.1.1. Lab bin The bin walls were made of three pieces of plywood lined with plexiglass and

a piece of transparent plexiglass at the front of the bin. The bin was 2400 mm tall, and was rectangular in cross section with a width of 400 mm and a length of 1000 mm. The bin hopper was constructed by putting two plywood plates lined with plexiglass inside the bin and the hopper half angle could be adjusted from 30° to 90° by changing the length of the plywood plates. A sliding gate opening was used to control discharge (Figure 4.1.).

4.1.2. Half bin To simulate effects of insert on stress distribution in ground feed in *Lab bin* an axisymmetric model was developed (Figure 4.2.(a)).

4.1.3. Full bin To simulate effects of the mounting method of the insert on stress distribution in ground feed in *Lab bin* a *Full bin* model was developed (Figure 4.2.(b)). Three mounting conditions were simulated:

- (1) Asymmetrically mounted insert rotated at 30° with hinged joint,
- (2) Symmetrically mounted insert with hinged joint, and
- (3) Symmetrically mounted insert with fixed joint.

4.1.4. Farm bin An axisymmetric model of a farm size bin (2 m diameter, 4 m high excluding the hopper) was developed to study the effects of insert and storage bin parameters on stress distribution inside ground feed (Figure 4.2.(c)).

In all the bins hopper geometry was discretized into 6-noded triangular and 8-noded quadrilateral elements (except for slip elements which must be 4-noded quadrilateral elements), varying in size from smallest at hopper outlet to largest at bin top. Filling of bin was simulated in 10 increments and draw-down initiation was simulated in one time step. Six different parameters were studied in the *Farm bin* analysis (Table 4.1.)

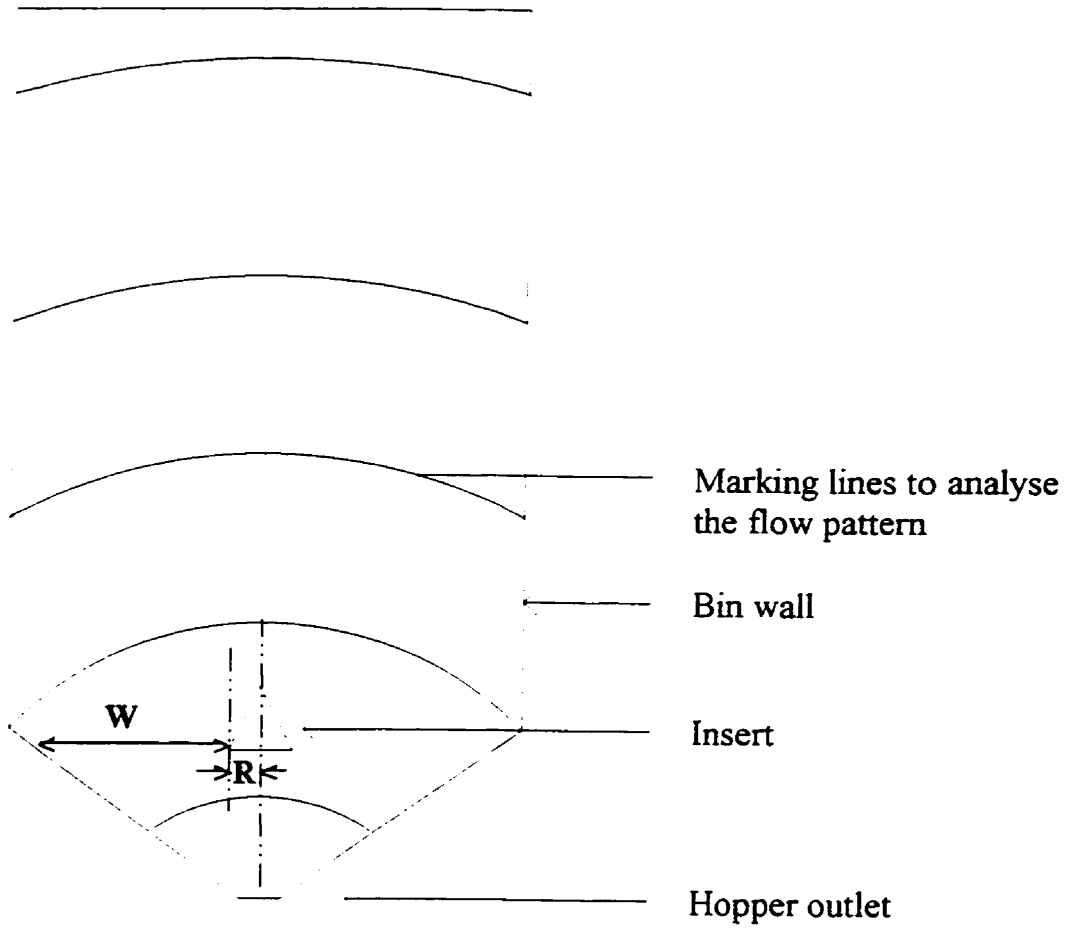
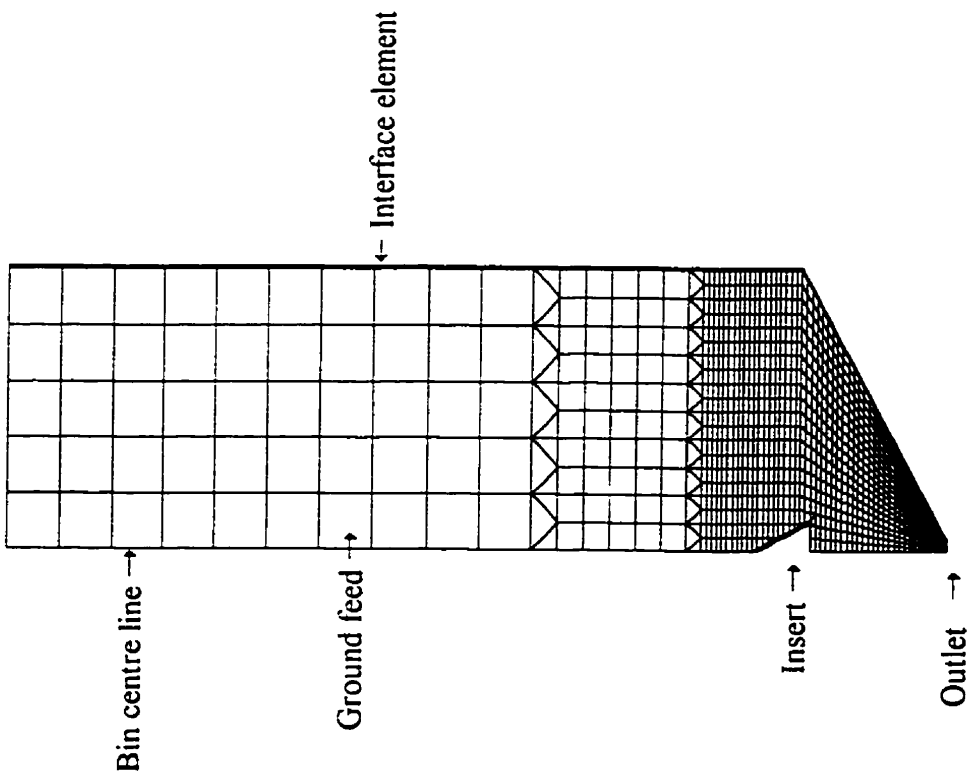
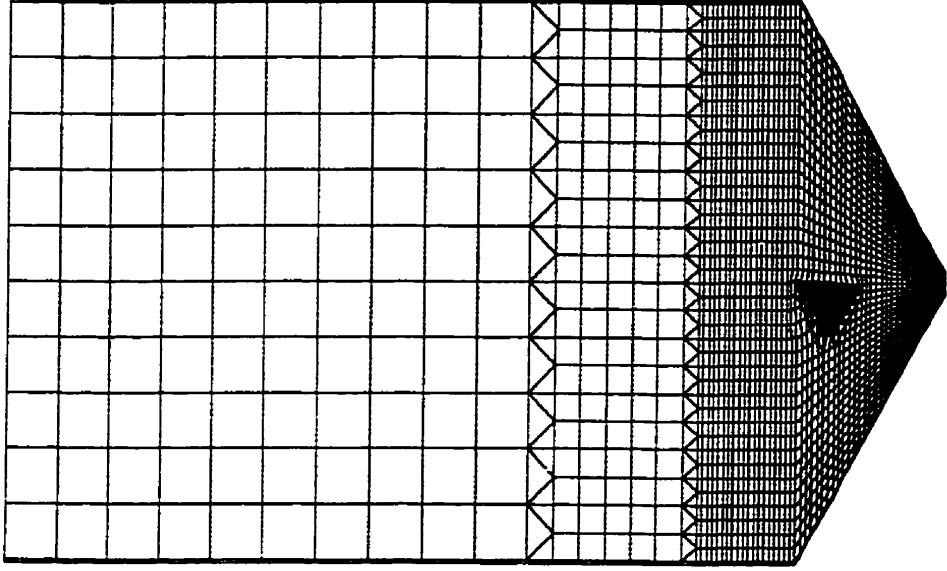


Figure 4.1. Schematic of *Lab Bin*

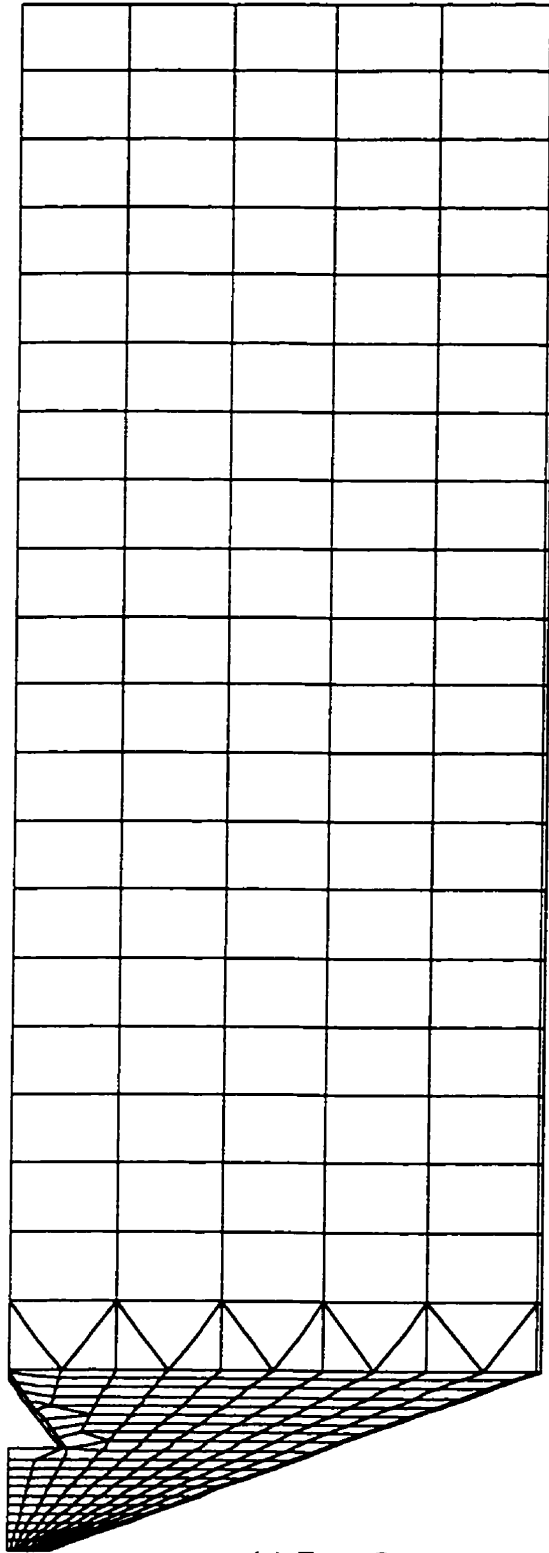


(a) *Half Bin*



(b) *Full Bin*

Figure 4.2. Bin models (a) *Half Bin*, (b) *Full Bin*, and (c) *Farm Bin*



(c) *Farm Bin*

Figure 4.2.

Table 4.1. Parameter combinations used for *Farm bin* study

Insert Location*	Insert Size	Insert Friction	Hopper Outlet*	Hopper Slope**	Bin Friction
(mm)	(mm)	K_{shear} (kN/m)	(mm)		K_{shear}
200	100	1	60	10 ⁰	1
300	150	10	100	20 ⁰	10
400	200	10 ²	160	30 ⁰	10 ²
500	250	10 ⁴	240	40 ⁰	10 ⁴
600	300	10 ⁶	320	50 ⁰	10 ⁶

Measured from hopper outlet to the bottom of the insert

* Hopper outlet size for full size hopper (not for asymmetric half)

** Hopper slope referred in this study is measured w.r.t horizontal

While analysing the effect of a parameter, the parameter under consideration was assigned different value in each of five tests whereas the rest of the parameters were kept constant and were assigned the 'mid value' (shaded values in Table 4.1.). The values of the parameters were chosen in such a way that they covered a range of possibilities. Since the size of hopper changed with change in parameter in study of effect of hopper outlet and hopper slope, the insert was placed such that its bottom remained at the junction of bin wall and hopper for all the cases.

In the simulations where insert location and insert size keeps changing, it is more appropriate to represent the insert-hopper arrangement as a non-dimensional number i.e. W/R ratio (Johanson 1966). Here R is the distance between the edge of the insert to the centre line of the bin and W is the distance between the edge of the insert and the side wall of the hopper

(Figure 4.1.). The R/W ratios for *Half bin* and *Full bin* are given in Table 4.2.

Table 4.2. R/W ratios for *Half bin* and *Full bin*

Insert location from hopper bottom (mm)	R (mm)	W (mm)	R/W
85	50	117	0.42
130	50	195	0.25
175	50	273	0.18
260	50	420	0.12
350	50	450	0.11
450	50	450	0.11

Half Bin(a)

Insert location from hopper bottom (mm)	R (mm)	W (mm)	R/W
200	100	327	0.30
300	100	501	0.19
400	100	674	0.15
500	100	848	0.12
600	100	900	0.11

Full Bin(b)

Size of the insert	R	W	R/W
(mm)	(mm)	(mm)	
100	50	724	0.06
150	75	699	0.11
200	100	674	0.15
250	125	649	0.19
300	150	624	0.24

Full Bin(c)

For granular materials, Johanson (1966) determined the critical values of W/R ratio which would result in the mass flow. The advantage of using this ratio is that it alone accounts for any change in size of hopper, slope of hopper, size of insert, and/or location of insert. Experimental results of Johanson (1966) indicate that the critical W/R values are independent of the slope angle of insert.

4.2. Description of SIGMA/W

SIGMA/W is a finite element software product that can be used to perform stress and deformation analyses of earth structures. SIGMA/W is a 32-bit, graphical software product that operates under Microsoft Windows 95 and Windows NT. SIGMA/W includes three executable programs; DEFINE, for defining the model, SOLVE for computing the results, and CONTOUR for viewing the results. The DEFINE program enables problems to be defined by drawing the problem using Computer Aided Drafting, (CAD) interface. Once a data file is created with DEFINE, the problem is solved using the SOLVE program. CONTOUR is used to graphically display the analysis results computed by SOLVE.

4.2.1. Units Any set of units can be used in a SIGMA/W analysis. However, the units must be used consistently throughout the analysis. For example, if the geometry is defined in meters, then deformation is in meters. Units must be selected for length, force and unit weight. The unit weight of water was set as 9.801 which then set the units to SI units. Table 4.3. shows examples of consistent sets of units.

Table 4.3. Examples of consistent sets of units in SIGMA/W

Property	Units	SI	Imperial
Geometry	L	meters	feet
Unit Weight of Water	F/L^3	kN/m^3	pcf
Soil Unit Weight	F/L^3	kN/m^3	pcf
Cohesion	F/L^2	kPa	pcf
Pressure	F/L^2	kPa	psf
Force	F	kN	lbs.
E (modulus)	F/L^2	kPa	psf

4.2.2 Convergence criteria In all non-linear analyses, it is necessary to use iterative techniques to obtain acceptable solutions. Non-linear analyses exist when a soil property is dependent on the computed results. For example, the stiffness modulus E is dependent on the stress state, but the stresses are dependent on the stiffness. This means that the analysis has to be done many times until there is a reasonable match between the element properties and the computed stresses. When the analysis has produced an acceptable match, the solution is deemed to have converged. As discussed in the Convergence Criteria in Appendix A, SIGMA/W uses two convergence criteria: the displacement criterion and the unbalanced load criterion. The displacement criterion checks the ratio of the vector norm of incremental

displacements in an iteration to the vector norm of the total displacements in the load step. The unbalanced load criterion compares the unbalanced load in an iteration to the applied load in the load step as a percentage ratio. When the percentage ratio becomes equal to or less than the defined convergence criteria, iterations stop and solution is deemed to have converged to the true solution. Trial runs showed that the solution for most of the tests converged within the first five iterations and remained almost unchanged thereafter. Reducing the convergence criteria below 1% resulted in an increase in computational time, however no change took place in the final result. A convergence criterion of 1% and a maximum number of iterations of 25 were found adequate for all the problems.

4.2.3. Simulating filling During a sequential fill placement simulation, forces due to the self-weight of each layer were applied to the finite element grid as the material was being placed. Load of each successive layer was transferred to the layers below. The stresses and displacement caused by the fill were added to the previous stress and displacement data and were then taken as initial condition for the following layer of fill. Time-step was defined as a numeric sequence with increment equal to one. The time-step was used in SIGMA/W to define a logical order which governed the sequence of filling.

4.2.4. Simulating draw-down initiation During simulation of incipient flow conditions, restraint to the bottom most nodes for y-displacement was removed and draw-down was initiated in a single time step.

4.2.5. Viewing results Contours were plotted for y-effective stress and x-effective stress for filling and draw-down initiation (Figure 4.3.). Contours for filling were plotted after the tenth fill. Twenty five contours were plotted for *Half bin* and *Full bin* at an increment of 1 kPa

while twenty five contours were plotted for Farm bin at an increment of 2kPa for a range of 0 to 24 kPa and 0 to 48 kPa, respectively because for all the simulations, the stresses remained in that range. Grey shades were used to fill the space between two contours. White color was used as starting contours at 0 kPa and black color was used as last contour. Region having stresses less than 0 kPa or greater than 24 kPa (*Half bin* and *Full bin*) and 48 kPa (*Farm bin*) was shown by white color.

4.3. Insert

Hao (1998) used triangular shaped inserts that were constructed from plexiglass (Figure 4.4.). The insert was 400 mm long with a cross-section of equilateral triangle of side 100 mm. Three holes were drilled at each end of the insert. The hole at the top was used to mount the insert so that it could swing sideways. Tests were also performed when the bottom holes were used to fix the insert in the bin firmly. To investigate the effect of insert location, Hao (1998) mounted the insert at 53, 83, 130, 174, 261, 350, and 450 mm above the outlet. The insert size used for the *Farm bin* simulations was 200 mm except for analysis where the insert size was a variable itself. In *the Half bin* and *the Farm bin* simulations, the insert formed part of the bin centre line (Figure 4.2(a)) where as in *Full bin* insert was made of linearly elastic elements (Figure 4.2(b)) of negligible body weight and very high modulus of elasticity in order to minimise the effects body weight and stresses developed in insert being transferred to the ground feed.

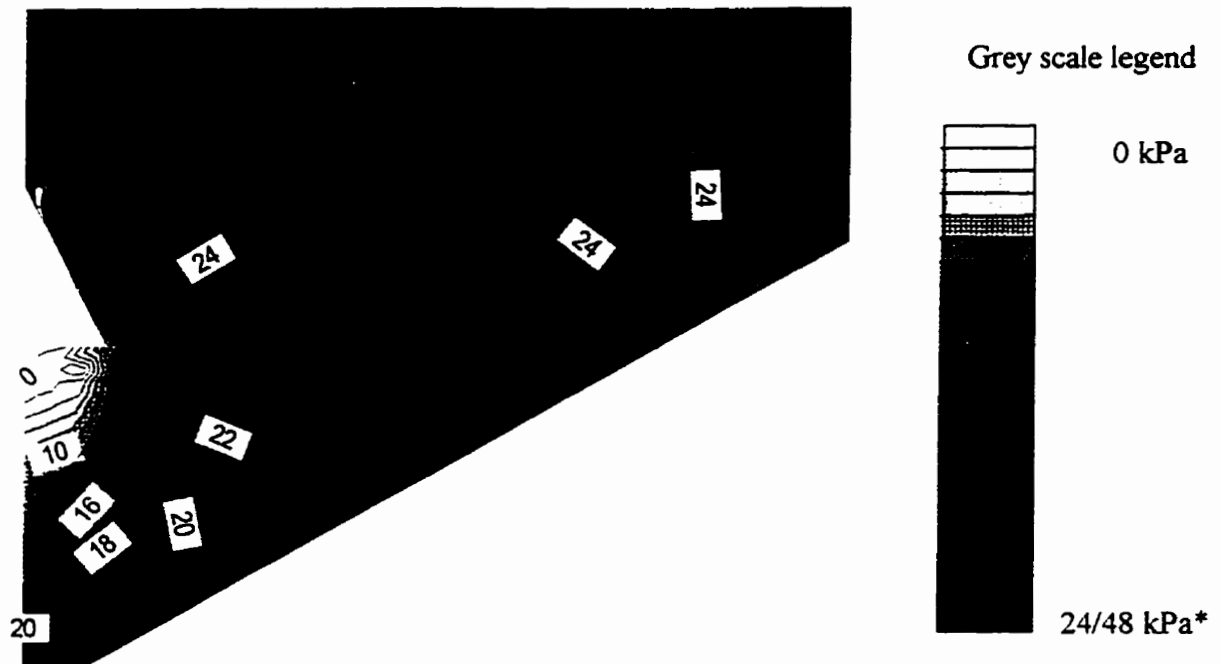


Figure 4.3. A typical stress contour plot with color legend

* Depending on half bin/full bin

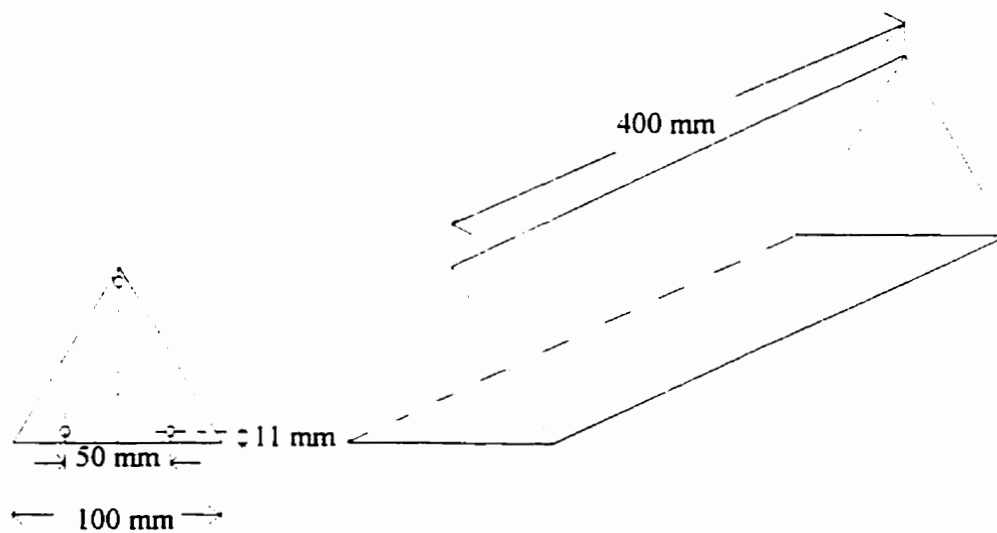


Figure 4.4. Schematic of insert (elevation and isometric view) used by Hao (1998)

4.4. Ground Feed

Ground feed used in triaxial tests in this study was same as the test material used by Hao (1998). The composition and some physical properties of ground feed are listed in Table 4.4. and Table 4.5., respectively.

Table 4.4. Composition of ground feed used in experiments of Hao (1998)

Material	Content (%)
Crushed barley	59.1
Soya-meal	12
Canola meal	10
Calcium carbonate	8.2
Tallow	6.4
Fish meal	2
Vitamin premix	1
Calcium phosphate	0.8
Mineral premix	0.5

Particle density was determined using a pycnometer. There is no standardized procedure to determine moisture content of ground feed, however, ASAE (1993) specifies procedure to determine moisture content of barley, which is 130^o and 20 hours. Since the primary content of ground feed was barley, the samples were kept in oven at 130^o for 24 hours and moisture content was determined on wet basis.

Table 4.5. Physical properties of ground feed used in experiments of Hao (1998)

Physical Properties	Values
Bulk density, kg/m ³	638.9
Effective angle of the internal friction, degree	27.2
Angle of the wall friction, degree	10.5
Cohesion among ground feed particles, kPa	1.6
Unconfined yield strength, kPa	2.9
Moisture content, % wb.	9.48 *
Particle Density, kg/m ³	1608.7 *

* Values determined by author

4.5. Interface Between the Stored Material and the Structure

Interfaces between ground feed and bin wall and between ground feed and insert were modeled using a four-noded quadrilateral element (Appendix A.12.). Using the Slip Surface material model, a SIGMA/W user can specify stiffness in two orthogonal directions. These directions are parallel and perpendicular to the long side of the element. A slip surface element is linear elastic element that has a resistance to compression (normal stiffness) and a resistance to sliding (shear resistance) but no resistance to tension. The isotropic behavior is modelled by defining normal and shear stiffness as:

$$K_{\text{normal}} = \frac{\text{force}}{\text{unit normal deformation in thickness}}$$
$$K_{\text{shear}} = \frac{\text{force}}{\text{unit shear deformation along the length}}$$

K_{normal} is set to a high value to indicate that the slip element has little or no compressibility, and K_{shear} is set to a low value to allow for slippage along the surface when simulating friction at the interface. When the value of K_{shear} is changed, the ability of the element to slip changes. This property of the slip elements has been used to simulate frictional resistance to slippage for various conditions. When there is tension in the slip element (i.e., negative normal stress), K_{normal} and K_{shear} are set to zero. In order to model a slip surface, a slip element should be rectangular and relatively thin. SIGMA/W treats the longer side of a slip element as length and the shorter side as thickness. Stresses in a slip element are obtained from the neighboring elements above and below. In these neighboring elements, stresses are first extrapolated from the Gauss points to the interface nodes. Then, from these nodes, SIGMA/W interpolates for values at the Gauss point using shape functions.

Slip elements were used to model the interface between ground feed and the storage bin wall and the interface between the insert and ground feed. As mentioned above, the value of K_{shear} determines the extent of slippage. A parametric study is needed to test the sensitivity of the results to K_{shear} values because the behavior of ground feed at the K_{shear} values used in simulations and the equivalent friction to the K_{shear} values is not known. In order to have consistency in simulations, K_{normal} was kept as 10^6 kN/m in all the models and K_{shear} was kept as 100 kN/m in model bins simulating no-insert condition and effects of insert location, insert size, hopper outlet, hopper slope, and effect of insert location and mounting methods. K_{shear} was varied from 1 to 10^6 for interface elements to simulate effects of change of bin wall friction and insert friction on stress distribution.

4.6. Constitutive Relationship for Ground Feed

The Cam-clay model is a critical state model as well as an elastic, plastic hardening model. Its formulation in SIGMA/W is based on presentations by Atkinson and Bransby (1978), and Britto and Gunn (1987). More detailed background on the theory of the Cam-clay model can be found in these references. In this section, only the information required to explain the SIGMA/W formulation is presented. The Cam-clay model uses effective stress parameters. In the following discussion, effective stresses are denoted by a superscript ($'$).

The general concept of using a hardening plasticity model to describe the stress-strain behavior of soils was first proposed by Drucker (1957). In constructing the critical state model, Roscoe *et al.* (1963) took some proposals of Drucker, and produced a model of soil behavior which managed to reproduce, for the first time, the description of volumetric response under shear. What really sets the critical state models apart from the previous elasto-plastic models is the critical state line in q - p' plots. This allows a consistent and realistic treatment of both drained and undrained tests. Figure 4.5(a) shows, schematically, volume change versus pressure plots for a sample comprising of loading (normal consolidation line) and unloading-reloading (overconsolidation line). Consider a stress state on the overconsolidation line. An increase in applied stress causes the stress state to move along the overconsolidation line towards the normal consolidation line. Once past the intersection of the two lines, any further stress increase causes the stress state to move down the normal consolidation line. When Figure 4.5(a) is rotated counterclockwise through 90° , the overconsolidation and normal consolidation lines show the characteristic of an elastic-

hardening plastic stress-strain curve, illustrated in Figure 4.5(b). The overconsolidation line is analogous to the initial linear elastic portion, while the normal consolidation line is analogous to the hardening plastic portion of the stress-strain relationship. However, a significant difference is apparent when comparing cohesive soils with metal. With soils, elasto-plastic behavior is associated with both linear and volumetric strains. The von Mises and Tresca yield functions for metal suggest that one can hydrostatically compress metals indefinitely without yielding taking place.

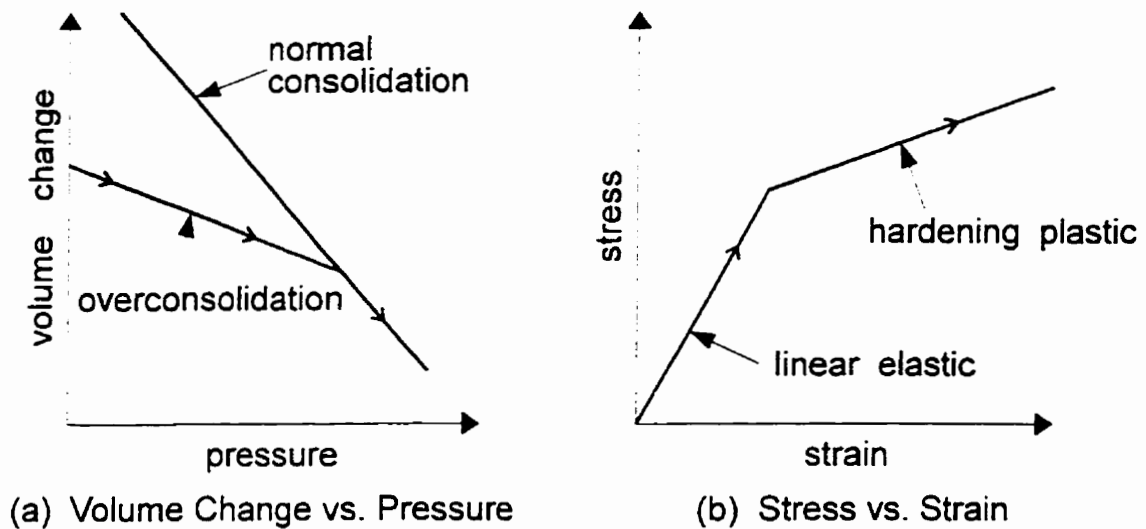


Figure 4.5. Analogy between volume-pressure and stress-strain relationships

4.7. Cam-clay Model Parameters

The Cam-clay model is an effective stress model which requires the following soil properties:

M Slope of the critical state line in the p' - q plane

The critical state line represents the final state of samples in triaxial tests when it is possible to continue to shear the sample with no change in imposed stresses or volume. p' is the mean effective pressure and q is the deviator stress applied to the sample. The mean effective pressure is defined as $(\sigma_1 + \sigma_2 + \sigma_3 - 3u)/3$ where σ_1 , σ_2 , and σ_3 are principal stresses in triaxial tests and u is the pore fluid pressure. The deviator stress is defined as the difference between major and minor principal stresses.

Γ Specific volume at the critical state when p' is 1.0 (or, $\ln(p')$ is 0)

When a critical state line is projected on the v - $\ln(p')$ plane, it lies parallel to the isotropic consolidation line. The intercept of the critical state line with the vertical axis at $\ln(p') = 0$ gives the parameter Γ .

κ Slope of the isotropic over-consolidation (unloading-reloading) line

λ Slope of the isotropic normal consolidation (loading) line

These parameters are illustrated in Figure 4.6. The critical state line shown in the p' - q plane is the locus of critical states projected onto that plane. The critical state line has a slope of, M , which is related to the angle of internal friction of the soil ϕ' . For the case of triaxial compression, M can also be expressed as:

$$M = \frac{6 \sin \phi'}{3 - \sin \phi'} \quad (4.1)$$

For this study, however, M was determined from the slope of the critical state line.

By definition, the specific volume, v , is related to the void ratio, e , through the following expression:

$$v = 1 + e \quad (4.2)$$

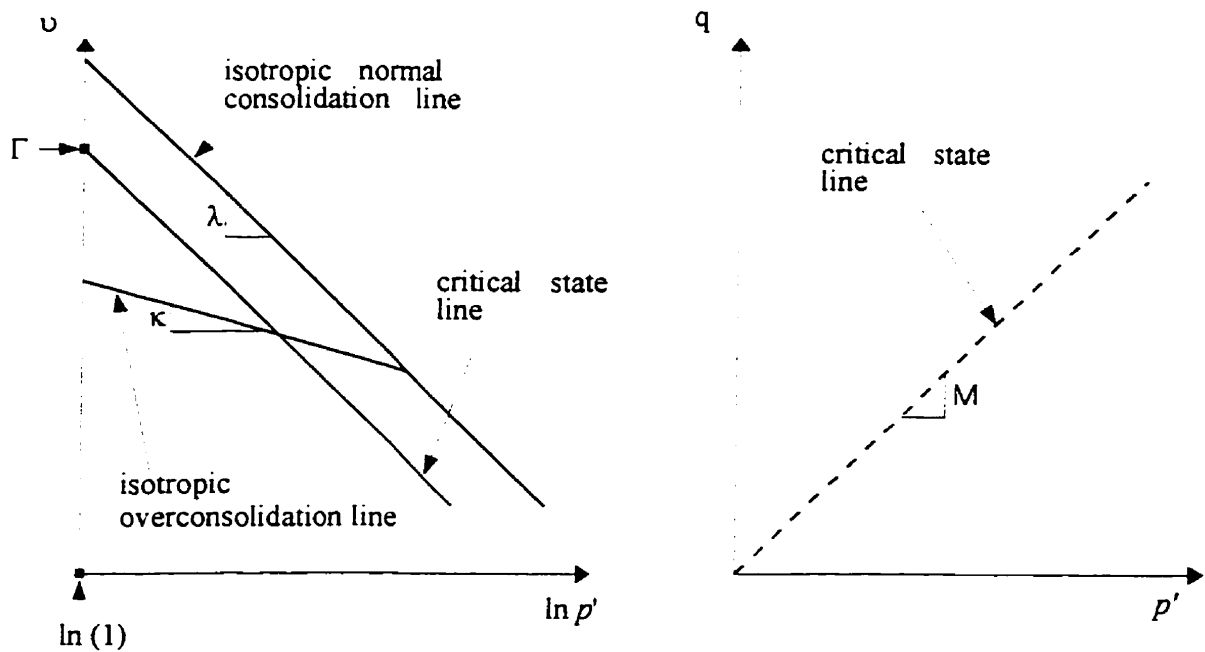


Figure 4.6. Definition of model parameters for Cam-clay

4.8. Determination of Parameters for Cam-clay Model

4.8.1. Triaxial apparatus The triaxial testing apparatus (Figure 4.7.) used was a T-1015Y (Soil Test Inc., IL). Axial loading was applied using a Universal Testing Machine (ATS Inc., PA). Stress and displacement data were acquired on an IBM compatible personal computer and confining pressure and pore pressures were measured using U-tube manometers.

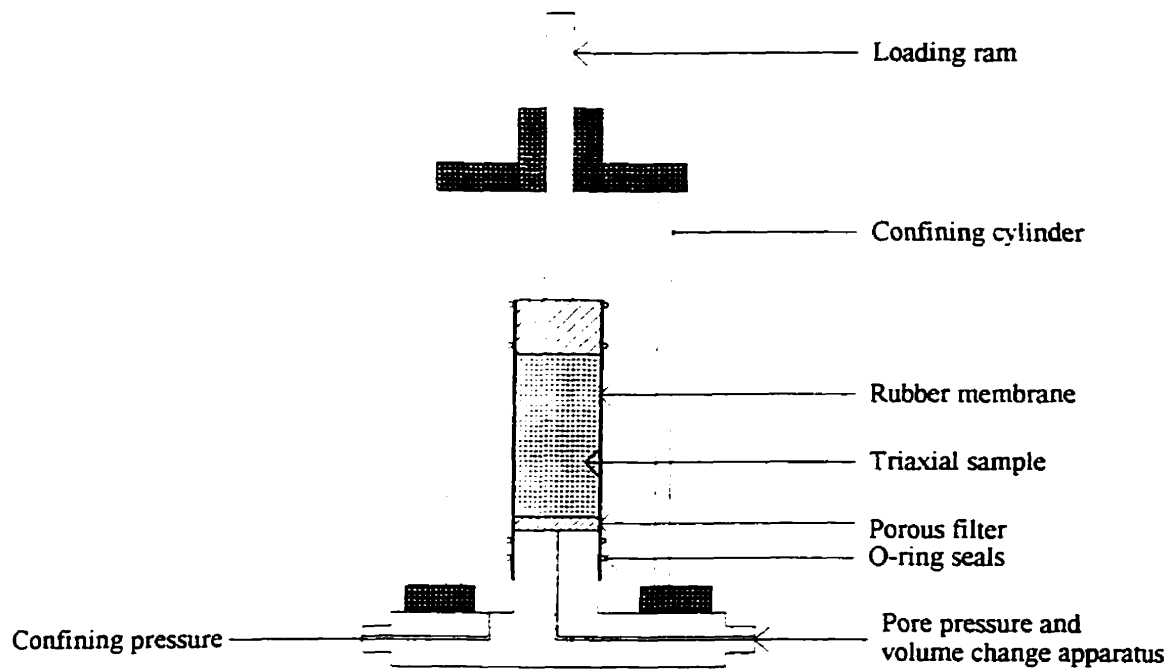


Figure 4.7. Triaxial test apparatus

4.8.2. Preparation of triaxial sample Samples were prepared using a 102 mm inner diameter mold. The mold was lined inside with a cylindrical rubber membrane which was used to confine the material. A constant vacuum of 10 kPa was applied between the mold and the membrane during filling so that the rubber membrane formed a smooth surface by adhering to the mold. In the absence of any existing guidelines (Tripodi *et al.* 1995) and to ensure consistency in all the samples, a filling procedure was adopted. The procedure consisted of placing a porous circular stone at the bottom and then placing a layer of approximately 300 g of material in a conical hopper from where it dropped freely into the mold holding the sample. The material was compressed by uniformly tamping with a wooden rod and this was

repeated until the mold was full. The height to diameter ratio of the samples was kept as 2:1 in tests done to determine Cam-clay parameters. A vacuum of 10 kPa was also applied to samples through pore line during preparation in order to obtain uniform compaction. After the mold was filled, pore vacuum was increased to 20 kPa in order to get a free standing sample and simultaneously, the vacuum between the mold and the membrane was removed. After enclosing the sample in the triaxial chamber, a confining pressure of 20 kPa was applied and the pore vacuum was removed simultaneously. Confining pressure was then adjusted according to test requirements.

4.8.3. Parameters Triaxial tests were performed on ground feed to determine the constitutive parameters for the Cam-clay model. Apart from the three critical state parameters λ , k , and M , an additional parameter Γ , representing the initial condition of material, was required. All critical state parameters were determined directly from three different triaxial tests: drained compression, undrained compression, and hydrostatic compression.

In order to determine Γ , the initial void ratio e_0 of samples used in isotropic tests was determined from the initial bulk density and particle density. Parameter Γ was then determined from parameters λ , κ , and N which is the intercept of the Normal Consolidation Line (NCL) and the $\ln(p')=0$ axis (Figure 4.6.), where NCL is the loading portion of the isotropic test. The tests carried out were as follows (Linton *et al.* 1988):

1. Four conventional triaxial tests at confining pressures of 20, 40, 75, and 100 kPa. These are referred to as drained tests. Four replicates were performed at each confining pressure.

2. Four constant volume triaxial tests, each at confining pressures of 20, 40, 75, and 100 kPa.

These tests are referred to as undrained tests. Two replicates were performed at each confining pressure.

3. Four hydrostatic compression tests with a loading and three unloading-reloading cycles.

These tests are referred to as isotropic compression tests.

Since all the tests were designed for soils, particularly in saturated states, confining pressures are normally applied using a liquid medium. However, given that the ground feed was in an unsaturated state and had low moisture content when compared to saturated soils, it was more appropriate to use air as the pressurising medium, as performed by Zhang *et al.* (1987) and Tripodi *et al.* (1994). Because of the large specimen size and relatively low confining pressure (compared with soil tests), using water may create a pressure gradient along the specimen. Therefore, air is a better choice for confining medium for triaxial tests..

4.8.4. Conventional triaxial compression (CTC) test: In drained tests, the specimen was axially compressed along the longitudinal axis (Figure 4.8.). The sample tested was in the form of a cylinder, hence two of the principal stresses σ_2 and σ_3 were always equal. In the CTC stress path, the sample was subjected to an initial confining stress $\sigma_0 = \sigma_1 = \sigma_2 = \sigma_3$. Due to confining pressure, the volume of the sample decreased thereby decreasing the volume of voids. The air occupying the voids was expelled out and hence the pore pressure increased. The pore line valve was kept open for complete drainage of air so that pore pressure u_e became equal to zero. Then σ_2 and σ_3 were kept constant while σ_1 was increased by deforming the sample axially applying a constant 0.083 mm/s displacement through the moving cross head. The drainage valve was kept open to allow complete dissipation of the resulting pore pressure u_d developed due to deviatoric stress. Here σ_1 was the major principal stress and

σ_2 and σ_3 were the intermediate and minor principal stresses, respectively. In the drained test, the total stress was equal to the effective stress since the pore pressure was zero. At failure, the maximum effective principal stress was $\sigma'_1 = \sigma_3 + \Delta\sigma_f$ where $\Delta\sigma_f$ was the deviator stress at failure. The minimum effective principal stress was $\sigma'_3 = \sigma_3$.

The results from the series of drained triaxial tests were plotted on q_{peak} versus p' plot. Regression analysis was done on peak point data versus p' obtained for drained tests and slope of the regressed line was determined. Peak points referred to the points when the sample experienced the maximum stress difference for the corresponding mean effective stress applied to the material. The slope of this line, connecting the peak points was denoted by M , which is a material parameter. Parameter M is the critical state parameter as it represents the final state of sample in triaxial tests when it is possible to continue to shear the sample with no change in imposed stresses or volume of the sample.

4.8.5. Undrained test: Undrained tests for powders pose particular problems, since by definition, they are constant volume tests. For dry compressible powders, constant volume is not possible, since there are no saturated states as with soils. For undrained tests, pore line was closed and pore pressure change was monitored, while mass of sample remained constant. In the undrained test, the specimen was first consolidated by a confining pressure σ_3 and full drainage from the specimen was allowed. After complete dissipation of excess pore pressure u_e generated by confining pressure, the deviator stress $\Delta\sigma$ was increased until the failure of the specimen occurs (Figure 4.9.). During the phase of axial loading, the drainage line from the specimen was closed. Since drainage was not permitted, the pore pressure due to deviator stress, u_d , in the specimen increased which indicated that the sample was not over consolidated. Simultaneous measurements of $\Delta\sigma$ and u_d were made during the test. The peak

data point in undrained tests is used to determine the sample's undrained strength and the critical state parameter M as determined in drained tests.

4.8.6. Isotropic compression test: Hydrostatic or isotropic tests consisted of loading and unloading-reloading cycles. These cycles were achieved by varying pressure in increments (Figure 4.10.). This was carried out in the triaxial apparatus with the axial loading ram locked clear of the sample top cap. The initial void ratio of the sample was determined from the particle density and the mass and initial volume of the sample which was determined at the time of preparation of sample by weighing the quantity of material used to prepare the sample and the height and diameter of the sample. The state of stress in isotropic consolidation lies on the diagonal of the principal stress space and consequently there are no shear stresses i.e. $\sigma_1 = \sigma_2 = \sigma_3 = \sigma_c$ where σ_c is the cell pressure in the triaxial apparatus. In terms of the relative invariants, the state of stress in isotropic compression is:

$$q = q' = 0,$$

$$p = \sigma_c,$$

$$p' = \sigma_c - u$$

The stress path of a normally consolidated material on $e - \ln p'$ plot is called the isotropic normal consolidation line. When the sample was unloaded, because of its elastoplastic nature, the unloading path did not retrace the loading path and instead took a different path. However, when the material was reloaded, it retraced the unloading path up to the point where unloading was initiated. The slope of the loading path was denoted by λ and the slope of unloading-reloading path was denoted by κ . The final value of λ and κ were determined by averaging the values of λ and κ in the loading and the unloading-reloading cycles, respectively in isotropic tests.

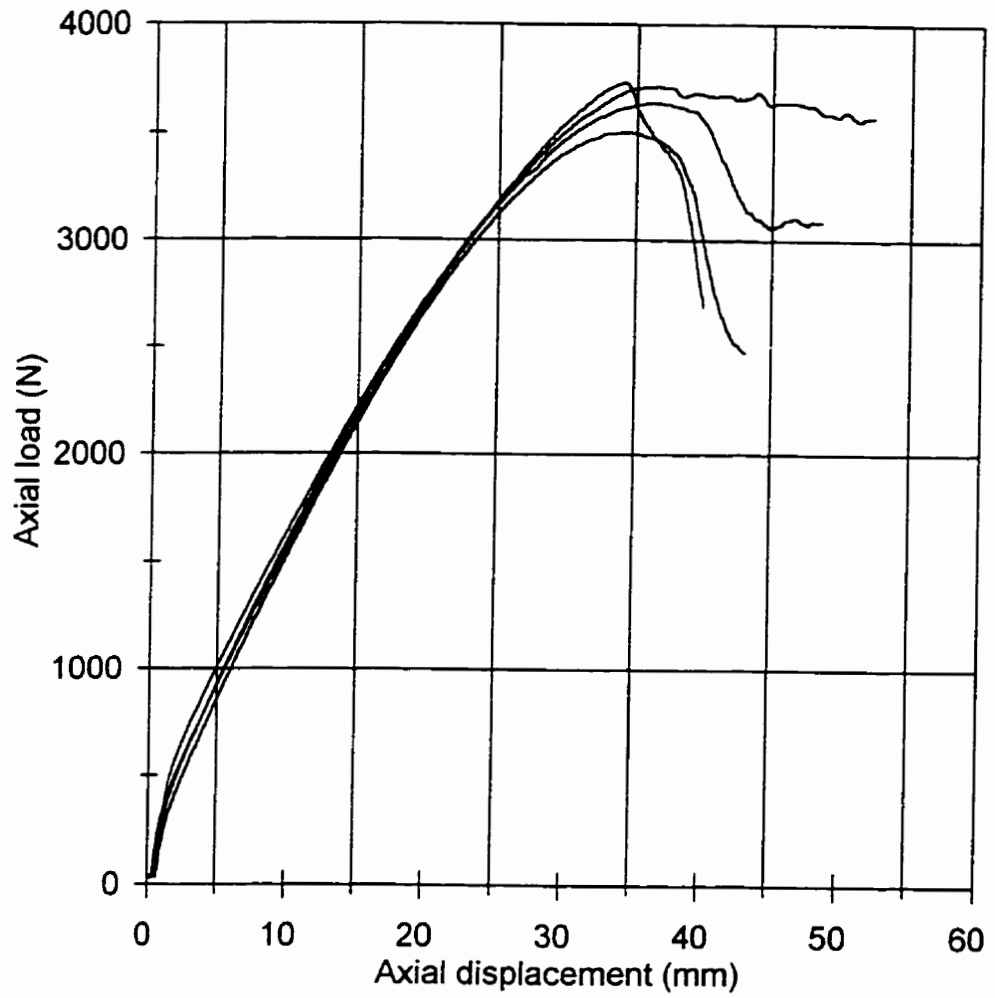


Figure 4.8. Load curve for drained tests

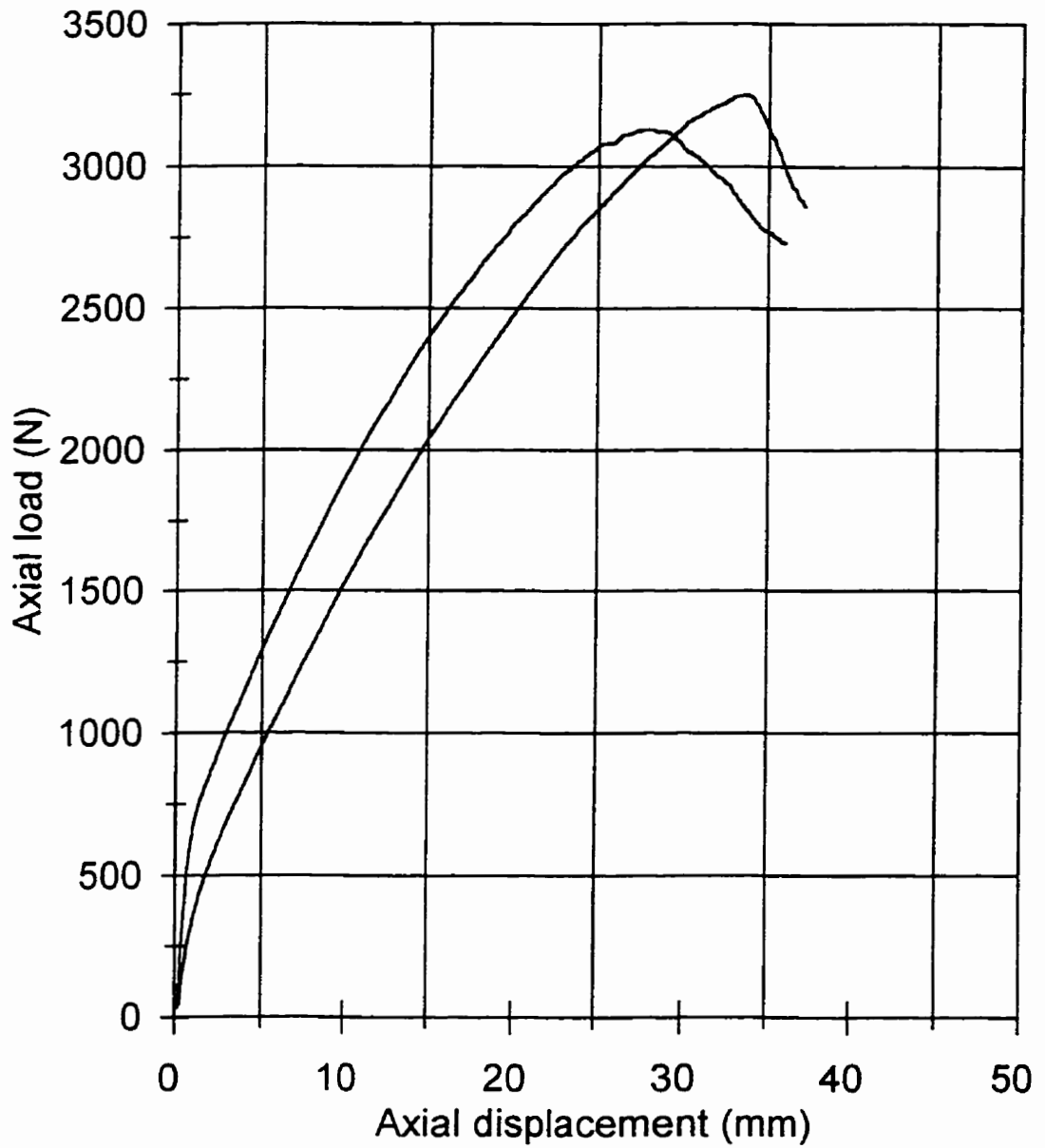


Figure 4.9. Load curve for undrained tests

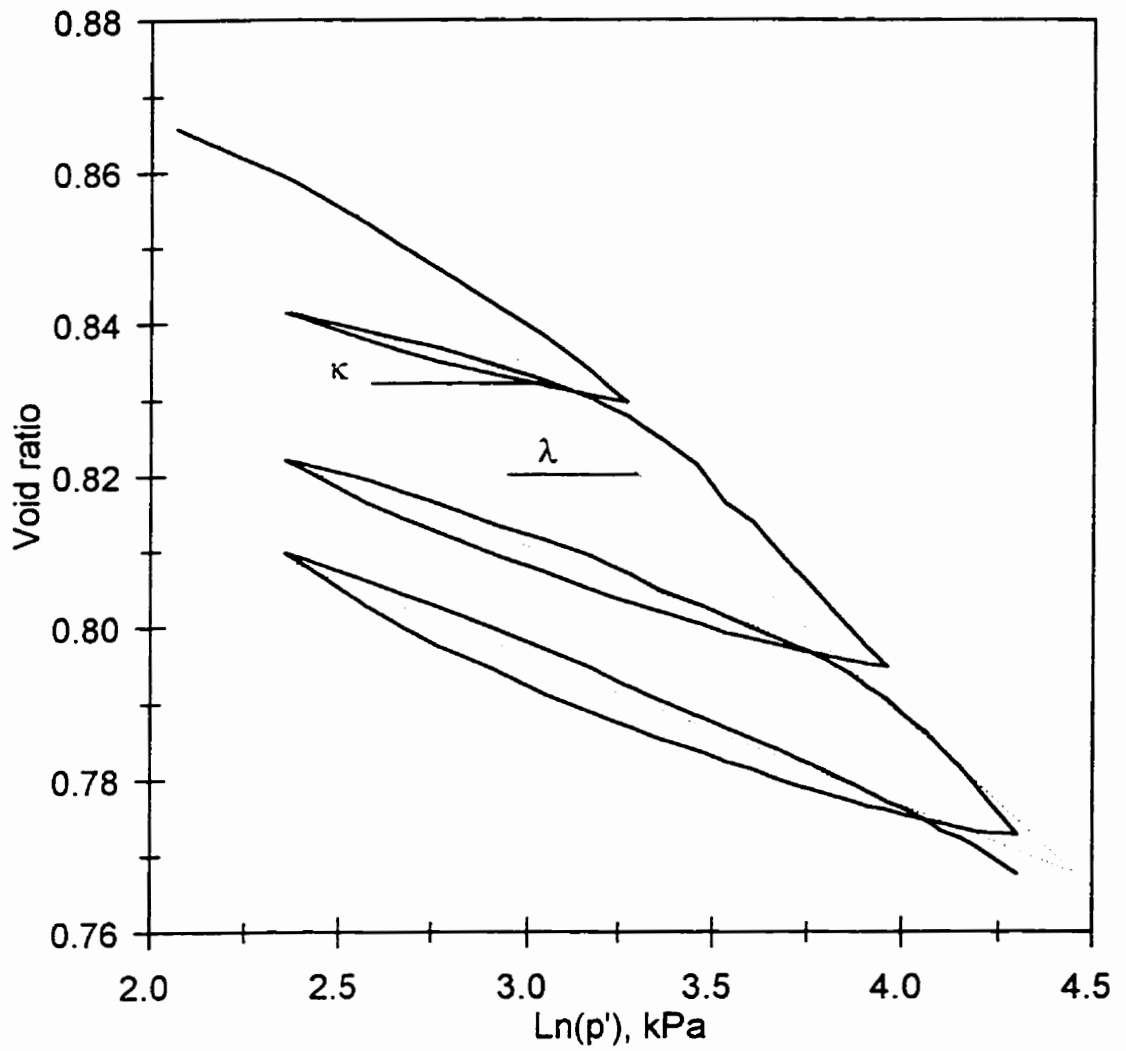


Figure 4.10. Three cycle isotropic test on ground feed

4.9. Yield Function, Cam-clay Model

The yield function for Cam-clay, as illustrated in Figure 4.11., can be expressed in terms of stress invariants p' and q as follows (Atkinson and Bransby, 1978):

$$F = \frac{q}{Mp'} + \ln\left(\frac{p'}{p'_x}\right) - 1 \quad (4.3)$$

where:

p'_x = the peak mean effective stress and is the value of p' at the critical state line.

The peak mean effective stress, p'_x , is related to the pre-consolidation pressure, p'_c , by:

$$\begin{aligned} \ln p'_x &= \ln p'_c - 1 \\ p'_x &= p'_c / 2.71828 \end{aligned} \quad (4.4)$$

The stress invariants p' and q are alternative forms of the first stress invariant, I_1' , and the second deviatoric stress invariant, J_2 , respectively.

$$p' = \frac{I_1'}{3} \quad (4.5)$$

and,

$$q = \sqrt{3J_2} \quad (4.6)$$

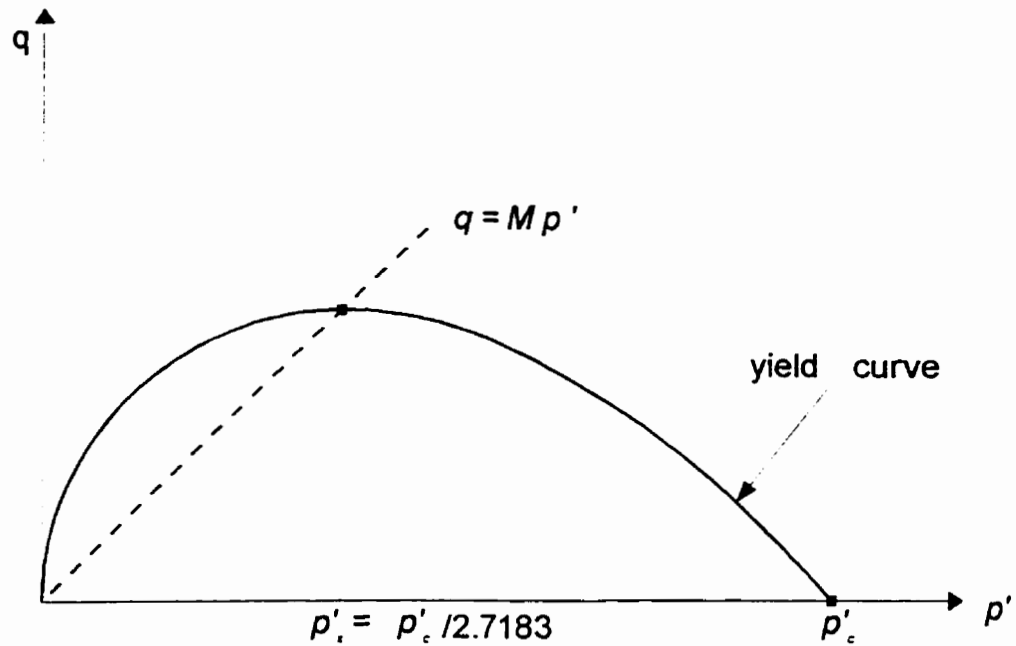


Figure 4.11. Yield curve for the Cam-clay model

By definition, the first stress invariant, I_1' , can be expressed in terms of effective stresses as

$$I_1' = \frac{1}{3}(\sigma'_x + \sigma'_y + \sigma'_z) \quad (4.7)$$

and the second deviatoric stress invariant, J_2 , can be written as

$$J_2 = \frac{1}{6}[(\sigma_x - \sigma_y)^2 + (\sigma_y - \sigma_z)^2 + (\sigma_z - \sigma_x)^2] + \tau_{xy}^2 \quad (4.8)$$

The second deviatoric stress invariant, J_2 , is the same for either total or effective stresses.

Equations for the overconsolidation line and the critical state line can be used to calculate the

mean peak stress, p'_x . As illustrated in the Figure 4.12., the specific volume at critical state,

v_x , for a particular overconsolidation line can be written as,

$$v_x = v + \kappa \ln p' - \kappa \ln p'_x \quad (4.9)$$

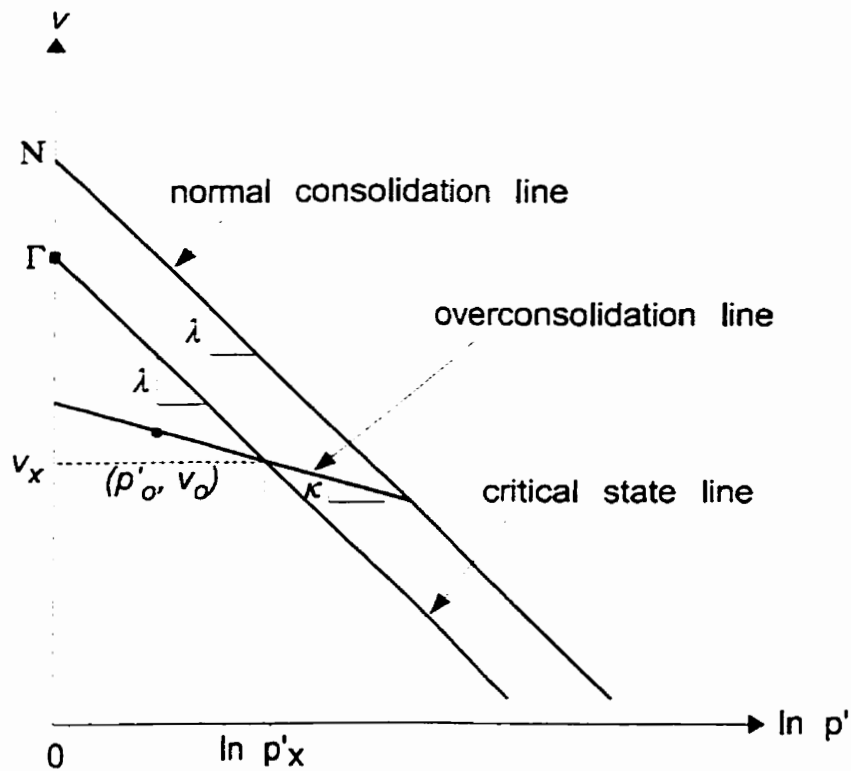


Figure 4.12. Definition of Soil Parameters for Cam-clay Model

From the critical state line, the same specific volume, v_x , can also be calculated using:

$$v_x = \Gamma - \lambda \ln p'_x \quad (4.10)$$

Eliminating the specific volume, v_x , from these two equations gives the following expression

for the mean peak stress, p'_x .

$$p'_x = \exp\left(\frac{\Gamma - v - \kappa \ln p'}{\lambda - \kappa}\right) \quad (4.11)$$

4.10. Constitutive Equations in Matrix Format

In SIGMA/W, soil plasticity is formulated using the theory of incremental plasticity. Once an elastic-plastic material begins to yield, an incremental strain can be divided into elastic and plastic components. The relationship between the plastic component of incremental stress and incremental strain is defined using a plasticity matrix. The plastic matrix $[C_p]$ is developed using the yield function, F . In the following discussion, subscripts e and p denote elastic and plastic state, respectively.

As shown in Equation 4.11, the mean peak stress, p'_x , is a function of the specific volume, V . If it is postulated that a change in the mean peak stress, p'_x , can only be caused by a plastic deformation in the specific volume, an incremental change in the yield function, F , is given by:

$$dF = \left\langle \frac{\partial F}{\partial \sigma'} \right\rangle \{d\sigma'\} + \frac{\partial F}{\partial p'_x} \frac{\partial p'_x}{\partial v^p} dv^p = 0 \quad (4.12)$$

From a given set of normal and overconsolidation curves, an incremental plastic change in specific volume can be expressed as:

$$dv^p = dv - dv^e = -(\lambda - \kappa) \frac{dp'}{p'} \quad (4.13)$$

The incremental plastic specific volume is related to the incremental plastic volumetric strain through:

$$dv^p = v_0 d\varepsilon_v^p \quad (4.14)$$

where:

dv^p = incremental plastic specific volume

v_0 = initial specific volume

$d\varepsilon_v^p$ = incremental plastic volumetric strain

Since only elastic strains can cause stresses to change, the incremental effective stress constitutive relationship can be written as follows.

$$\begin{aligned} \{d\sigma'\} &= [C'_e] (\{d\varepsilon\} - \{d\varepsilon_p\}) \\ &= [C'_e] \left(\{d\varepsilon\} - \lambda_p \left\{ \frac{\partial G}{\partial \sigma'} \right\} \right) \end{aligned} \quad (4.15)$$

where:

$[C'_e]$ = effective elastic matrix

G = plastic potential function

λ_p = (plastic) scaling factor.

Substituting $\{d\sigma'\}$, from Equation 4.15, into Equation 4.12 gives:

$$\left\langle \frac{\partial F}{\partial \sigma'} \right\rangle [C'_c] \{d\varepsilon\} = \left\langle \frac{\partial F}{\partial \sigma'} \right\rangle [C'_c] \lambda_p \left\{ \frac{\partial G}{\partial \sigma} \right\} - \frac{\partial F}{\partial p'_x} \frac{\partial p'_x}{\partial v^p} dv^p \quad (4.16)$$

The plastic increment in specific volume, dv^p , can be calculated from the original specific volume and the incremental plastic volumetric strain, $d\varepsilon_v^p$.

$$dv^p = v_o d\varepsilon_v^p = v_o \lambda_p \left(\frac{\partial G}{\partial \sigma'_x} + \frac{\partial G}{\partial \sigma'_y} + \frac{\partial G}{\partial \sigma'_z} \right) \quad (4.17)$$

Applying the associated flow rule (i.e. the plastic potential function, G , is the same as the yield function, F), the following expression is obtained for the plastic scaling factor, λ_p .

$$\lambda_p = \frac{\left\langle \frac{\partial F}{\partial \sigma'} \right\rangle [C'_c]}{\left\langle \frac{\partial F}{\partial \sigma'} \right\rangle [C'_c] \left\{ \frac{\partial F}{\partial \sigma'} \right\} - \frac{\partial F}{\partial p'_x} \frac{\partial p'_x}{\partial v^p} v_o F_m} \{d\varepsilon\} \quad (4.18)$$

where:

$$F_m = \frac{\partial G}{\partial \sigma'_x} + \frac{\partial G}{\partial \sigma'_y} + \frac{\partial G}{\partial \sigma'_z} = \frac{\partial F}{\partial \sigma'_x} + \frac{\partial F}{\partial \sigma'_y} + \frac{\partial F}{\partial \sigma'_z} \quad (4.19)$$

A relationship between incremental stress and incremental strain is obtained by substituting λ_p into Equation 4.15.

$$\{d\sigma'\} = ([C'_e] - [C'_p])\{d\epsilon\} \quad (4.20)$$

where:

$$[C'_p] = \frac{[C'_e] \left\{ \frac{\partial F}{\partial \sigma'} \right\} \left\langle \frac{\partial F}{\partial \sigma'} \right\rangle [C'_e]}{\left\langle \frac{\partial F}{\partial \sigma'} \right\rangle [C'_e] \left\{ \frac{\partial F}{\partial \sigma'} \right\} - \frac{\partial F}{\partial p'_x} \frac{\partial p'_x}{\partial v^p} v_o F_m} \quad (4.21)$$

and is termed the plasticity matrix.

4.11. Modified Cam-clay Model

In this study, constitutive equations based on modified Cam-clay model were used to develop the finite element models of storage bins. Modified Cam-clay model addresses two particular dissatisfactions with the original Cam-clay model: the point on the yield locus and the predicted value of K_0 (the coefficient of earth pressure at rest). The shear strains predicted by Cam-clay model were high at low stress ratios and it predicted a value of $K_0 = 1$ for a normally consolidated soil where measured values are normally in the range of 0.5 to 0.7. In order to account for the discrepancies, the assumption for the dissipated work was changed and hence the flow rule got modified. This resulted the yield function of modified Cam-clay model to be of a shape of an ellipse instead of hyperbolic. The yield curve for the modified Cam-clay model is illustrated in Figure 4.13.

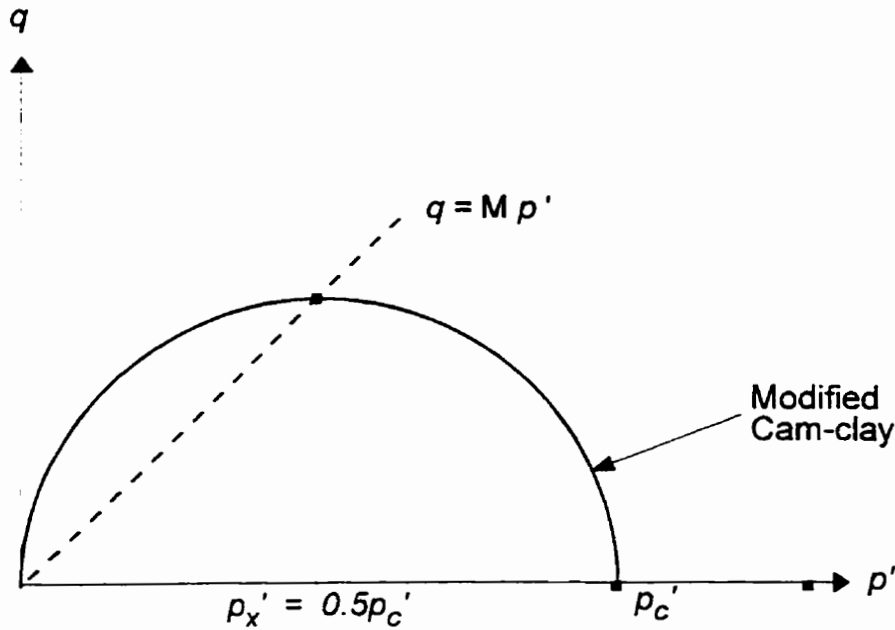


Figure 4.13. Yield function for modified Cam-clay

The yield function for the Modified Cam-clay model is given by the following equation (Britto and Gunn, 1987):

$$q^2 = M^2 p' p'_c - M^2 p'^2 \quad (4.22)$$

where:

p'_c = preconsolidation pressure

The parameters used to define the Modified Cam-clay model are M , Γ , κ , and ν . These parameters are the same as those used for the Cam-clay model as discussed in the previous section.

Similar to the Cam-clay model, SIGMA/W uses the mean peak stress, p'_x , to determine the size of the yield locus for the Modified Cam-clay model. The mean peak stress, p'_x , is the pressure when a soil reaches its critical state. At the critical state, the shear stress, q , is given by the following equation.

$$q = Mp'_x \quad (4.23)$$

Substituting this value of shear stress, q , into Equation 4.22 gives,

$$p'_c = 2p'_x \quad (4.24)$$

Therefore, the yield function, F , for the Modified Cam-clay model can be written as:

$$F = \frac{q^2}{p'} + M^2 p' - 2M^2 p'_x \quad (4.25)$$

The derivatives of the yield function, F , with respect to stress invariants p' and q are respectively:

$$\frac{\partial F}{\partial p'} = M^2 - \frac{q^2}{p'^2} \quad (4.26)$$

$$\frac{\partial F}{\partial q} = \frac{2q}{p'} \quad (4.27)$$

The terms $\left\{ \frac{\partial p'}{\partial \sigma} \right\}$, $\left\{ \frac{\partial q}{\partial \sigma} \right\}$, $[C_e]$ and $\frac{\partial p'_x}{\partial v^p}$ are the same as those used for the Cam-clay model.

The remaining variables in the plastic matrix, $[C_p]$, for modified Cam-clay are:

$$F_m = M^2 - \frac{q^2}{p'^2} \quad (4.28)$$

$$\frac{\partial F}{\partial p'_x} = -2M^2 \quad (4.29)$$

Except for the differences noted in the following discussion, the procedure to define the initial condition of the Modified Cam-clay model is the same as that for the Cam-clay model described in the previous section. In SIGMA/W if a preconsolidation pressure is not defined by the user, it is calculated using:

$$p'_c = \frac{1}{M^2 p'_{\max}} (q_{\max}^2 + M^2 p'^2_{\max}) \quad (4.30)$$

where q_{\max} and p'_{\max} are the maximum deviator stress and peak mean effective stress experienced by the material in the past.

Another change in modified Cam-clay model is that the vertical distance between the isotropic NCL and CSL becomes $(\lambda - \kappa) \ln 2$ instead of $(\lambda - \kappa)$. The interception of the isotropic normal consolidation line with the vertical axis (i.e. $\ln p' = 0$), N is given by (Britto and Gunn 1987):

$$N = \Gamma + (\lambda - \kappa) \ln 2 \quad (4.31)$$

4.12. Model Parameters

The parameters used in finite element models in SIGMA/W are listed in Table 4.6.

Table 4.6. List of parameters used in finite element model in SIGMA/W

PARAMETERS*	VALUE
Over consolidation ratio	1
Poisson's ratio	0.35
λ	0.045
κ	0.016
M	1.977
Γ	2.003
Bulk density (kg/m ³)	638.9
Convergence criteria (displacement norm)	1%
Maximum. number of iterations	25
Number of fill	10

*Details discussed in the Results and Discussion section

Over consolidation ratio, which is defined as the ratio of maximum vertical stresses in the past to that at the present was taken as 1 since it is assumed that all the stresses in the material are relieved during the process of filling the bin when it is loosely dropped into the storage bin. The parameters λ , κ , M, Γ , and Poisson's Ratio were determined by triaxial tests. Bulk density of ground feed was determined using a pycnometer. Other parameters were decided by making careful observations in trial simulations to get accurate results and optimum performance of the program.

4.13. Model Verification

The finite element model was verified in two steps for its ability to predict the stress-strain behavior of ground feed. First step was to compare the experimental results of triaxial tests with the results of the simulation of triaxial test on SIGMA/W (Appendix D). The second step was to compare the vertical and horizontal stresses on the bin wall determined by SIGMA/W with those calculated using Janssen's equations. The triaxial tests were simulated at confining pressures of 40, 75, and 100 kPa and the parameters M and λ were determined. Parameter M was determined from the slope of the line obtained by joining the peak deviatoric stress points in q - p' plot (Appendix D). Parameter λ was determined by plotting the critical state line in the e - $\ln(p')$ space and determining the slope of the line (Appendix D). The intercept of the critical state line with the vertical axis at $\ln(p')=0$ gave the value of parameter Γ . Parameter κ was determined by simulating unloading-reloading cycle in an isotropic test and determining the slope of loading-unloading lines (Appendix D). The parameters were then compared to the values determined by actual triaxial tests.

The triaxial test was simulated by first establishing the initial stress conditions due to confining pressure and then applying the displacement. The unloading-reloading was simulated by specifying the state of triaxial sample due to confining pressure as the initial condition and at first reducing the confining pressure and then increasing the confining pressure. The values of parameters obtained by simulation of triaxial tests are listed in Table 4.7. and compared to the values obtained by experiments.

Table 4.7. Comparison of modified Cam-clay parameters as determined from simulation of triaxial tests and actual triaxial tests.

Parameter	Value determined by experiments	Value determined from simulations
M	1.977	1.787
λ	0.045	0.057
κ	0.016	0.016
Γ	2.003	2.024

The vertical and horizontal stresses on the bin wall were calculated using the Janssen's equations (Shamlou 1988). The results of calculations are mentioned in Appendix D. It may however be noted that these equations were developed for granular materials assuming that the ratio of horizontal to vertical pressure is constant everywhere in the bin and is independent of the magnitude of prevailing stresses. The bin-loads obtained by calculations were compared to the results of simulation on bin with no insert condition for *Half bin*.

5. RESULTS AND DISCUSSION

5.1. Finite Element Model

5.1.1 Property parameters of ground feed The parameters for the modified Cam-clay model were determined by drained, undrained, and isotropic triaxial tests. The load-displacement curves for all the drained and undrained tests and $e-\ln(p')$ curves for isotropic consolidation tests are plotted in Appendix B. The high value of r^2 (>0.99) indicates consistency in results for parameter M . The coefficients of variation for λ and κ was high (Table 5.1.). This could be attributed to the convex nature of the loading curve and hysteresis in the unloading-reloading cycle. The loading curve was convex downward as reported by Tripodi *et al.* (1995). Parameter Γ , which was determined by finding intercept of loading curve with vertical axis at $\ln(p') = 0$ had least coefficient of variation of all the parameters. Over consolidation ratio (OCR), which is the ratio of maximum vertical stress in the past to that at the present, was taken as 1, as it was assumed that the material was not subjected to any higher stress before or at the time it was filled in the storage bin. Poisson's ratio of 0.35 was determined for ground feed from the triaxial tests by measuring the axial deformation required to create a lateral deformation of 10 mm (Appendix C). The value of 10 mm was chosen as it occurred within the linear part of the loading curve for drained tests and provided sufficient magnitude to measure the deformations with least possible error. The height to diameter ratio for these samples was kept as 1:1. Hence Poisson's ratio was expressed as the ratio of lateral deformation to axial deformation. Lateral deformations were measured using a calliper whereas axial deformations were directly recorded by the data acquisition system. Moisture content and particle density were determined for ground feed before starting the

triaxial tests (Appendix C). The moisture content was 9.48% (wet basis) and particle density was 1608.7 kg/m³. The in-bin bulk density of ground feed was 638.9 kg/m³. Particle density was used to determine the void ratio in triaxial test samples as the volume of sample and weight of material was known for each sample.

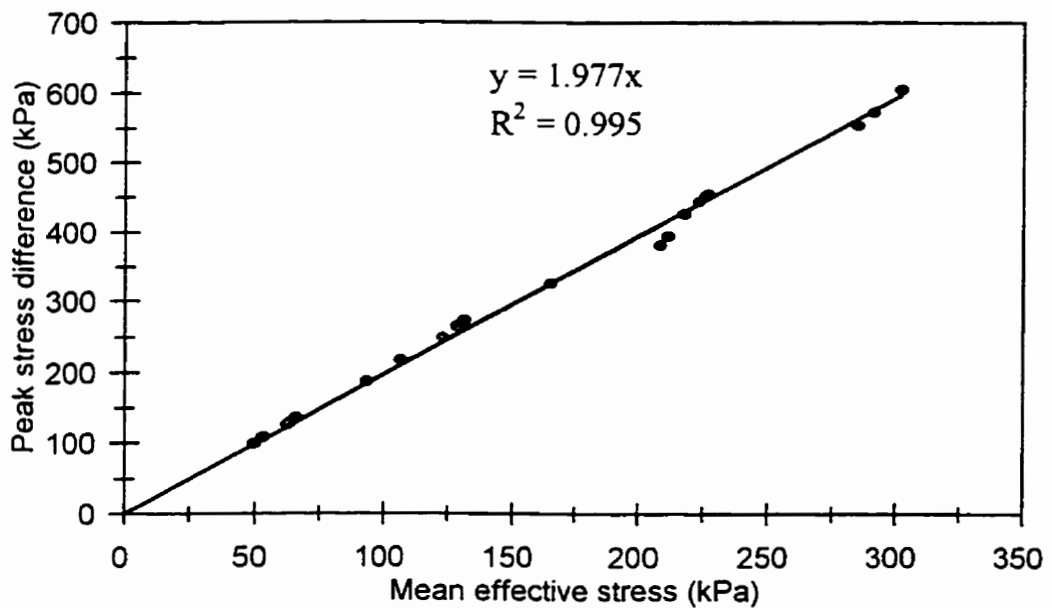


Figure 5.1. Critical state line determined for ground feed from regression analysis on drained and undrained test data

Table 5.1. Analysis of triaxial test data to determine parameters λ , κ , and Γ

Isotropic Test	Slope			Intercept
	Loading (λ)	Unloading (κ)	Reloading (κ)	Γ
Test 1	0.031253	0.012510	0.013014	1.964754
	0.048976	0.016136	0.018750	2.021780
	0.054120	0.018273	0.021564	2.039053
Test 2	0.031710	0.017395	0.019771	1.968127
	0.044902	0.013216	0.018007	2.004463
	0.058535	0.011678	0.017880	2.054253
Test 3	0.030195	0.012685	0.013652	1.929846
	0.049285	0.016408	0.017983	1.990610
	0.053003	0.017904	0.017864	2.001122
Test 4	0.033729	0.014529	0.014186	1.973164
	0.050418	0.019795	0.019536	2.027781
	0.059816	0.021816	0.018909	2.063621
Mean		λ	κ	Γ
		0.045495	0.016811	2.003215
Standard Deviation		0.010497	0.002898	0.038349
Coefficient of variance (%)		23.07	17.23	1.91

5.1.2. Model verification The finite element model was verified in two steps. The parameters for modified Cam-clay model determined by the simulation (Table 4.7.) are close to the values determined by the triaxial experiments except for the parameter λ which is 20% higher. It may however be noted that the value of parameter $\lambda = 0.057$, as determined from simulations is close to the slope of third loading cycle in triaxial tests (Table 5.1.). Parameter M as determined from simulations is higher by 10% where as parameters κ and Γ are within 1% of the values determined by triaxial experiments.

The stresses determined by Janssen's equations (Appendix D) predict the horizontal and vertical wall stresses for initial filling (static pressures) and dynamic discharge pressures. For stresses during discharge, wall pressure in the hopper could not be determined as the equations failed for hopper angle = 60° and gave the ratio of total wall pressure to vertical pressure as less than one. The vertical bin loads for the main bin after filling are under-predicted by Janssen's equations whereas horizontal stresses calculated by Janssen's equations are close to the stresses determined by SIGMA/W. The horizontal and vertical stresses calculated for the bin during discharge by Janssen's equations are close to calculations by SIGMA/W (Appendix D).

5.1.3. Stress contour patterns in model bins The stress contours in the model bins formed a pattern which was common to all the bins for stresses after filling and stresses after draw down initiation.

For bins without the insert, the contours for y-effective stresses and x-effective stresses after filling were horizontal and increased towards the bottom of the bin. High stresses were observed for y-effective stresses at the transition of bin and hopper whereas for x-effective stresses at the transition of bin and hopper, a region of low stresses was observed. After the draw-down was initiated, the y-effective stresses at the bin-hopper transition further increased and x-effective stresses further decreased. The y-effective stresses at the hopper outlet reduced to zero and increased upwards.

For bins with the insert, the contours for y-effective stresses and x-effective stresses after filling completely changed as compared to the no-insert conditions. High stresses were observed for y-effective stresses at the transition of bin and hopper and along the side of the insert. Vertical stresses just below the insert reduced to zero and the stress contours appeared

to 'fan-out' from the edge of the insert towards the bottom and side of the hopper. For x-effective stresses a region of low stresses was observed at the transition of bin and hopper, however along the side of the insert, high stresses were observed. X-effective stresses also 'fanned-out' from the edge of the insert towards the bottom and centre-line of the hopper. After the draw-down was initiated, the y-effective stresses at the bin-hopper transition further increased and x-effective stresses further decreased. The x and y-effective stresses along the side of the insert further increased. The y-effective stresses at the hopper outlet reduced to zero and increased upwards and the spread of the 'fan' at the edge of the insert further increased thereby increasing area under reduced stresses.

5.2. Stress Distribution in *Half Bin*

The 'contour' option of SIGMA/W was used to view the contours for stress distribution in ground feed in model bins. Contours of y-effective stress and x-effective stress were plotted for filling and draw-down initiation conditions. The primary regions of interest were the area above the hopper outlet but below the insert and the area adjacent to the insert. Stresses in material in the bin above the insert level remained unaffected in all the cases and hence were not included in analysis. The numbers marked on the contours show the stress contour value in kPa. Variation in stresses was compared 'with respect to previous condition', which for example in Table 5.2. means that in column 'Stresses after filling', x-effective stress at 130 mm decreases w.r.t. 175 mm, and x-effective stress at 85 mm increases w.r.t. 130 mm condition. The increase or decrease in stresses as mentioned in table 5.2. was determined by visual inspection by comparing the area under the stress contours for different simulations.

5.2.1. Stress distribution after filling It can be seen from Table 5.2. and Figure 5.2.(a) that

placing an insert reduces stresses in both the vertical and horizontal directions, however placing an insert too high (450 mm and 350 mm) has little or no effect on stresses at the outlet. As the insert is lowered, vertical and horizontal stresses keep reducing. When the insert is placed too close (insert location 130 mm and 85 mm) to the outlet, horizontal stresses increase between the insert and hopper wall.

5.2.2. Stress distribution after draw-down initiation The variation in stress pattern after draw-down initiation remain the same as that after filling (Table 5.2.). In all cases, vertical stresses at the hopper outlet become zero or tensile (since the first contour starts at 0 and has white shade, the region having zero stresses or tensile stresses have the same contour and contour shade). It may be noted that as the insert is lowered, horizontal stresses in the region adjacent to the insert increase (Figure 5.2.(b)). This is in agreement to the observations made by early researchers that when the gap between the hopper wall and insert is reduced beyond a certain limit, chances of flow stoppage due to arch formation at the insert level increase.

The pattern of stress distribution and its variation with respect to change in location of insert indicates that maximum flowability would be obtained when the insert is placed at 175 mm ($R/W = 0.18$) from insert bottom because the consolidation stresses are least at the hopper outlet and hence the chances of arch formation are the least. Hao (1998) reported that flow properties increasingly improved as the insert was raised from 85 ($R/W = 0.42$) to 260 mm ($R/W = 0.12$). The flow properties did not improve further when the insert was mounted in the range of 260 to 450 mm ($R/W = 0.11$). Results of the simulation do show the trend of increase and decrease of flowability as observed by Hao (1998). The difference in the insert location for maximum flowability as determined by the simulations and as determined by Hao (1998) can be attributed to different conditions at the time of experiment, such as frictional

characteristics of the *Lab bin*, in comparison to parameters used in simulations of *Half bin*.

Table 5.2. Effect of insert location on stresses near the hopper outlet for *Half bin*

Insert Location from hopper bottom (R/W)	Stresses after filling		Stresses after draw-down initiation	
	Y-effective	X-effective	Y-effective	X-effective
	stress	stress	stress	stress
No insert				
450 mm (0.11)	↓	↓	↓	↓
350 mm (0.11)	↓	↔	↓	↔
260 mm (0.12)	↓	↓	↓	↓
175 mm (0.18)	↓	↓	↓	↓
130 mm (0.25)	↓	↓	↓	↑
85 mm (0.42)	↓	↑	↓	↑

↑ increase in stresses w.r.t. pervious condition

↓ decrease in stresses w.r.t. pervious condition

↔ stresses remain unchanged w.r.t. pervious condition

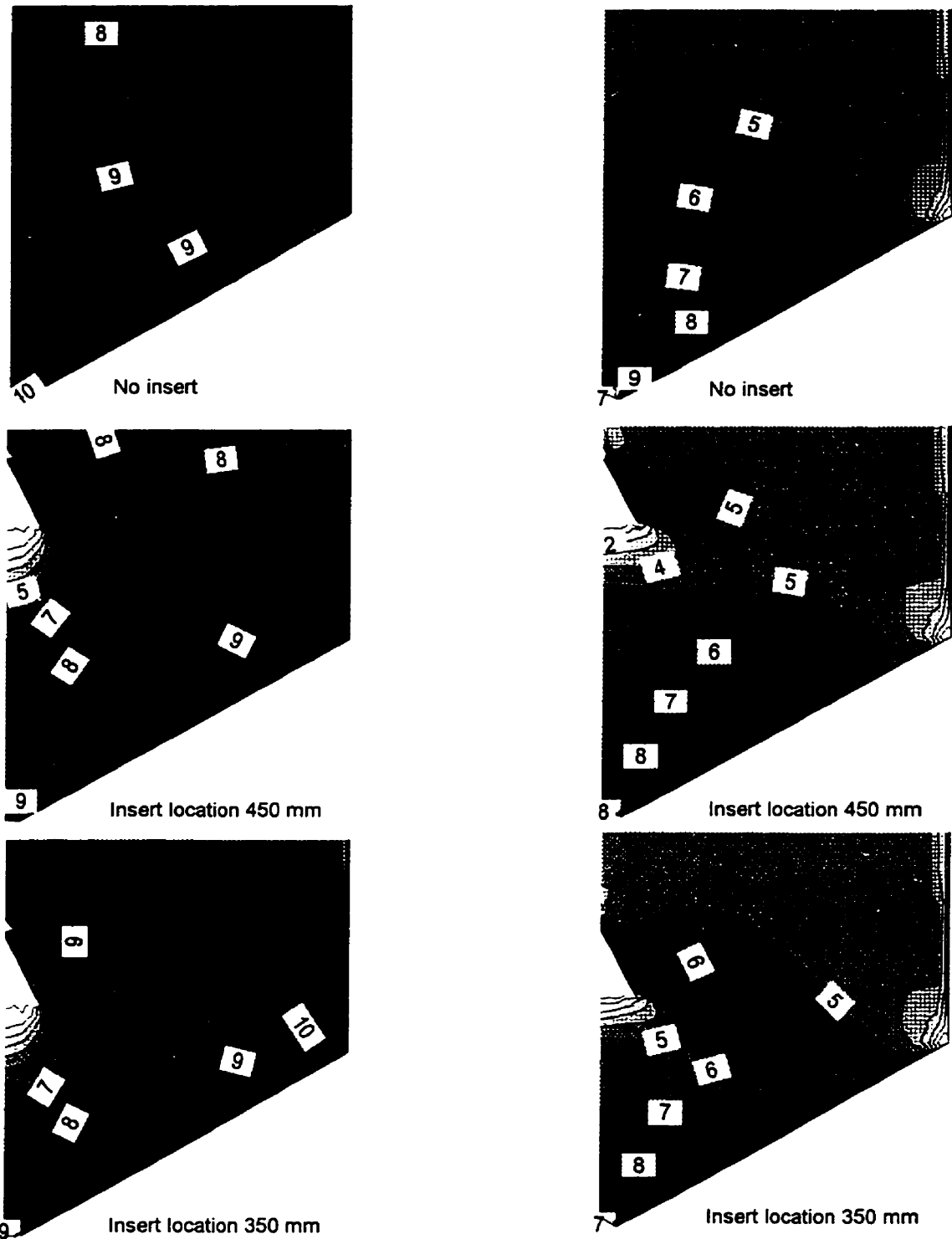


Figure 5.2.(a) Effect of insert location on stress distribution in *half bin* after filling but prior to draw down initiation. Y-total stress (left column) and x-total stress (right column)

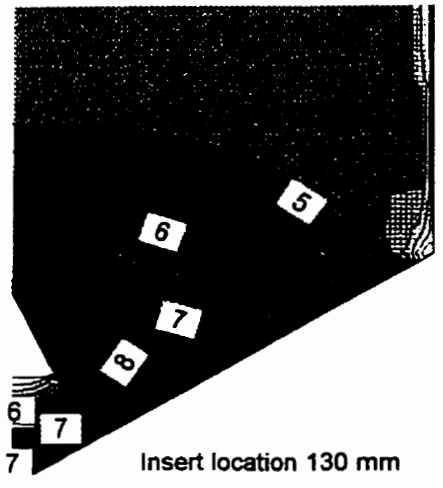
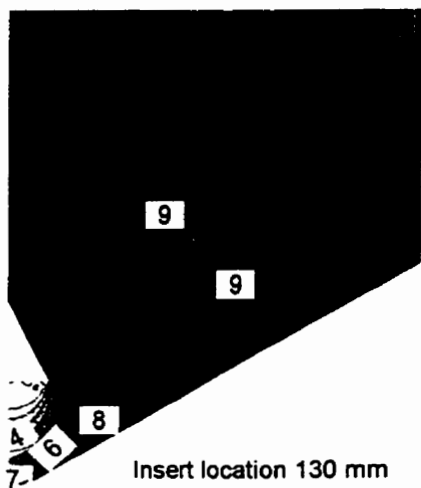
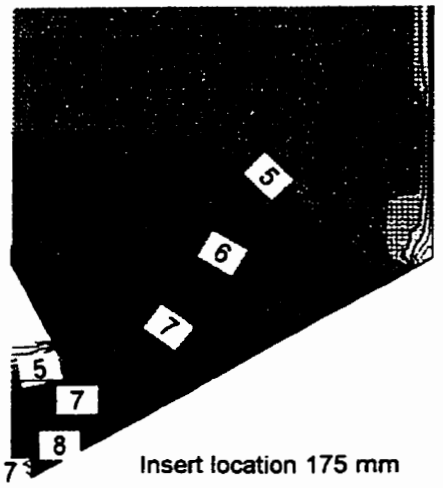
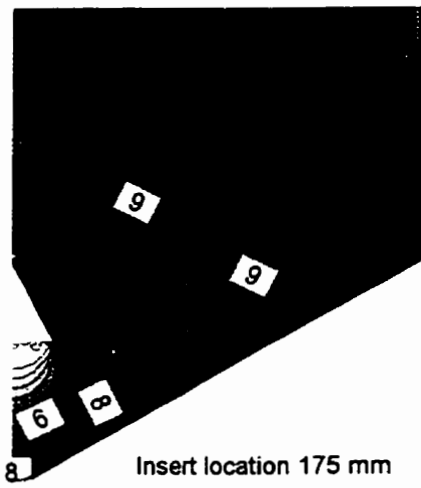
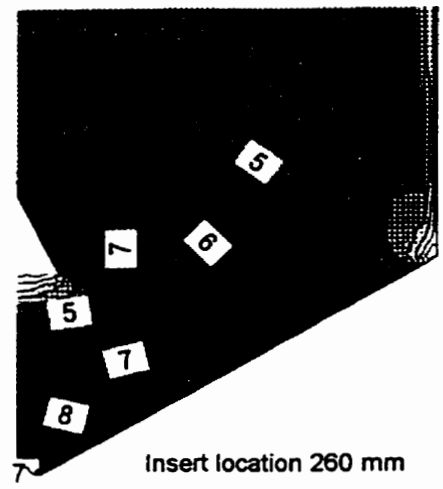
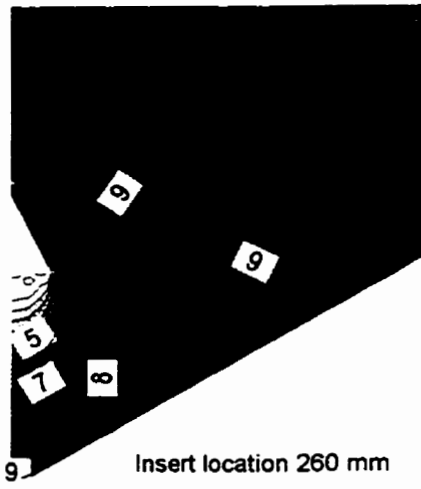


Figure 5.2.(a)

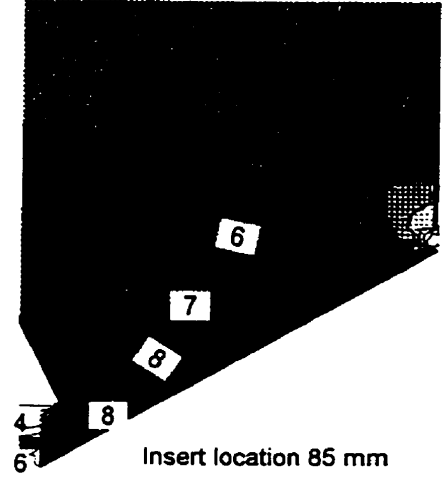
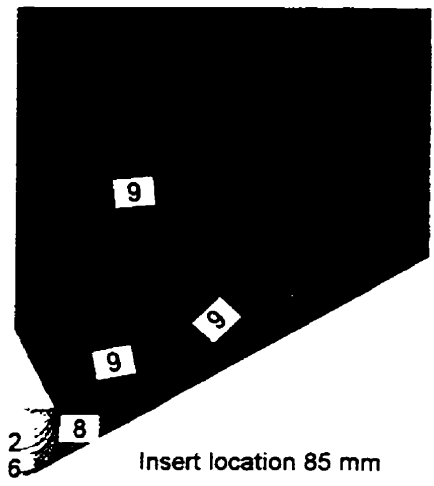


Figure 5.2.(a)

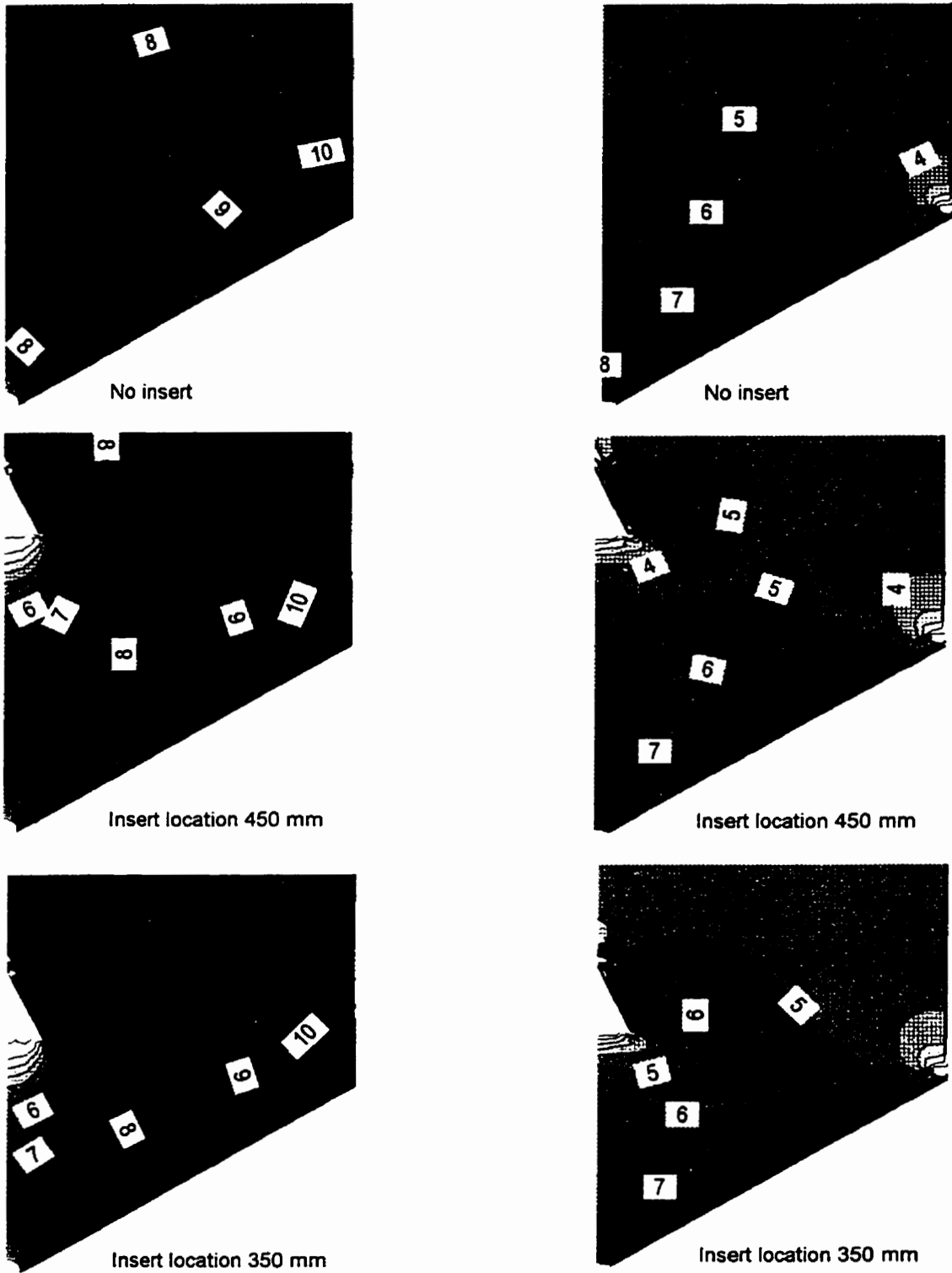


Figure 5.2.(b) Effect of insert location on stress distribution in *half bin* after draw down initiation. Y-total stress (left column) and x-total stress (right column)

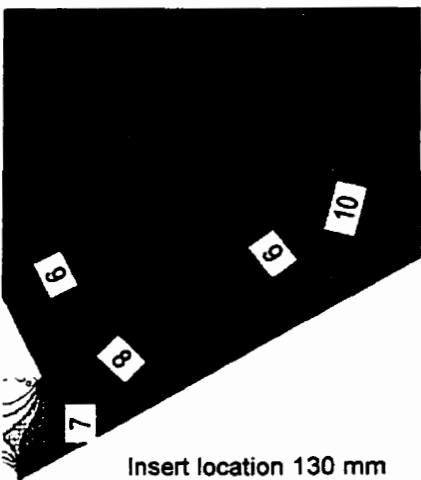
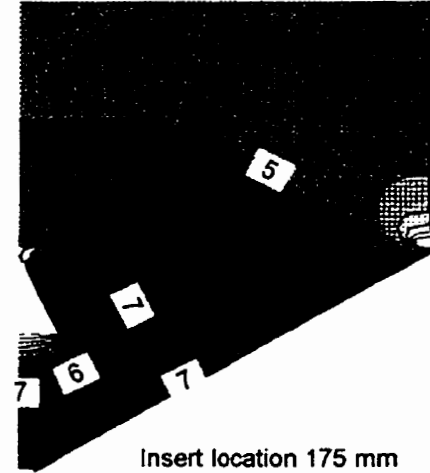
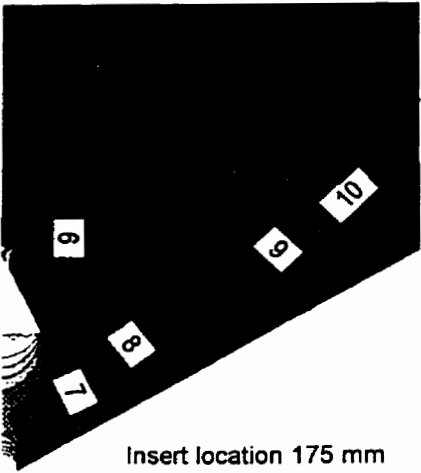
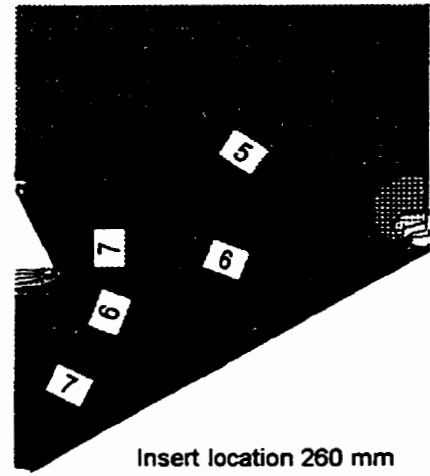
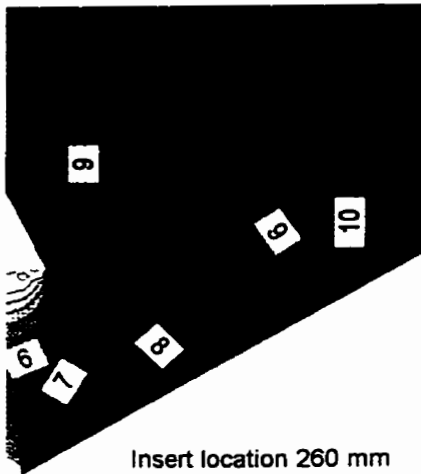


Figure 5.2.(b)

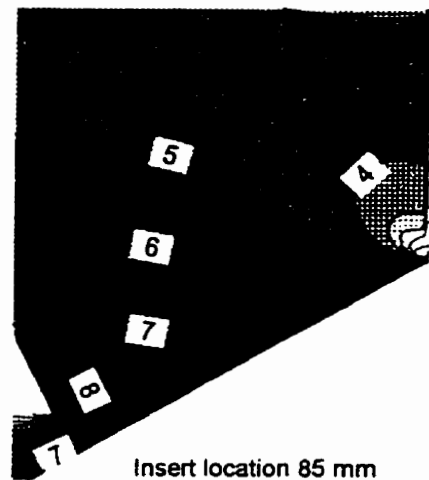
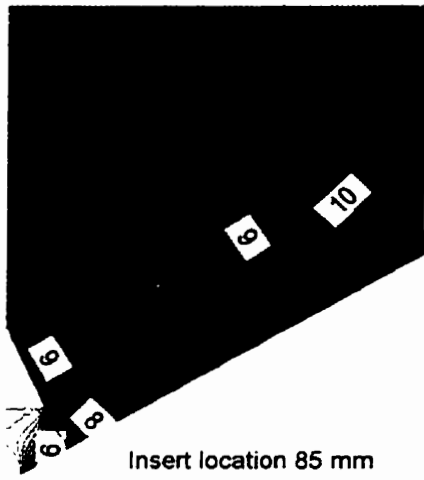


Figure 5.2.(b)

5.3. Stress Distribution in *Full Bin*

Simulations were carried out on *Full bin* in order to investigate the effect of mounting method of insert on stress distribution in ground feed. Contours were plotted and compared to stress distribution when no insert was placed in the bin.

5.3.1. Stress distribution after filling Table 5.3. and Figure 5.3.(a) show the results of contour plot for *Full bin*. Placing asymmetric hinged insert reduces both vertical and horizontal stresses. When symmetric fixed insert is placed in the bin, vertical stresses below the insert are further reduced whereas horizontal stresses remain the same. Replacing the symmetric fixed insert with the symmetric hinged insert does not produce any change in stress distribution in the simulation. It may be noted that since the model does not simulate dynamic conditions, the actual behaviour of hinged support in dynamic conditions can not be inferred.

5.3.2. Stress distribution after draw-down initiation Vertical and horizontal stresses decrease when the asymmetric hinged insert is placed in the bins compared to the no 'insert' condition. The vertical stresses decrease further when the symmetric fixed or the symmetric hinged insert is placed. It is interesting to note that despite the axial symmetry in the symmetric fixed insert and the symmetric hinged insert, the stress distribution after draw-down initiation does not remain symmetric. The model was checked for errors and simulations were repeated but the result was unaltered. This observation as of now remains unexplained and should be reinvestigated using some other finite element program for modified Cam-clay model. Hao (1998) found the rotated insert to be the most efficient of all. The inserts rotated when the normal stresses existing on the two sides of insert were unbalanced. When the insert rotated, the gap between one edge of the insert and the hopper wall increased and more material

flowed from that side.

Although the vertical stresses for the symmetric fixed insert decrease below the insert in comparison to the asymmetric hinged insert, high vertical stresses adjacent to the hopper could result in arch formation (dynamic or stable) at the insert level in the symmetric fixed insert case and thus explains better performance of rotated inserts. The ability of the insert to rotate allows it to adjust itself by rotating away from the side with high stresses and allowing a wider flow channel on that side thereby enhancing uniform flow behaviour and increased flowability.

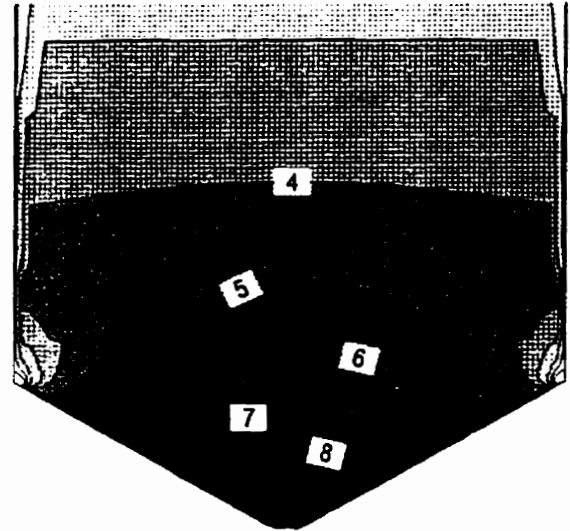
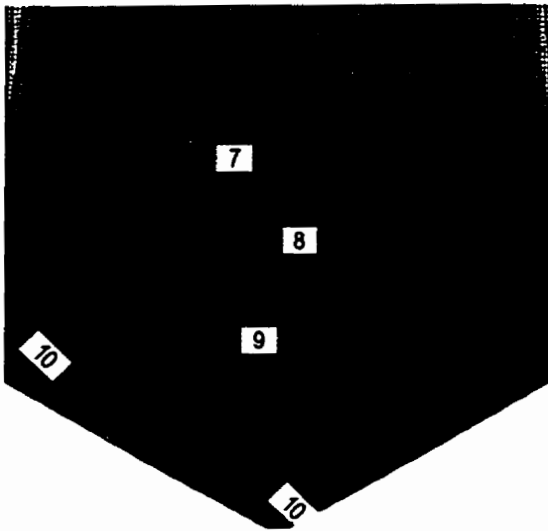
Table 5.3. Effect of insert location on stresses near the hopper outlet for *Full bin*

Mounting method of insert	Stresses after filling		Stresses after draw-down initiation	
	Y-effective	X-effective	Y-effective	X-effective
	stress	stress	stress	stress
No insert				
Asymmetric hinged	↓	↓	↓	↓
Symmetric fixed	↓	↔	↓	↓
Symmetric hinged	↔	↔	↔	↔

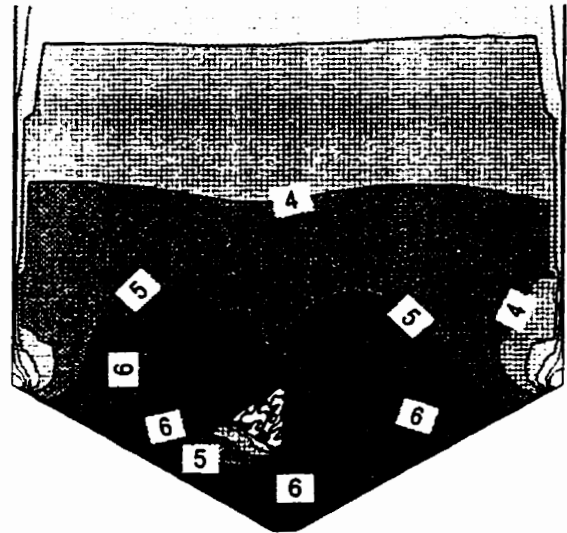
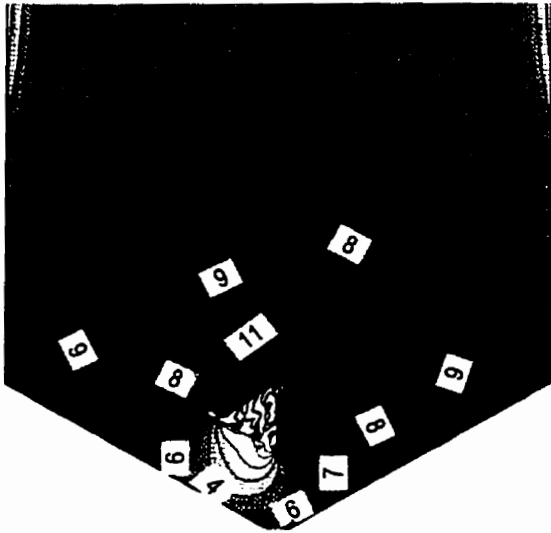
↑ increase in stresses w.r.t. pervious condition

↓ decrease in stresses w.r.t. pervious condition

↔ stresses remain unchanged w.r.t. pervious condition

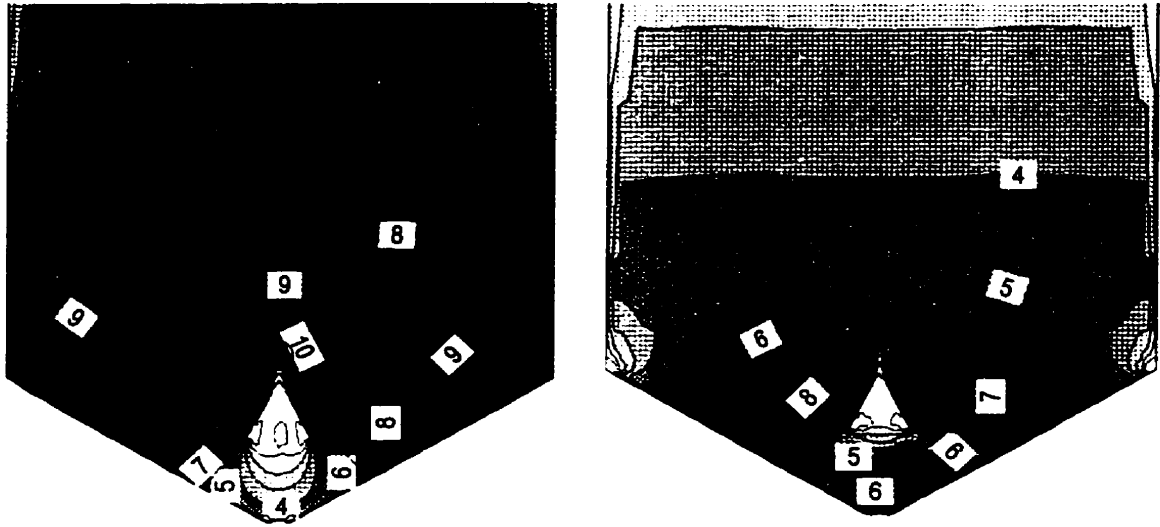


No insert

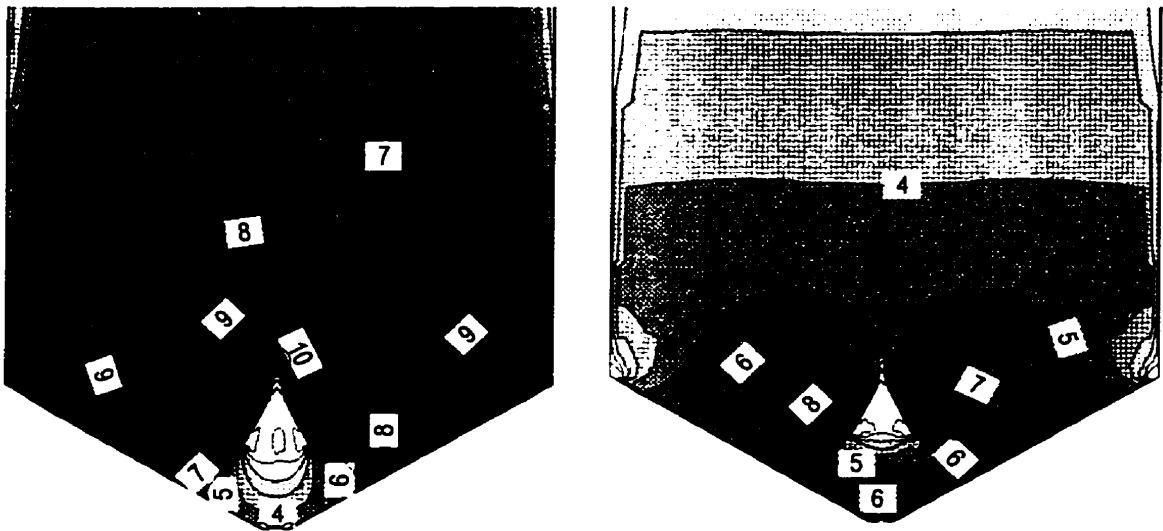


Asymmetric hinged insert at 175 mm

Figure 5.3.(a) Effect of insert mounting method on stress distribution in *full bin* after filling but prior to draw down initiation. Y-total stress (left column) and x-total stress (right column)

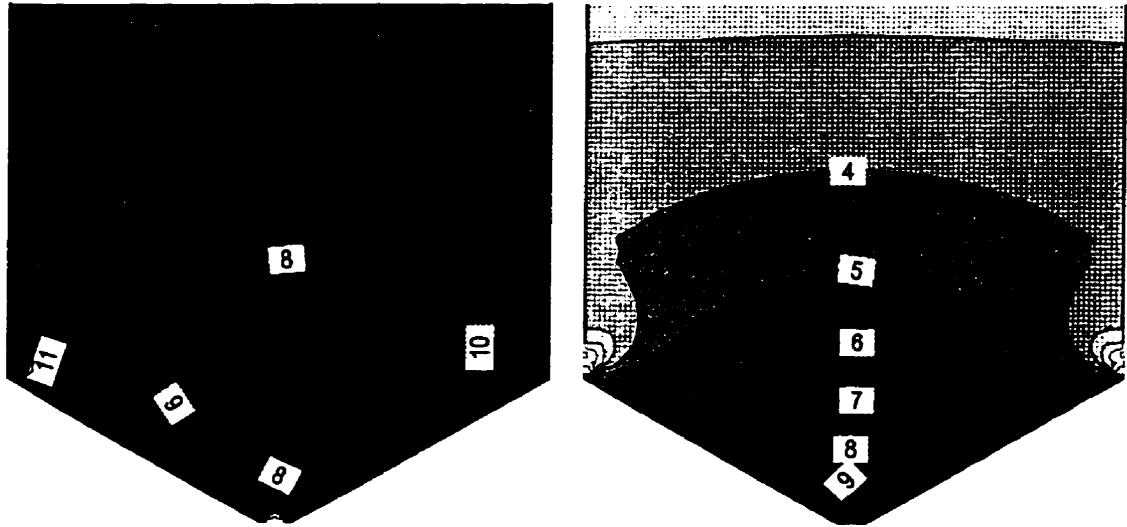


Symmetric fixed insert at 175 mm

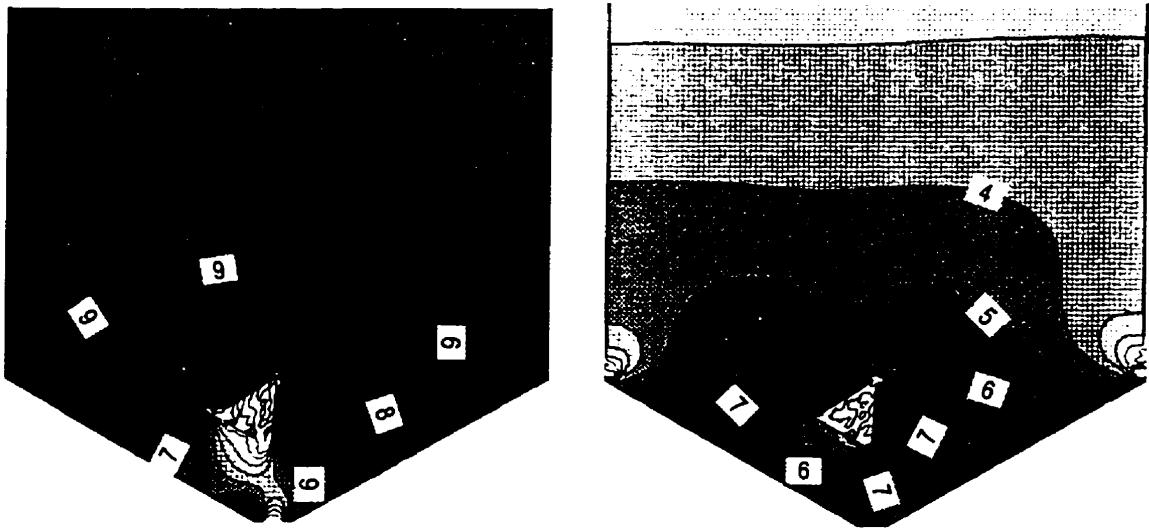


Symmetric hinged insert at 175 mm

Figure 5.3.(a)

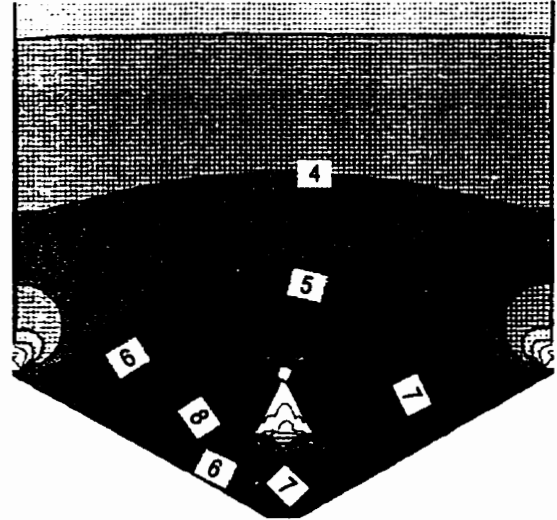
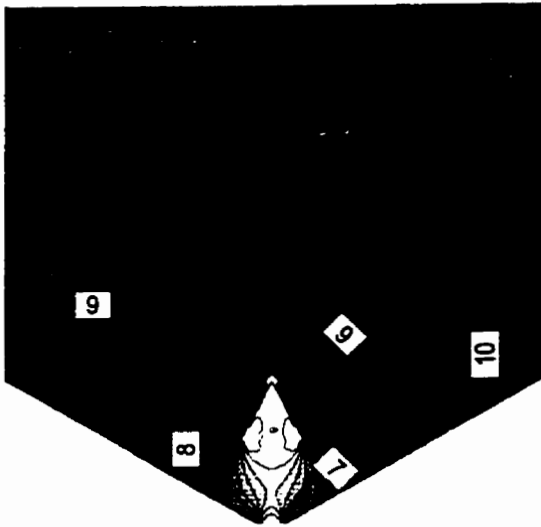


No insert

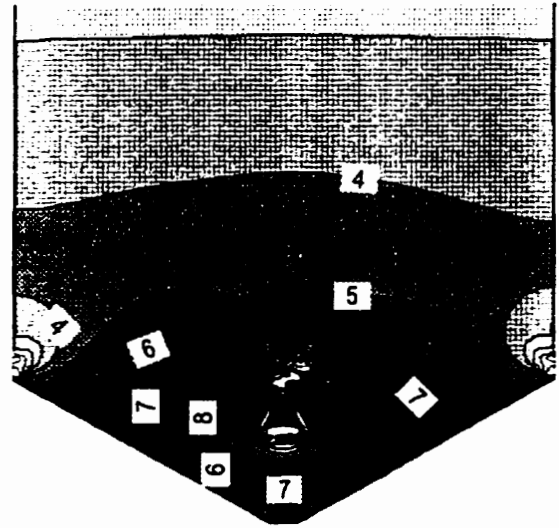
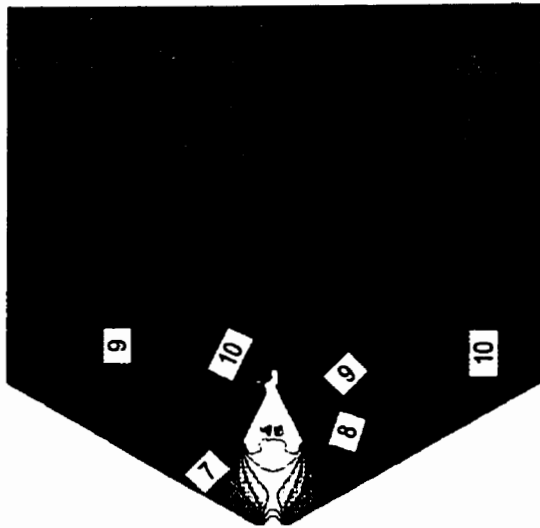


Asymmetric hinged insert at 175 mm

Figure 5.3.(b) Effect of insert mounting method on stress distribution in *full bin* after draw down initiation. Y-total stress (left column) and x-total stress (right column)



Symmetric fixed insert at 175 mm



Symmetric hinged insert at 175 mm

Figure 5.3.(b)

5.4. Effect of Insert Location on Stress Distribution in *Farm Bin*

Simulations were carried out on *Farm bin* in an effort to extend the finite element model to farm size storage bins. In this analysis, stress distribution in ground feed when stored in farm size bin was investigated and compared to results of the experiments by Hao (1998). Similarity in pattern of stress distribution was observed when stress contours were compared to *Half bin* analysis.

5.4.1. Stress distribution after filling It is evident from Table 5.4. and Figure 5.4.(a) that insert location influences the stress distribution in ground feed. Presence of an insert as high as 600 mm ($R/W = 0.11$) from hopper bottom reduces stresses in vertical and horizontal directions as compared to condition when no insert is present. Similar to *Half bin* analysis, horizontal and vertical stresses keep reducing as the insert is placed lower into the bin. When the insert is placed at 200 mm ($R/W = 0.30$) from hopper bottom, the horizontal stresses increase at the hopper outlet.

5.4.2. Stress distribution after draw-down initiation As the insert is placed lower in the hopper, the region near the outlet having zero or tensile vertical stresses increases (Figure 5.4.(b)). The stress distribution near the hopper outlet remains unchanged when insert is lowered from 600 to and 500 mm ($R/W = 0.12$), however appreciable changes take place as the insert is lowered to 400 mm ($R/W = 0.15$) and 300 mm ($R/W = 0.19$) (Figure 5.4.(b)). The zone of high stresses adjacent to the insert increases as the insert is further lowered to 200 mm.

The stress distribution indicates that maximum flowability can be expected when the insert is placed between 300 mm to 400 mm from hopper bottom. Insert at 200 mm may result in arch formation at the insert level. Further simulations need to be done at small increments of insert location between 300 mm and 400 mm as the stresses are least in that

condition. This would determine a precise insert mounting location which would result in least stresses in the bin. There is a minor increase in stresses when insert is moved from 300 mm to 400 mm however, since the distance between insert and hopper wall increases as the insert is moved from 300 mm to 400 mm, the chances of formation of arches when the flow starts decreases. Thus results from further simulations and experiments can be of help in deciding the appropriate location to mount the insert.

Table 5.4. Effect of insert location on stresses near the hopper outlet with change in insert location for *Farm bin*

Insert Location from hopper bottom (R/W)	Stresses after filling		Stresses after draw-down initiation	
	Y-effective stress	X-effective stress	Y-effective stress	X-effective stress
No insert				
600 mm (0.11)	↓	↓	↓	↓
500 mm (0.12)	↓	↔	↓	↔
400 mm (0.15)	↓	↓	↓	↓
300 mm (0.19)	↓	↓	↓	↓
200 mm (0.30)	↓	↓	↓	↓

↑ increase in stresses w.r.t. pervious condition

↓ decrease in stresses w.r.t. pervious condition

↔ stresses remain unchanged w.r.t. pervious condition

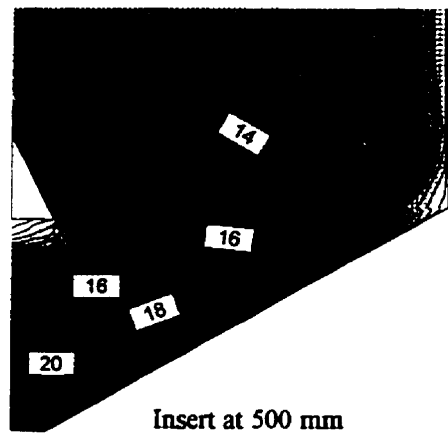
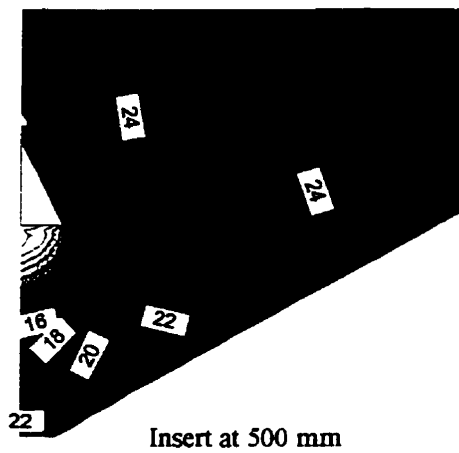
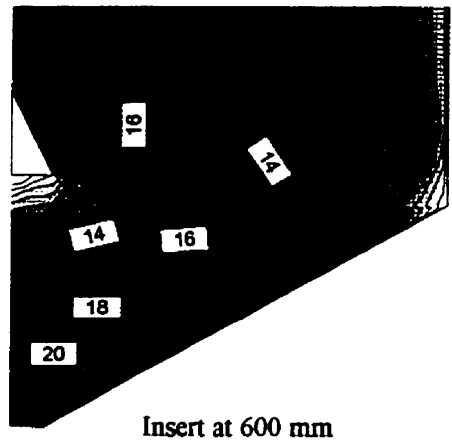
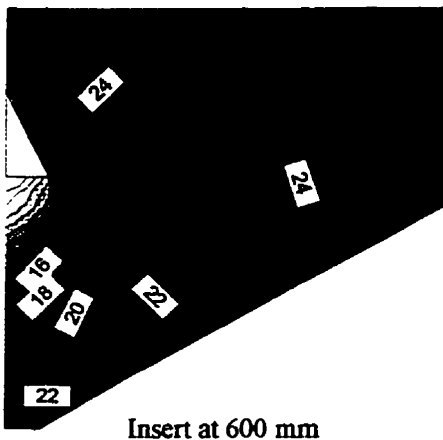
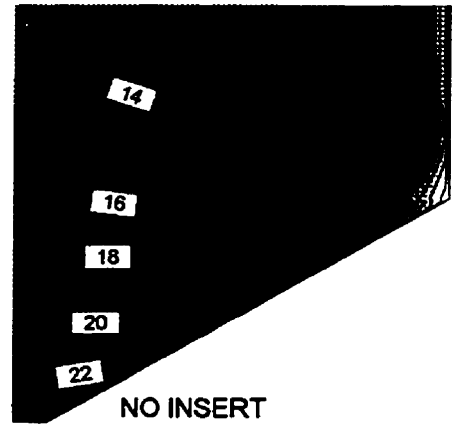
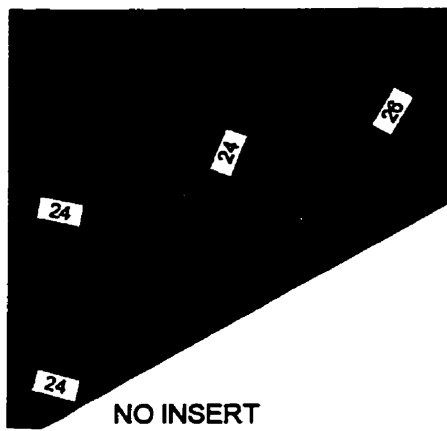
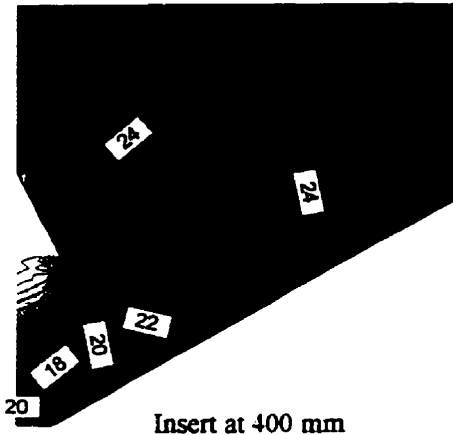
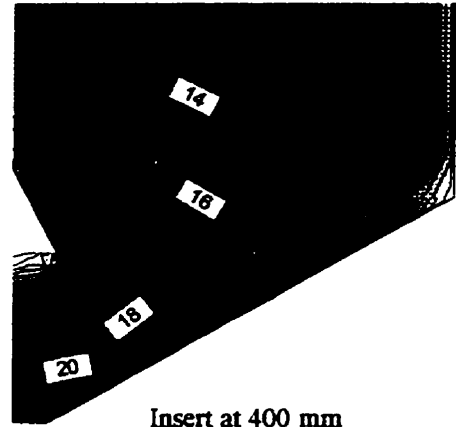


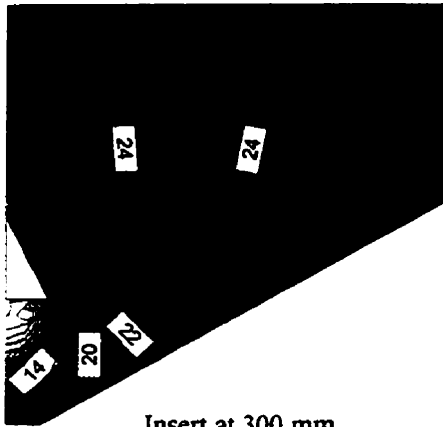
Figure 5.4.(a) Effect of insert location on stress distribution in *farm bin* after filling but prior to draw down initiation. Y-total stress (left column) and x-total stress (right column)



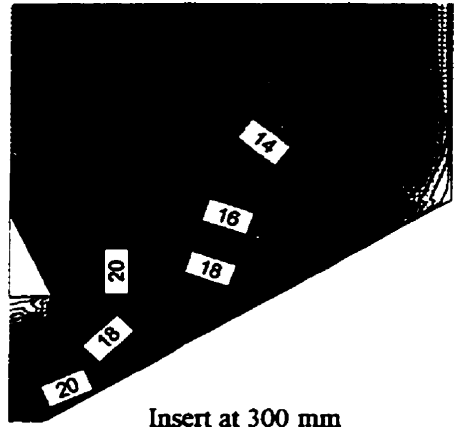
Insert at 400 mm



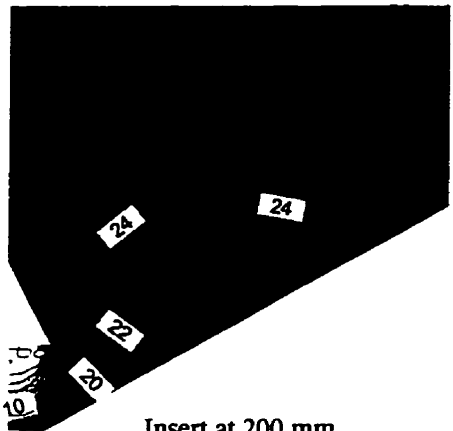
Insert at 400 mm



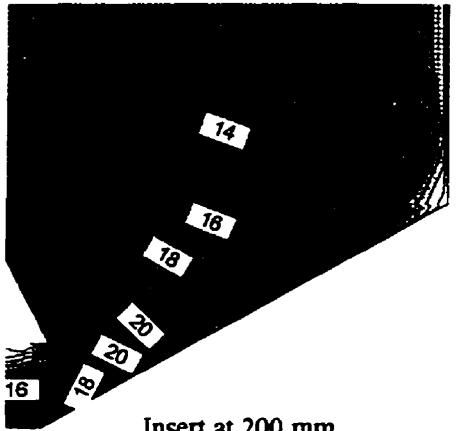
Insert at 300 mm



Insert at 300 mm



Insert at 200 mm



Insert at 200 mm

Figure 5.4.(a)

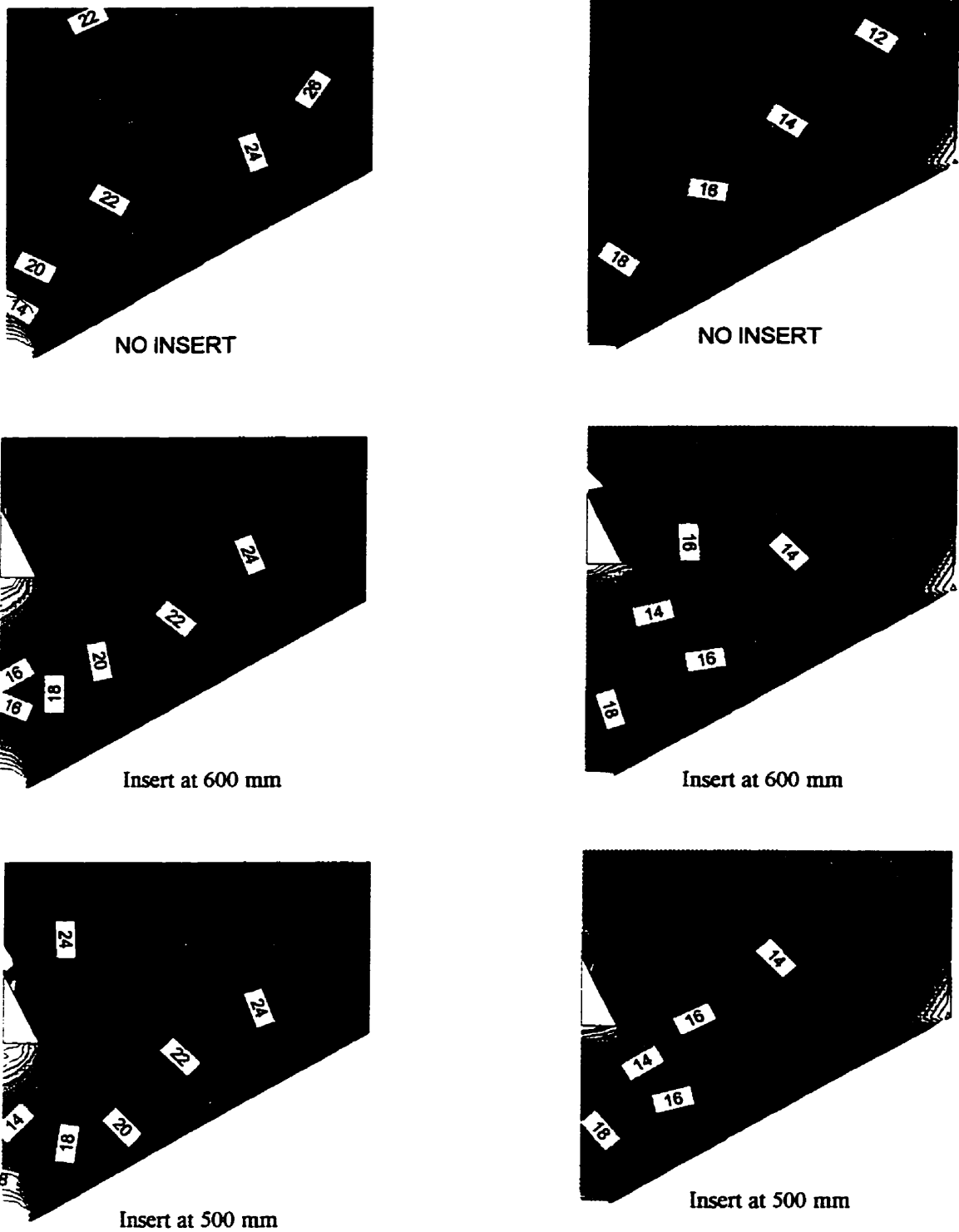
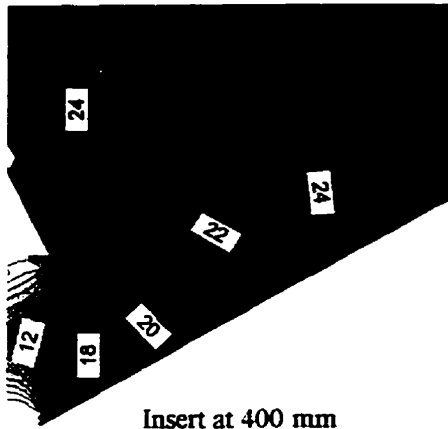
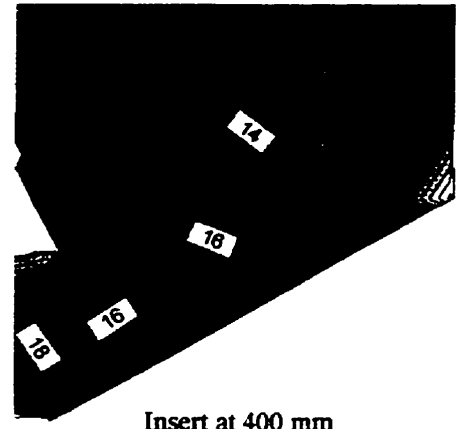


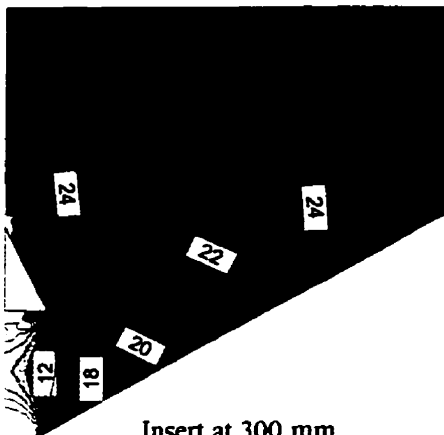
Figure 5.4.(b) Effect of insert location on stress distribution in *farm bin* after draw down initiation. Y-total stress (left column) and x-total stress (right column)



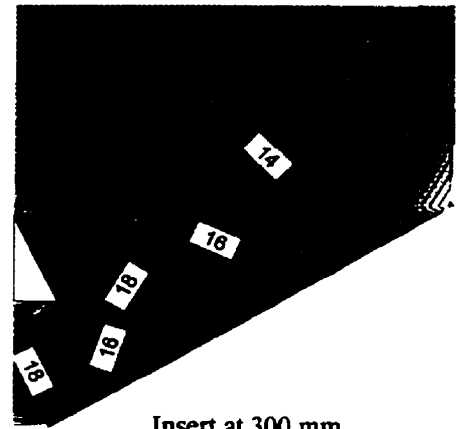
Insert at 400 mm



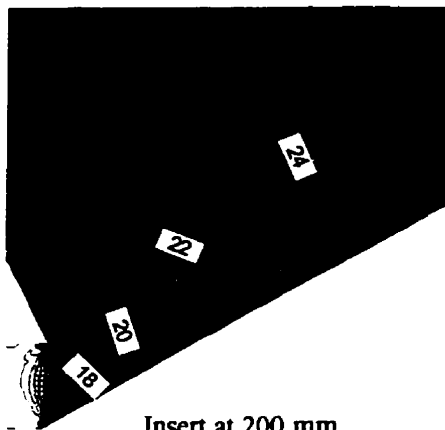
Insert at 400 mm



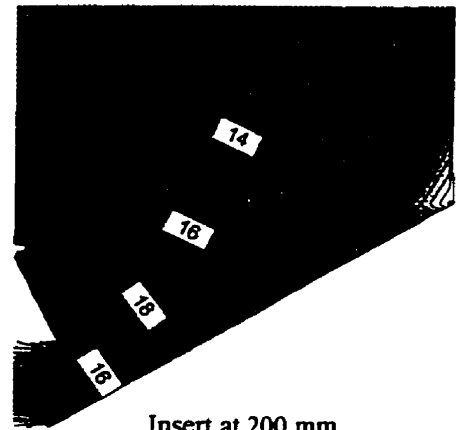
Insert at 300 mm



Insert at 300 mm



Insert at 200 mm



Insert at 200 mm

Figure 5.4.(b)

5.5. Effect of Insert Size on Stress Distribution in *Farm Bin*

In this analysis, the inserts were mounted at 400 mm from the hopper bottom. Due to the constraint in time, five insert sizes were simulated.

5.5.1. Stress distribution after filling Table 5.5. and Figure 5.5.(a) show that placing an insert as small as 100 mm ($R/W = 0.06$) decreases both the stress when compared to condition without insert. As the insert size is increased to 150 mm ($R/W = 0.11$), vertical stresses decrease where as horizontal stresses remain unchanged. When the insert size is increased to 200 ($R/W = 0.15$), 250 ($R/W = 0.19$), and 300 mm ($R/W = 0.24$), both the stresses decrease.

5.5.2. Stress distribution after draw-down initiation The pattern of stress distribution for different insert sizes is shown in (Figure 5.5.(b)). The horizontal stresses remain unchanged when insert size is increased from 100 mm to 150 mm. The horizontal and vertical stresses keep decreasing as the insert size is increased.

It can be inferred that flowability of the *Farm bin* keeps increasing as the insert size is increased. This inference should however be viewed with caution because as the insert size increases, the distance between insert and hopper wall decreases. As the gap narrows, the chances of arch formation increases. When the insert is too small (100 mm and 150 mm), the vertical and horizontal stresses at the outlet are as high as bin with no insert. This suggests that inserts of a very small size have little or no effect on flowability of stored material. From practical considerations, an excessively large inserts would require re-examining of the structural design because of the self weight of the insert where insert is to be used as a flow corrective device in an existing bin. The large size of insert would make installation of the insert difficult. Further simulations and experiments should be carried out with larger insert sizes along with experiments in model bins to establish the analogy between the insert size and

flowability.

Table 5.5. Effect of insert size on stresses near the hopper outlet

Insert Size (R/W)	Stresses after filling		Stresses after draw-down initiation	
	Y-effective stress	X-effective stress	Y-effective stress	X-effective stress
No insert				
100 mm (0.06)	↓	↓	↓	↓
150 mm (0.11)	↓	↔	↓	↔
200 mm (0.15)	↓	↓	↓	↓
250 mm (0.19)	↓	↓	↓	↓
300 mm (0.24)	↓	↓	↓	↓

↑ increase in stresses w.r.t. pervious condition

↓ decrease in stresses w.r.t. pervious condition

↔ stresses remain unchanged w.r.t. pervious condition

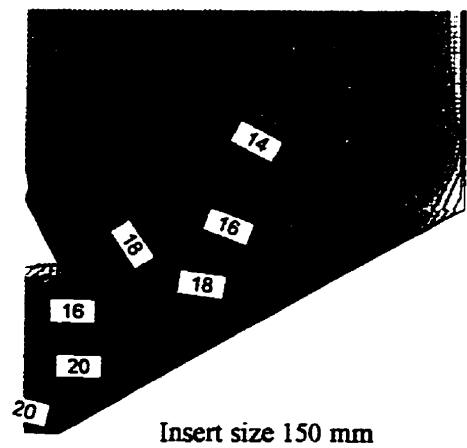
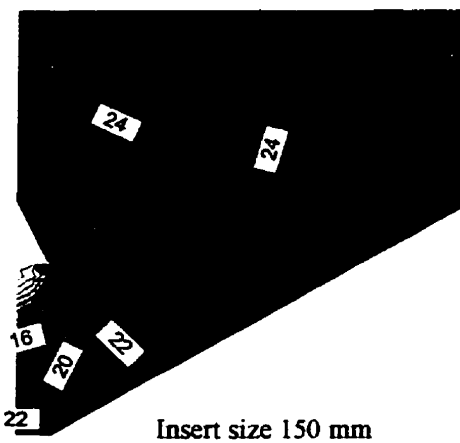
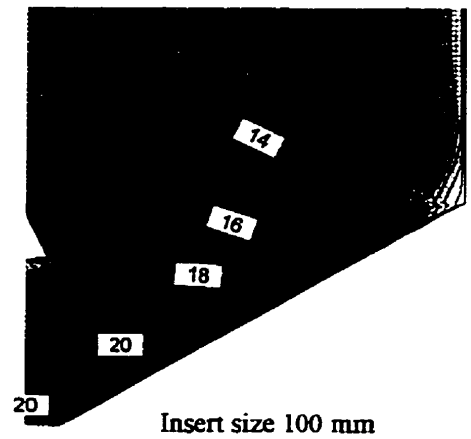
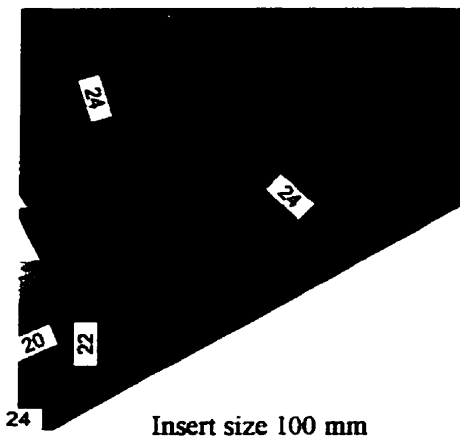
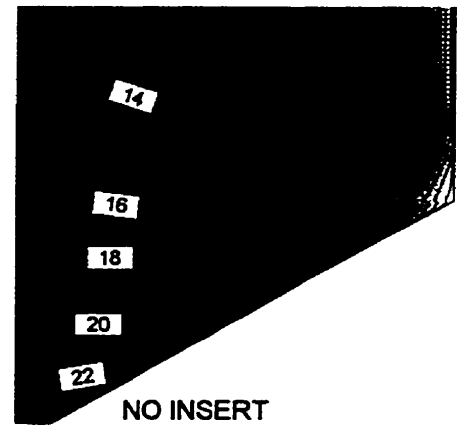
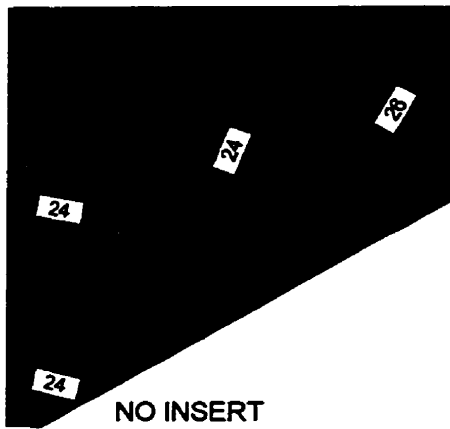


Figure 5.5.(a) Effect of insert size on stress distribution in *farm bin* after filling but prior to draw down initiation. Y-total stress (left column) and x-total stress (right column)

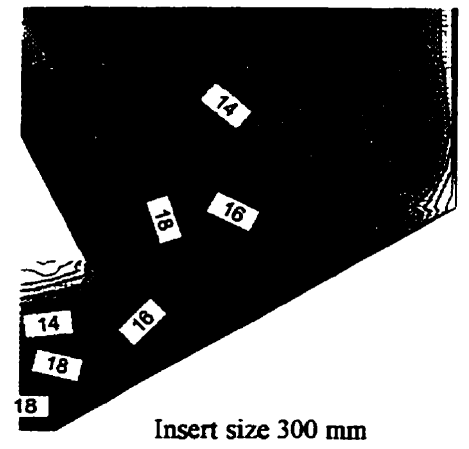
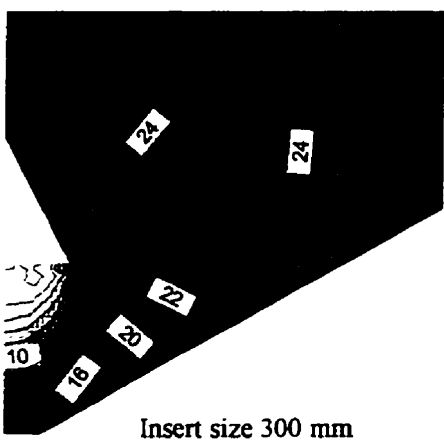
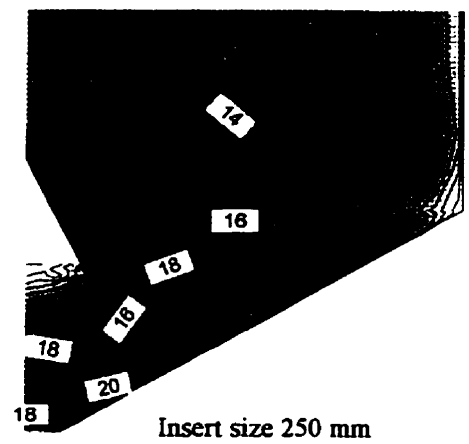
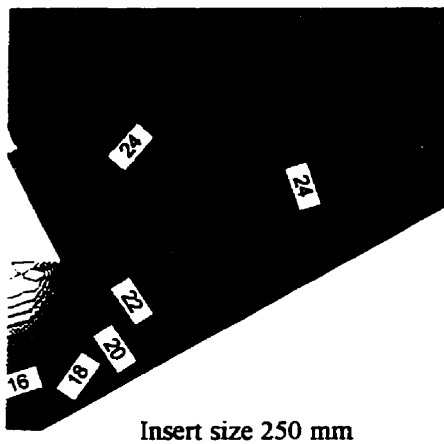
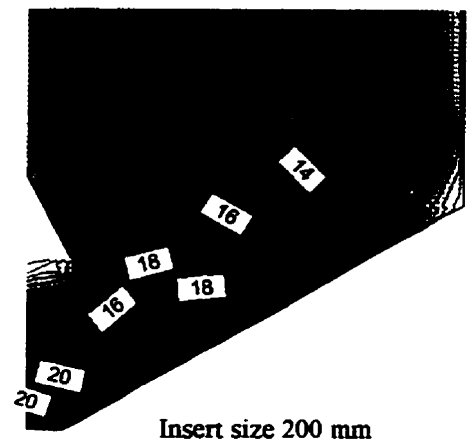
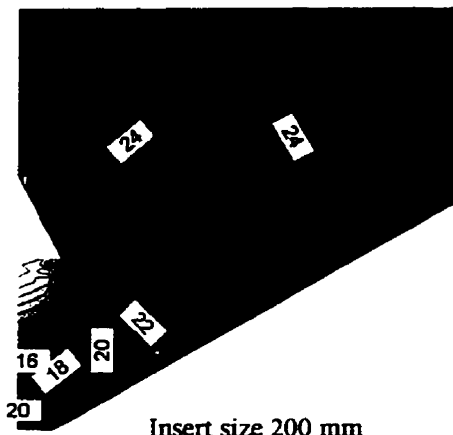


Figure 5.5.(a)

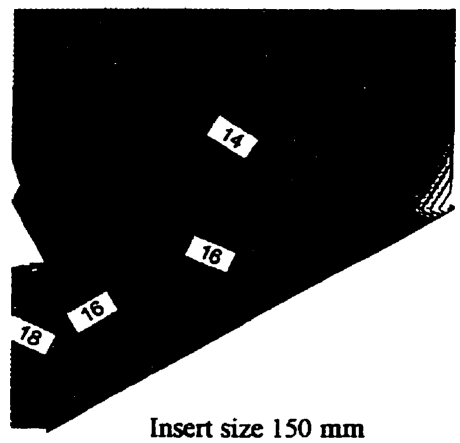
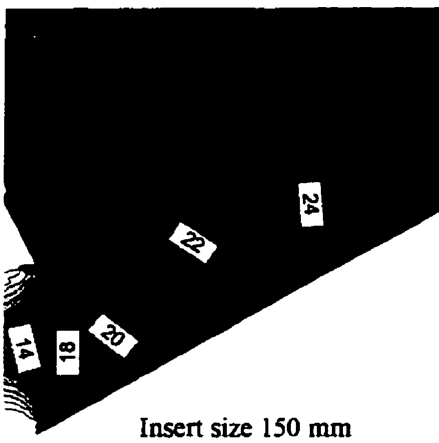
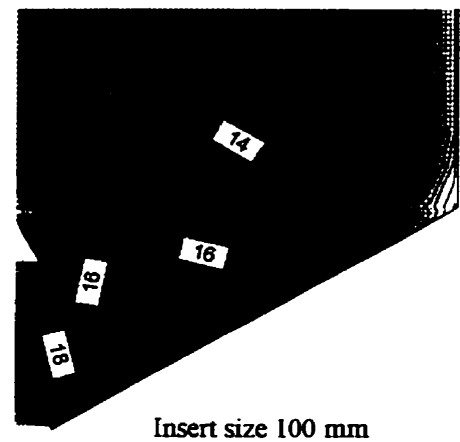
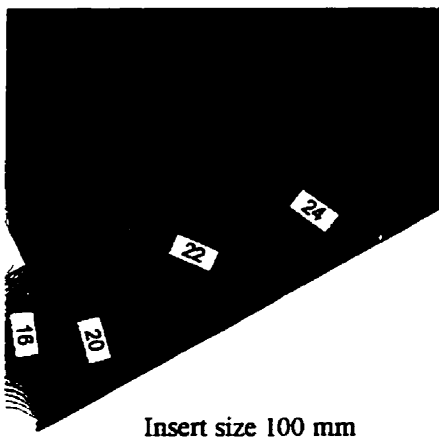
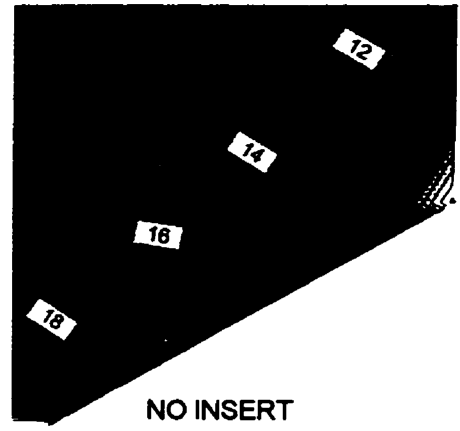
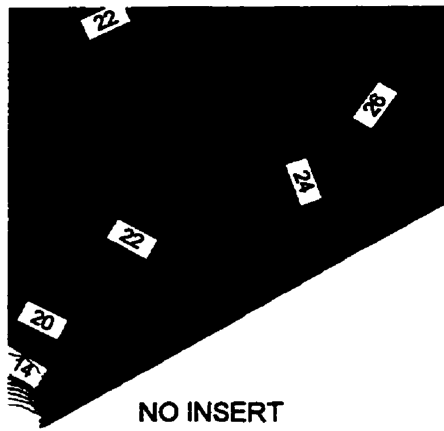
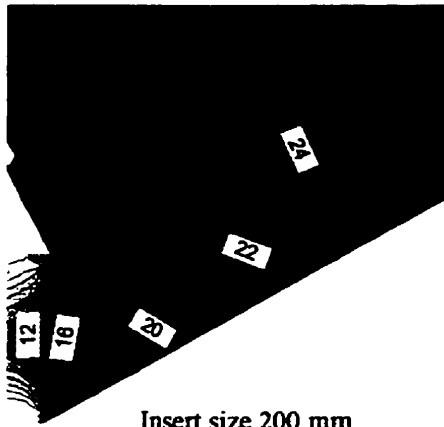
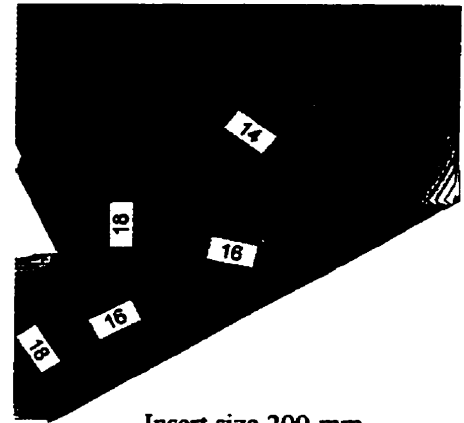


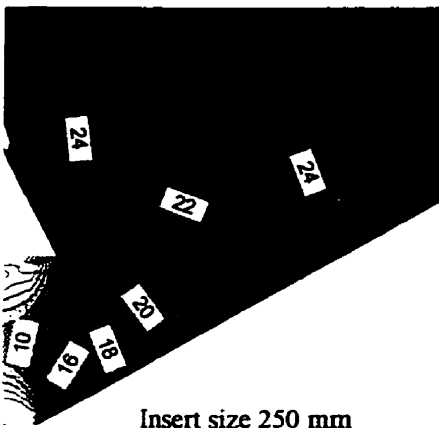
Figure 5.5.(b) Effect of insert size on stress distribution in *farm bin* after draw down initiation. Y-total stress (left column) and x-total stress (right column)



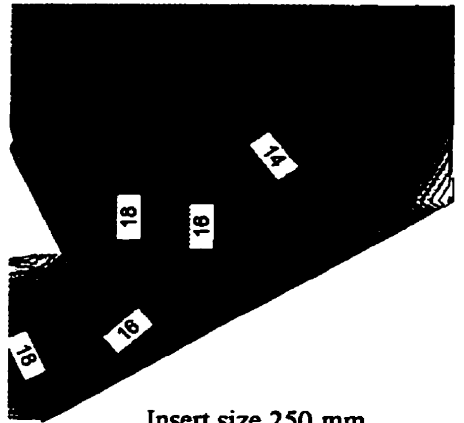
Insert size 200 mm



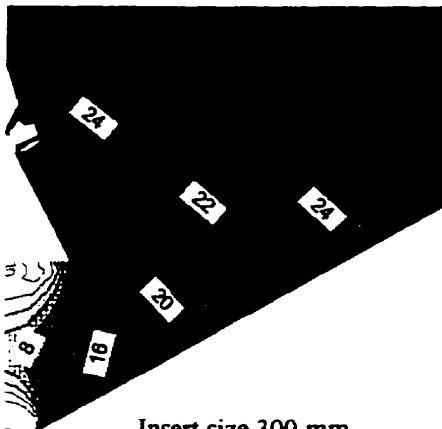
Insert size 200 mm



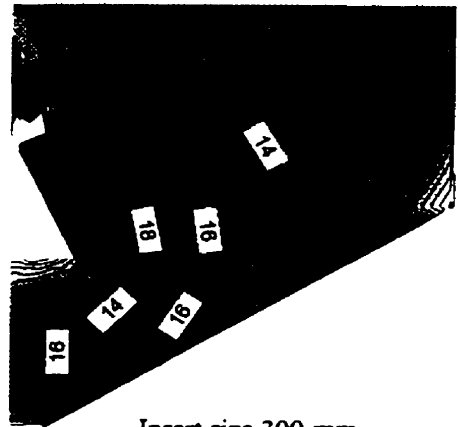
Insert size 250 mm



Insert size 250 mm



Insert size 300 mm



Insert size 300 mm

Figure 5.5.(b)

5.6. Effect of Insert Friction on Stress Distribution in *Farm Bin*

5.6.1. Stress distribution after filling As the friction of insert is reduced by reducing the value of K_{shear} from 10^6 to 10^4 kN/m, horizontal stresses increases. Reducing the friction any further does not change stresses in the horizontal direction (Table 5.6.). The vertical stresses remain unchanged as the insert K_{shear} is varied from 10^6 to 1 kN/m.

5.6.2. Stress distribution after draw-down initiation The variation in stress distribution is same as that after filling. It can be interpreted that placing an insert of very high friction may reduce chances of arch formation in storage bin by reducing the consolidation stresses in ground feed at the hopper outlet but at the same time can obstruct smooth flow of material along the insert. For a wide range of insert friction (K_{shear} 10^4 to 1 kN/m) there is no effect on stress distribution. This leads to the conclusion that insert of low surface friction should be used in storage bins because it promotes smooth flow along the walls of the insert and also because the consolidation pressure remains unaffected for a wide range of value of K_{shear}

Since the values of K_{shear} used by SIGMA/W are only indicative of slippage of slip element, a parametric study is needed to test the sensitivity of the K_{shear} values in terms of friction coefficient between the ground feed and insert surface. Experiments need to be carried out to determine correlation between the K_{shear} value and kinematic friction to establish physical significance of K_{shear} values that were used in the simulations.

Table 5.6. Effect of insert friction on stresses near the hopper outlet

Insert Friction K_{shear} kN/m	Stresses after filling		Stresses after draw-down initiation	
	Y-effective stress	X-effective stress	Y-effective stress	X-effective stress
10^6				
10^4	↔	↑	↔	↑
10^2	↔	↔	↔	↔
10	↔	↔	↔	↔
1	↔	↔	↔	↔

↑ increase in stresses w.r.t. pervious condition

↓ decrease in stresses w.r.t. pervious condition

↔ stresses remain unchanged w.r.t. pervious condition

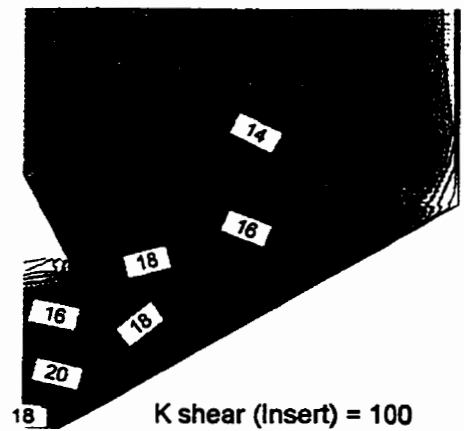
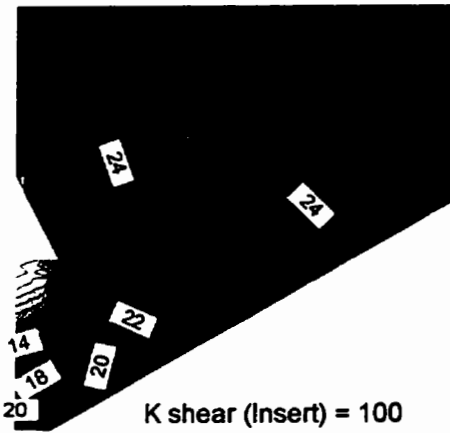
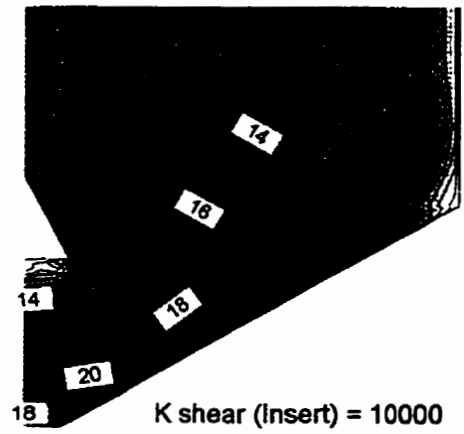
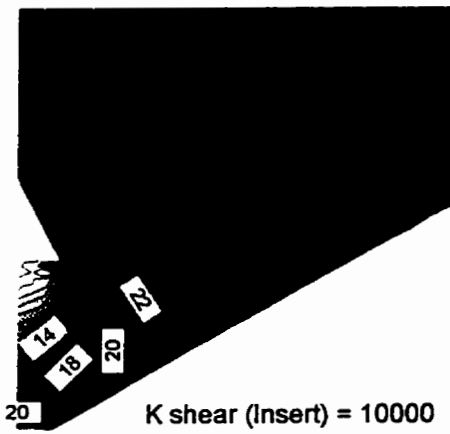
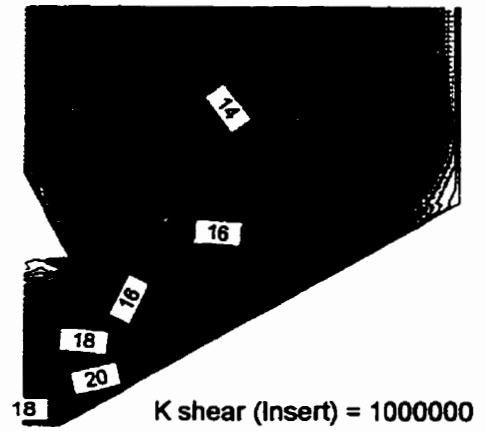
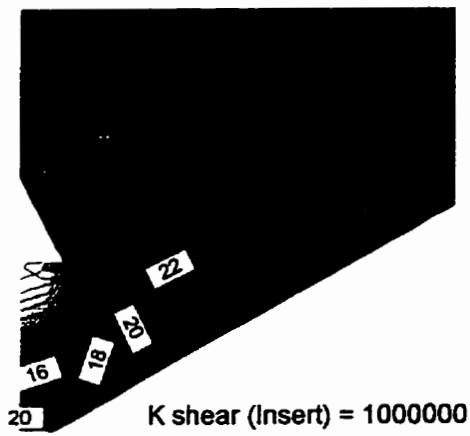


Figure 5.6.(a) Effect of insert friction on stress distribution in *farm bin* after filling but prior to draw down initiation. Y-total stress (left column) and x-total stress (right column)

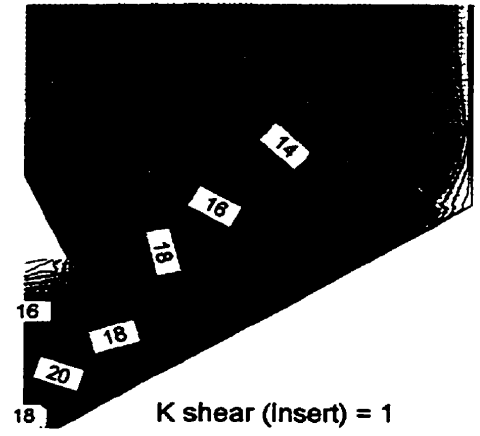
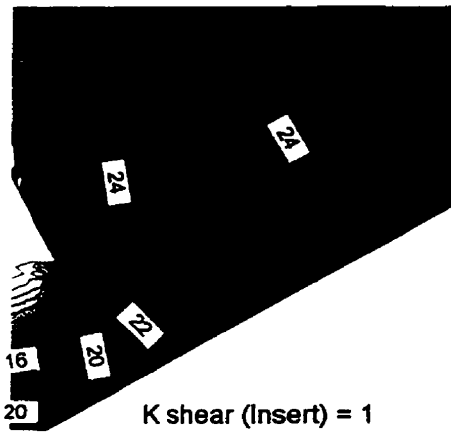
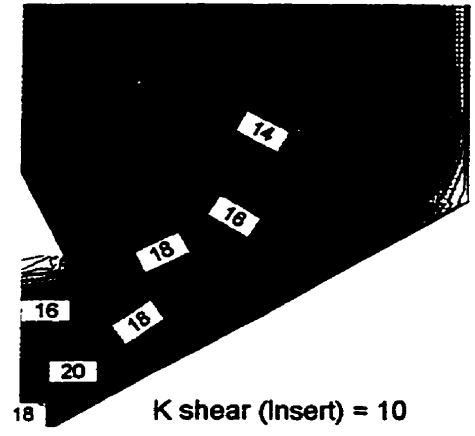
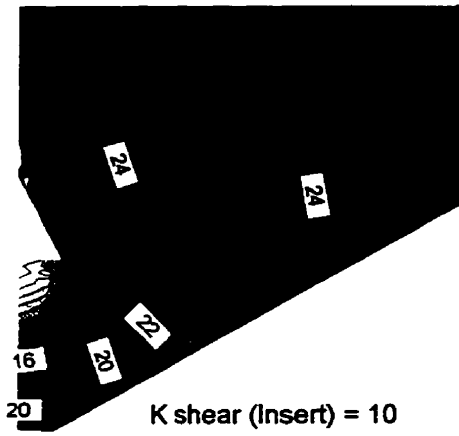


Figure 5.6.(a)

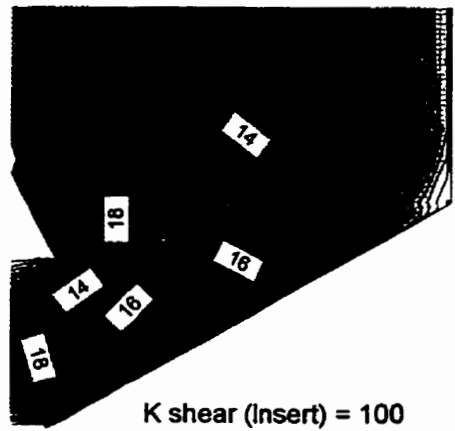
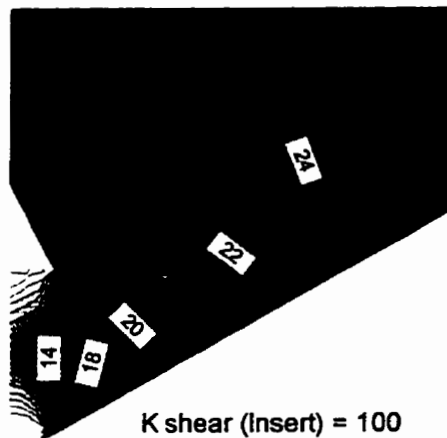
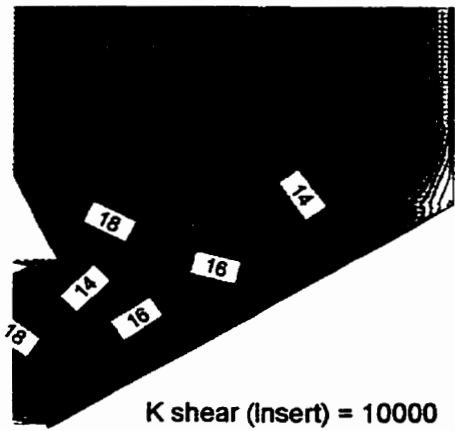
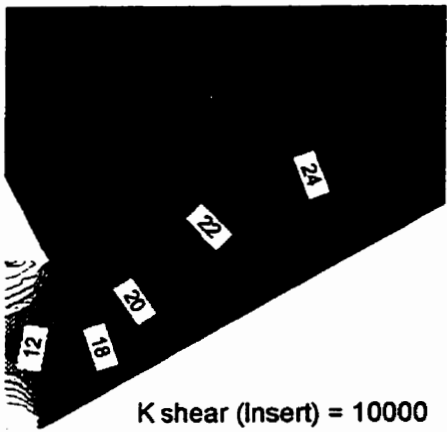
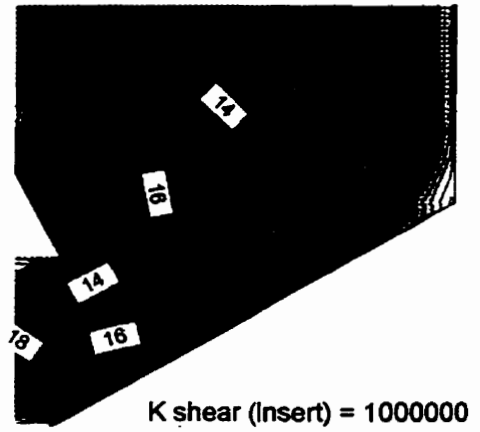
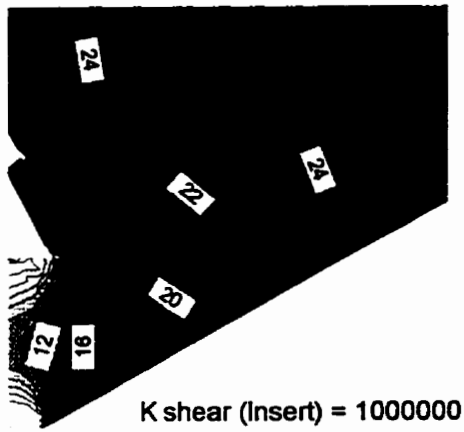


Figure 5.6.(b) Effect of insert friction on stress distribution in *farm bin* after draw down initiation. Y-total stress (left column) and x-total stress (right column)

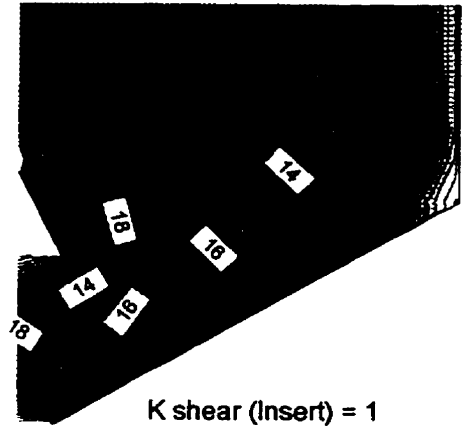
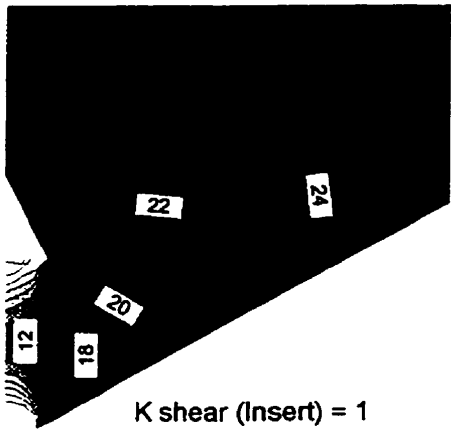
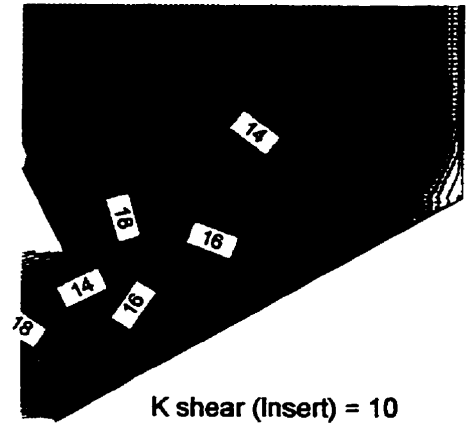
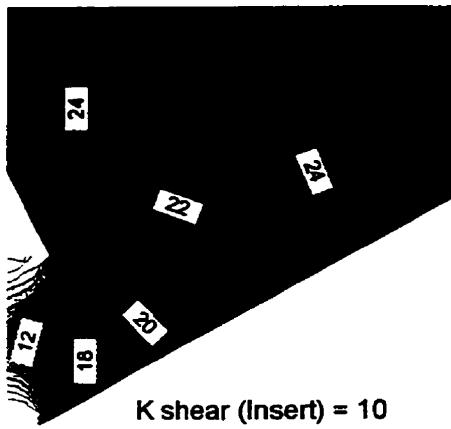


Figure 5.6.(b)

5.7. Effect of Size of Hopper outlet on Stress Distribution in *Farm Bin*

5.7.1. Stress distribution after filling Though the results of this analysis are predictable, this study helps reinforce the claim that for increased flowability in storage bin, the stress distribution should be such that the vertical and horizontal stresses should be minimum. When the outlet size is reduced from 320 mm to 240 mm and then to 160 mm, vertical stresses remain unchanged and horizontal stresses increase (Table 5.7.). This is because the movement of material near the hopper outlet is in radial direction. When the outlet size is gradually reduced, the horizontal surface to which the lateral loads are transferred is reduced hence the area of high horizontal stresses increases vertically. It can be noticed for stress contour of 20 kPa that the high stress zone steadily increases from the side of inclined hopper wall towards the centre line of the bin. Reducing the outlet size to 100 mm increases the vertical stresses and the horizontal stresses (Figure 5.7.(a)). Further reduction of outlet size to 60 mm does not change the horizontal or vertical stress distribution.

5.7.2. Stress distribution after draw-down initiation As the hopper outlet size is reduced, vertical and horizontal stresses first increase and then remain unchanged (Figure 5.7.(b)). The region of zero or negative stresses increases with increase in the size of hopper outlet.

The results of this simulation, as expected, clearly indicate that flowability of ground feed increases with increase in outlet size.

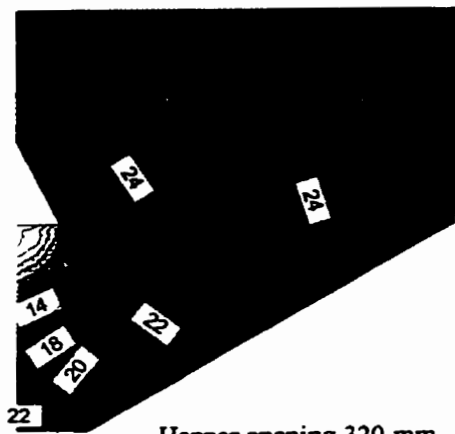
Table 5.7. Effect of hopper outlet size on stresses near the hopper outlet

Hopper outlet size	Stresses after filling		Stresses after draw-down initiation	
	Y-effective stress	X-effective stress	Y-effective stress	X-effective stress
320 mm				
240 mm	↔	↑	↑	↑
160 mm	↔	↑	↔	↔
100 mm	↑	↑	↔	↔
60 mm	↔	↔	↔	↔

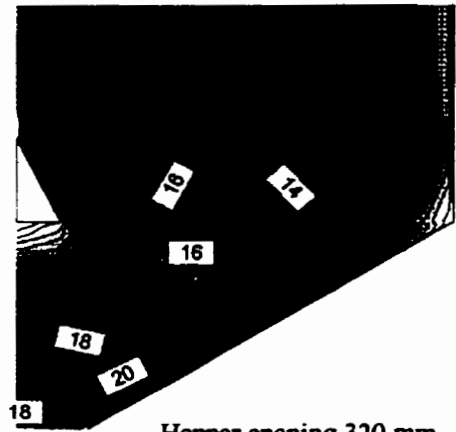
↑ increase in stresses w.r.t. pervious condition

↓ decrease in stresses w.r.t. pervious condition

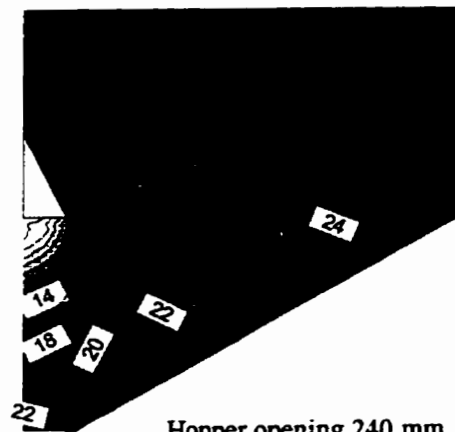
↔ stresses remain unchanged w.r.t. pervious condition



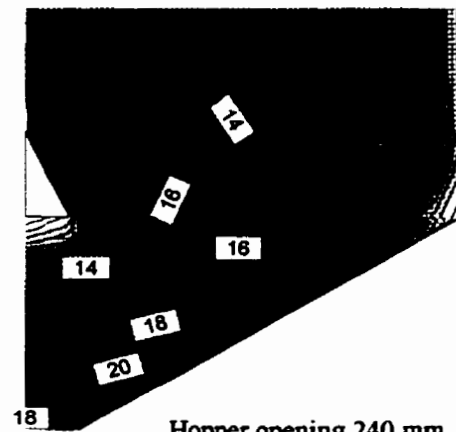
Hopper opening 320 mm



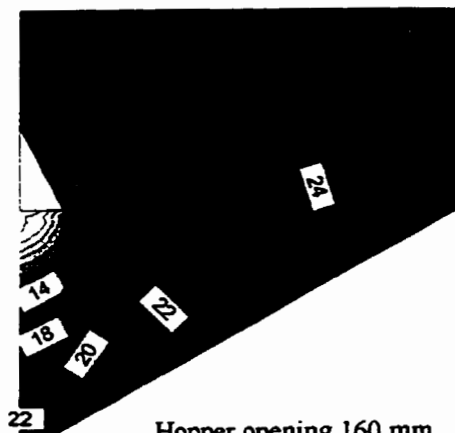
Hopper opening 320 mm



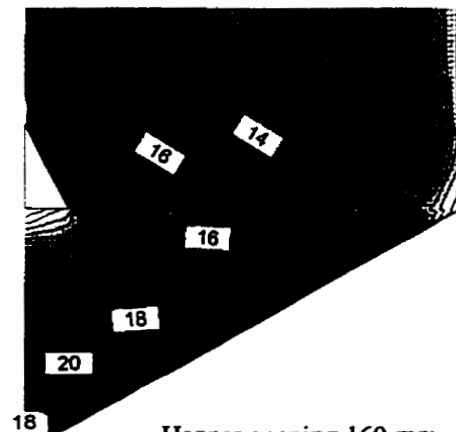
Hopper opening 240 mm



Hopper opening 240 mm



Hopper opening 160 mm



Hopper opening 160 mm

Figure 5.7.(a) Effect of size of hopper opening on stress distribution in *farm bin* after filling but prior to draw down initiation. Y-total stress (left column) and x-total stress (right column)

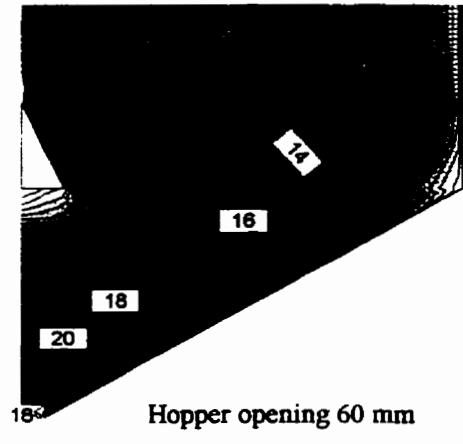
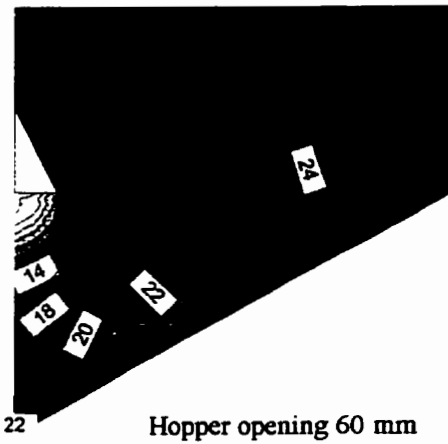
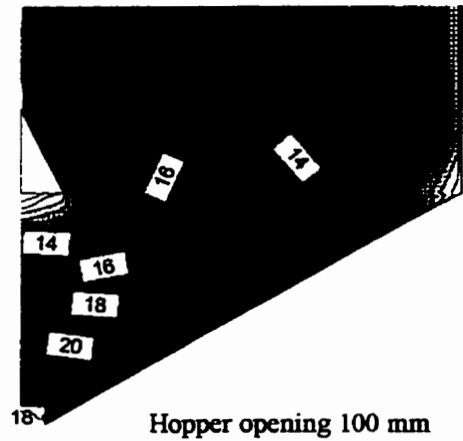
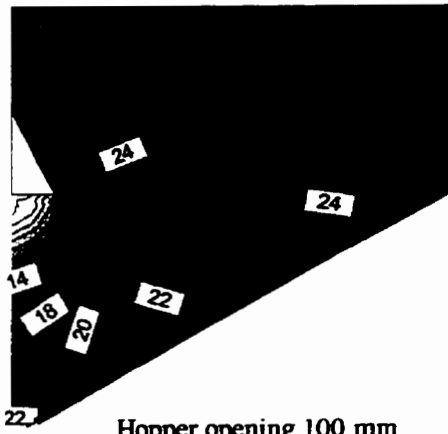
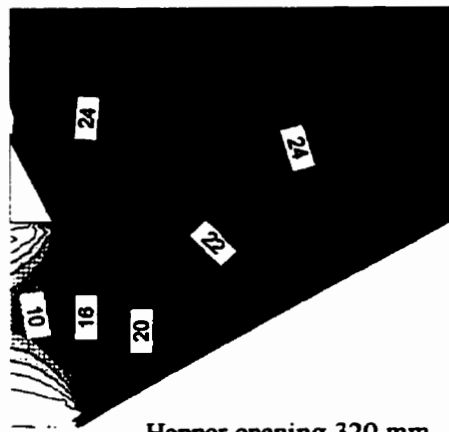
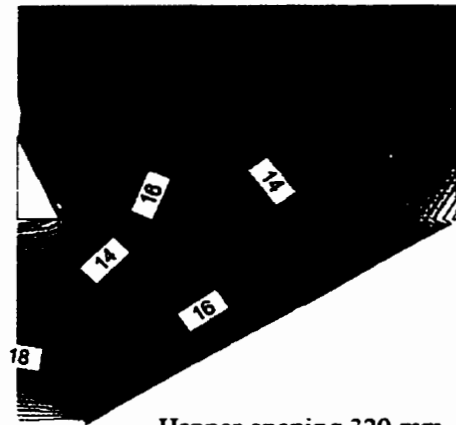


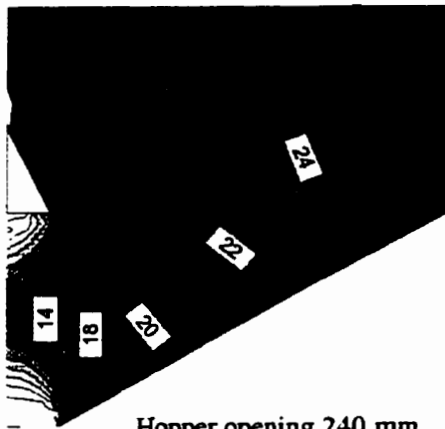
Figure 5.7.(a)



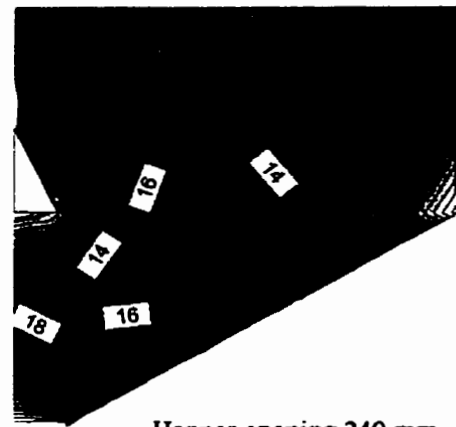
Hopper opening 320 mm



Hopper opening 320 mm



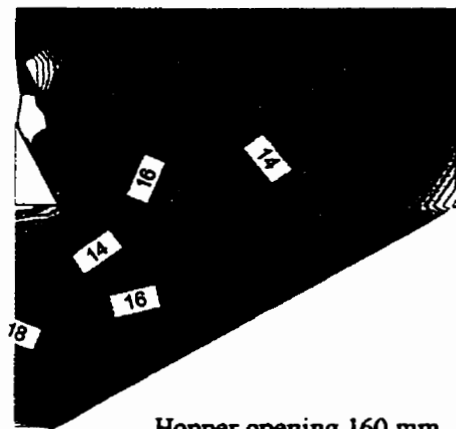
Hopper opening 240 mm



Hopper opening 240 mm

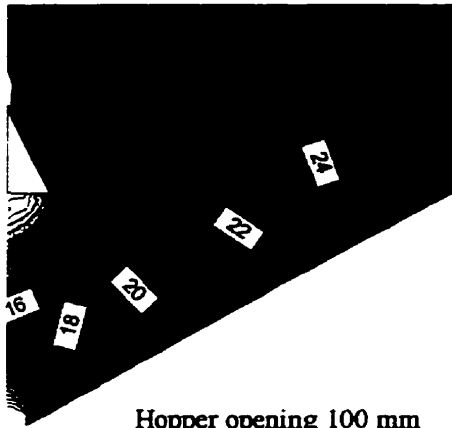


Hopper opening 160 mm

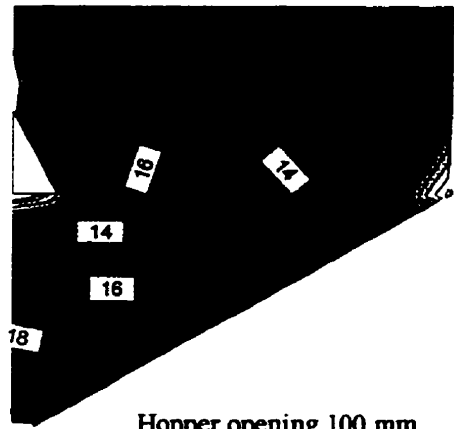


Hopper opening 160 mm

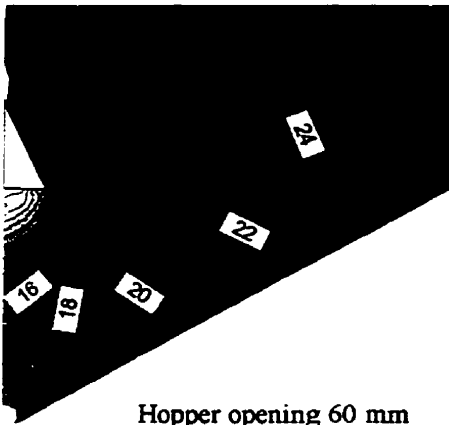
Figure 5.7.(b) Effect of size of hopper opening on stress distribution in *farm bin* after draw down initiation. Y-total stress (left column) and x-total stress (right column)



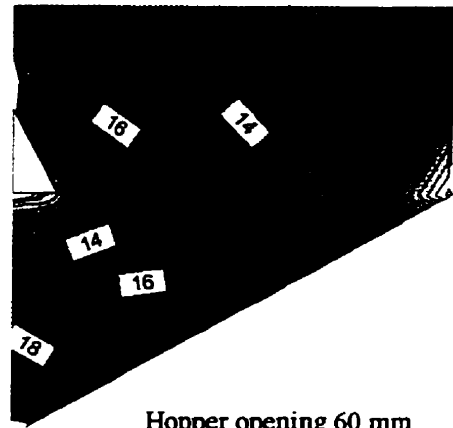
Hopper opening 100 mm



Hopper opening 100 mm



Hopper opening 60 mm



Hopper opening 60 mm

Figure 5.7.(b)

5.8. Effect of Hopper Slope on Stress Distribution in *Farm Bin*

In this analysis, since the height of hopper changed with the hopper slope, it was decided to place the insert in such a way that its bottom was always in line with the junction of bin and hopper. The effect of distance of hopper outlet from insert dominated over the influence of slope on the flowability of ground feed because when the distance between the insert and hopper outlet increased beyond a limit, the stresses at the outlet remained unaffected by the presence of the insert.

5.8.1. Stress distribution after filling For a slope of 50° , the vertical and horizontal stresses are high (Figure 5.8. (a)) as there is increased surcharge due to increased mass in the bigger hopper and stress distribution near the hopper outlet is unaffected by the insert. As the slope is reduced to 40° , the vertical and horizontal stresses decrease (Table 5.8.) due to reduced surcharge load. The effect of insert becomes prominent when the slope is reduced to 30° . High vertical stresses adjacent to the insert in bins with the hopper slope equal to 20° and 10° may tend to reduce flowability due to reduced gaps between the insert and hopper wall.

5.8.2. Stress distribution after draw-down initiation The horizontal stresses decrease with decrease in hopper slope and vertical stresses initially decrease and then increase despite the decreases in surcharge load (Figure 5.8. (b)). The region of zero or negative stresses increases with decrease in slope. The increase in vertical stresses could increase flowability of ground feed once the material is in incipient flow condition as the dynamic stresses would help break the arch.

It can be inferred from the stress distribution that the proximity of insert to the hopper outlet plays a major role in deciding the flowability of the material. In cases where stresses near the hopper outlet are influenced by the insert, chances of arch formation increase with

decrease in slope after filling of the bin however, after the draw down is initiated, the flowability may increase as the slope of hopper is reduced. This is because of high vertical stresses in the material at the hopper outlet which may tend to break the arches. Reducing the slope beyond a certain limit would reduce the flowability due to increased confining stresses adjacent to the insert.

Table 5.8. Effect of hopper slope on stresses near the hopper outlet

Hopper slope degree	Stresses after filling		Stresses after draw-down initiation	
	Y-effective stress	X-effective stress	Y-effective stress	X-effective stress
50				
40	↓	↓	↓	↓
30	↓	↓	↑	↓
20	↓	↓	↑	↓
10	↓	↓	↑	↓

↑ increase in stresses w.r.t. pervious condition

↓ decrease in stresses w.r.t. pervious condition

↔ stresses remain unchanged w.r.t. pervious condition

* hopper slope w.r.t. horizontal

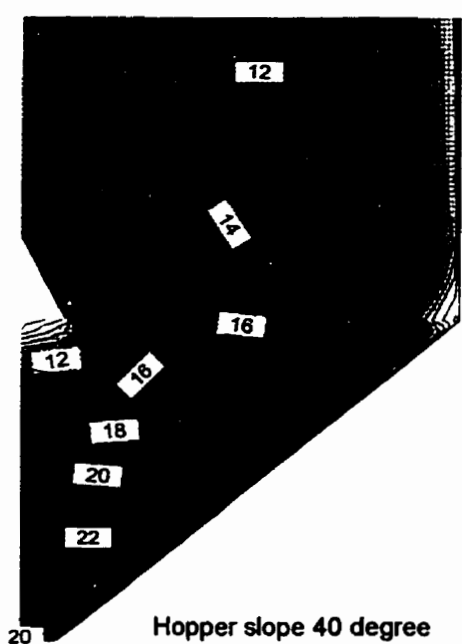
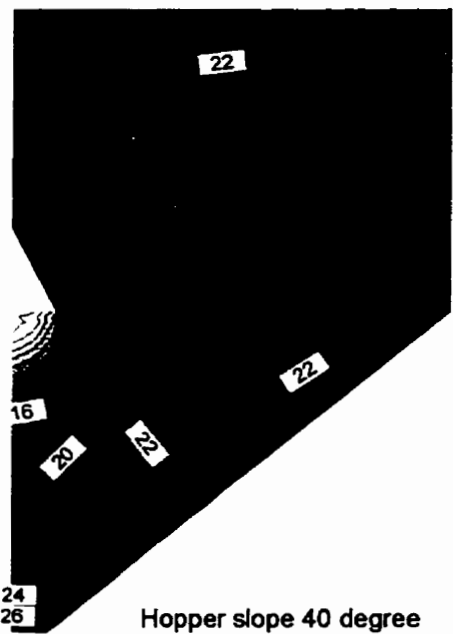
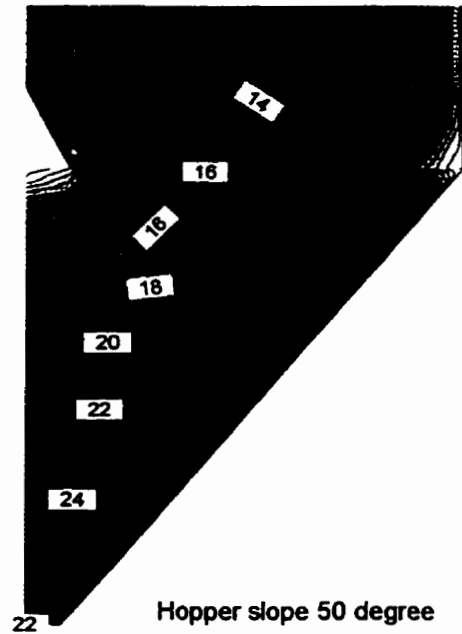
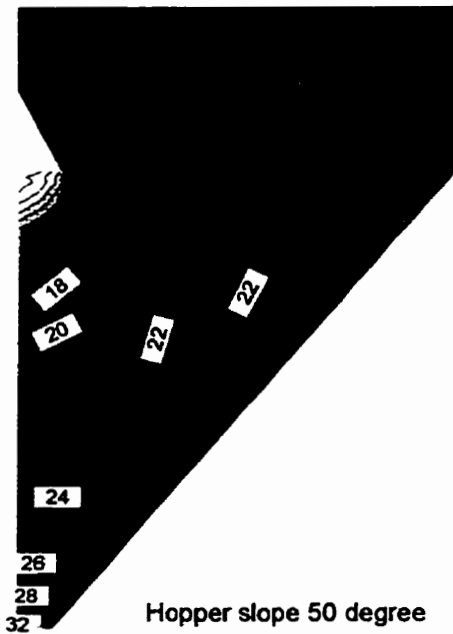


Figure 5.8.(a) Effect of hopper slope on stress distribution in *farm bin* after filling but prior to draw down initiation. Y-total stress (left column) and x-total stress (right column)

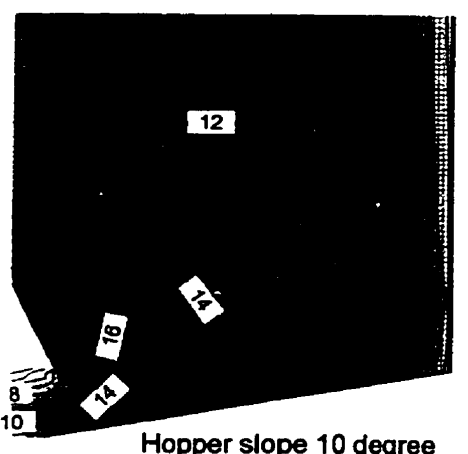
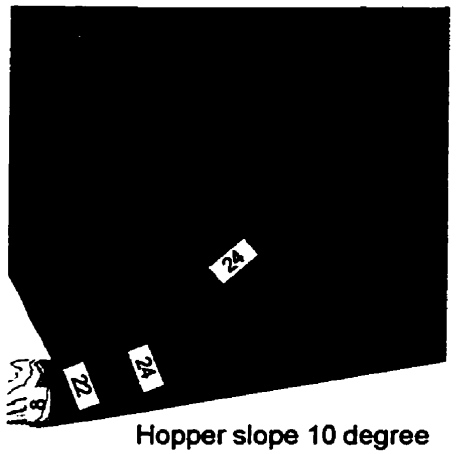
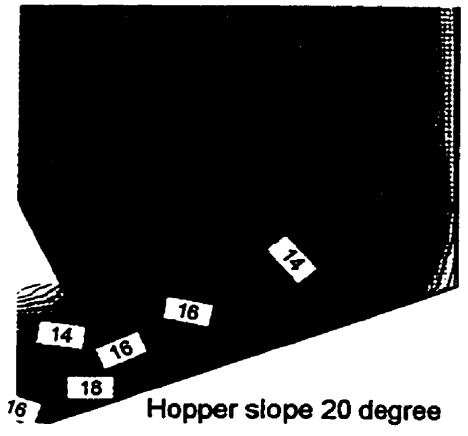
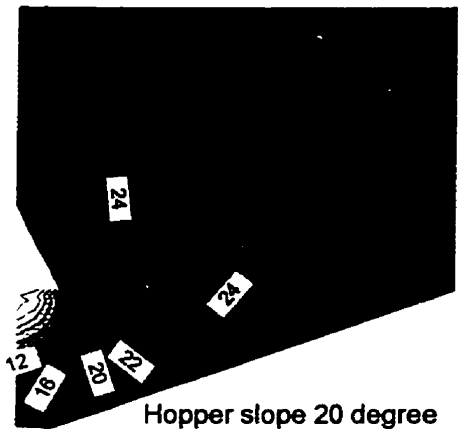
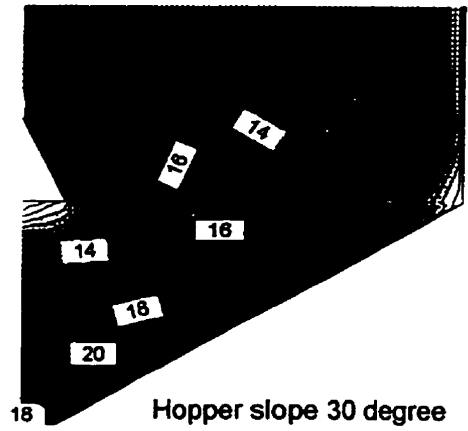
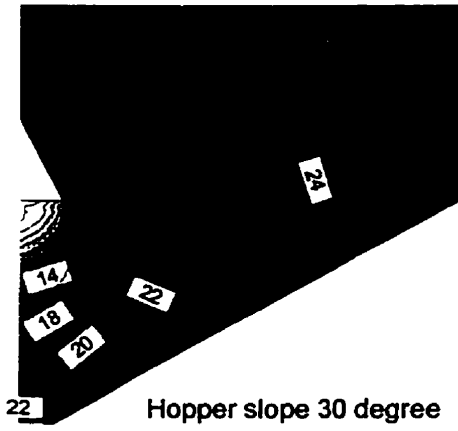
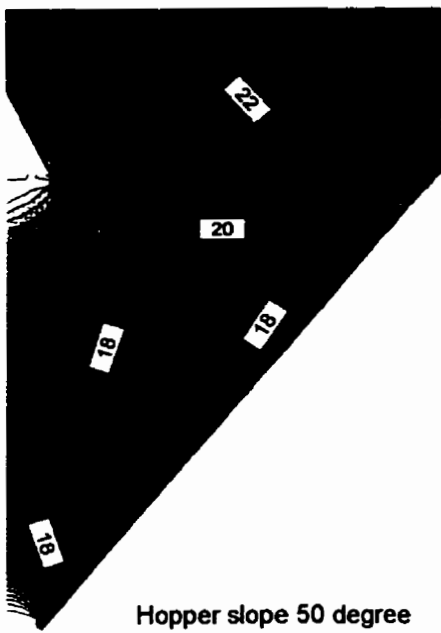
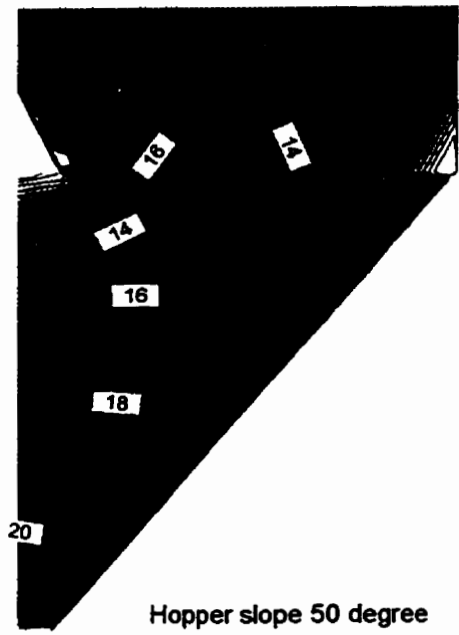


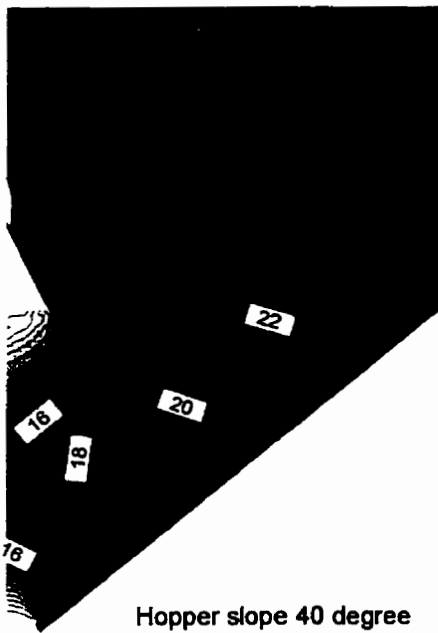
Figure 5.8.(a)



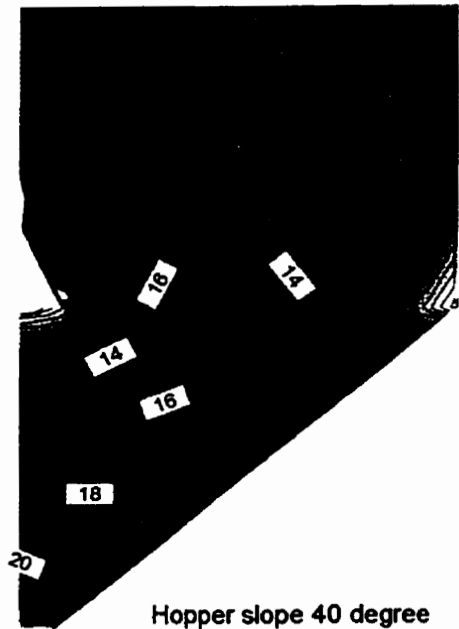
Hopper slope 50 degree



Hopper slope 50 degree

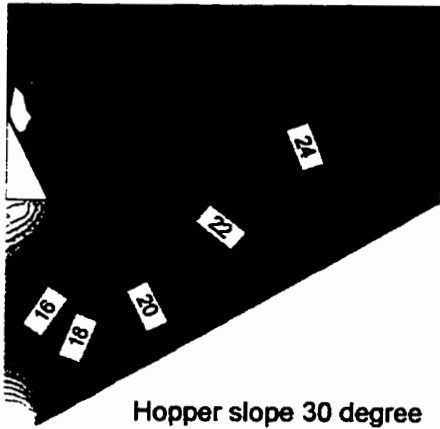


Hopper slope 40 degree

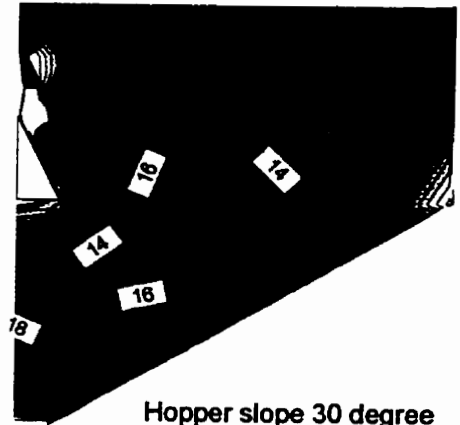


Hopper slope 40 degree

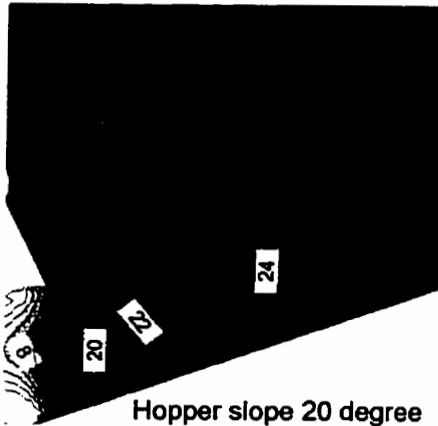
Figure 5.8.(b) Effect of hopper slope on stress distribution in *farm bin* after draw down initiation. Y-total stress (left column) and x-total stress (right column)



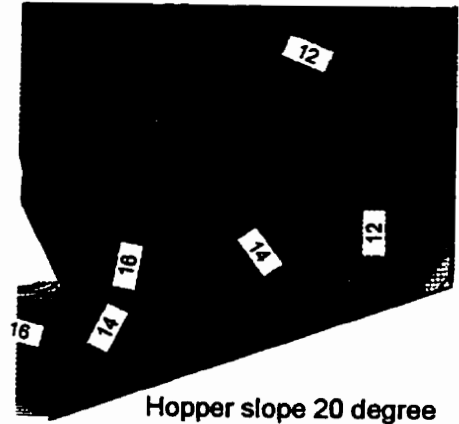
Hopper slope 30 degree



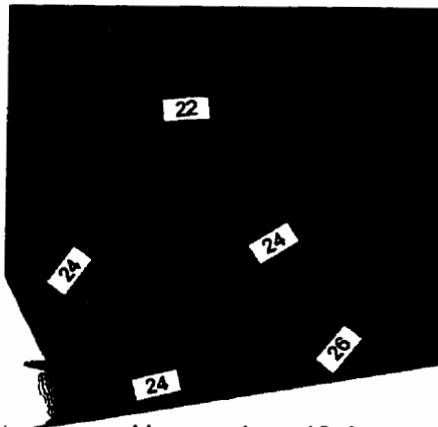
Hopper slope 30 degree



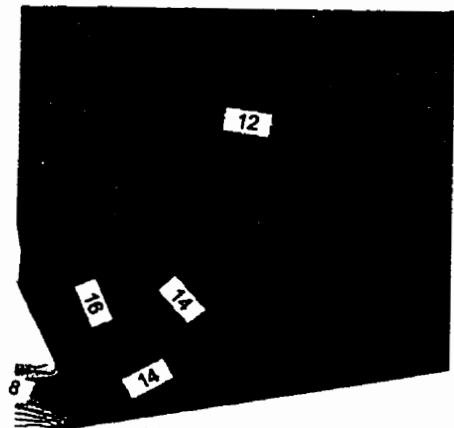
Hopper slope 20 degree



Hopper slope 20 degree



Hopper slope 10 degree



Hopper slope 10 degree

Figure 5.8.(b)

5.9. Effect of Bin wall Friction on Stress Distribution in *Farm Bin*

5.9.1. Stress distribution after filling Bin wall friction has major influence on the stress distribution. Horizontal and vertical stresses increase at the hopper outlet as the wall friction is decreased (Figure 5.9.(a)). Horizontal stresses remain unchanged when K_{shear} is reduced from 10 kN/m to 1 kN/m (Table 5.9.).

5.9.2. Stress distribution after draw-down initiation Reducing the value of K_{shear} initially increases the horizontal and vertical stresses. The stresses remain unchanged as the value of K_{shear} is reduced below 10^2 kN/m for vertical and horizontal stresses.

The movement of material during filling or during compaction under succeeding layers of fill is not retarded by smooth wall which means transfer of load to the material instead of bin wall. This increase in surcharge load results in increased stresses. The results indicate that when storage bin having smooth side walls is filled with ground feed, the chances of arch formation increase after filling of the storage bin due to high confining stresses, provided that the arch can be supported at its ends by the friction between material and hopper wall. Since the friction at the support of arch also reduces, it may result in sliding of the material along with the arch thereby resulting in flow despite high consolidation stresses. High stresses after draw-down initiation furthermore suggest that improved flow can be expected as the dynamic stresses would help slide the arch along with the material.

As mentioned earlier, since the values of K_{shear} used in SIGMA/W are only indicative of slippage, the results of simulation should be substantiated with experimental evidence and as of now be read with caution.

Table 5.9. Effect of bin wall friction on stresses near the hopper outlet

Bin Wall Friction K_{shear} kN/m	Stresses after filling		Stresses after draw-down initiation	
	Y-effective stress	X-effective stress	Y-effective stress	X-effective stress
10^6				
10^4	↑	↑	↑	↑
10^2	↑	↑	↑	↑
10	↑	↑	↔	↔
1	↑	↔	↔	↔

↑ increase in stresses w.r.t. pervious condition

↓ decrease in stresses w.r.t. pervious condition

↔ stresses remain unchanged w.r.t. pervious condition

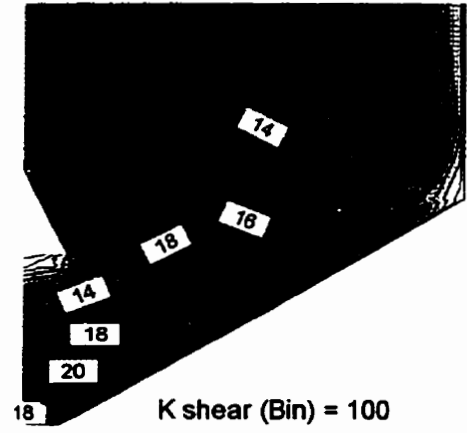
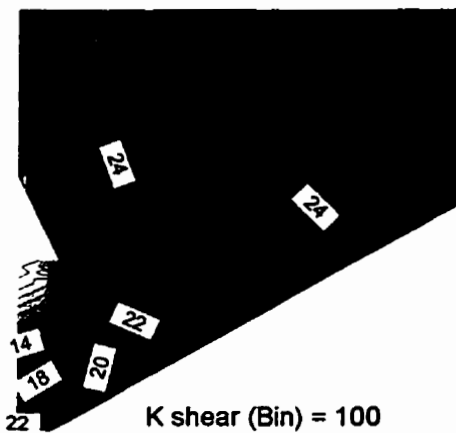
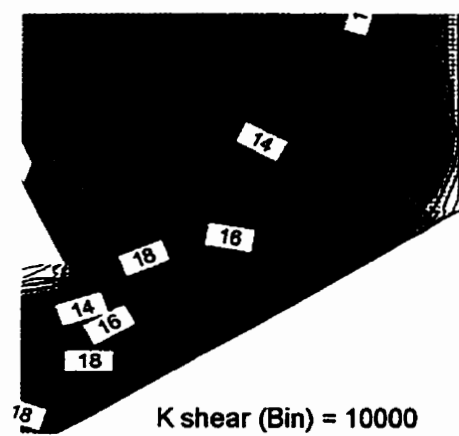
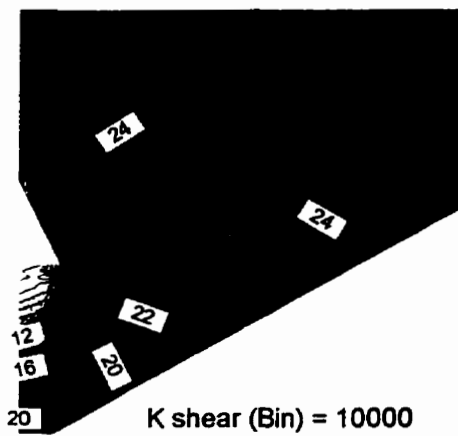
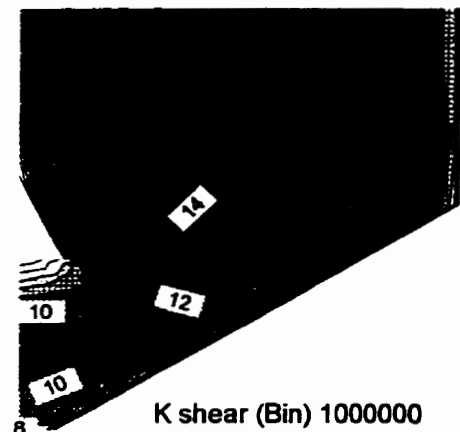
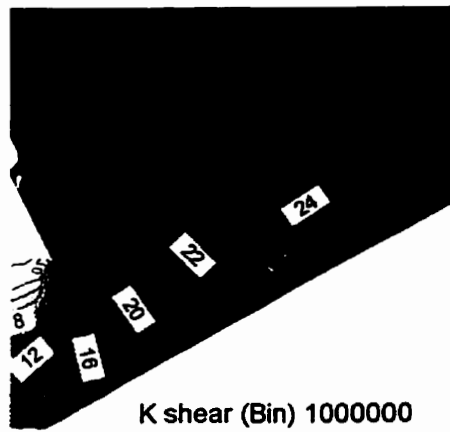


Figure 5.9.(a) Effect of bin wall friction on stress distribution in *farm bin* after filling but prior to draw down initiation. Y-total stress (left column) and x-total stress (right column)

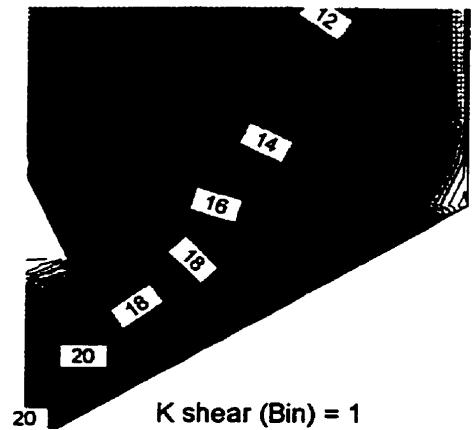
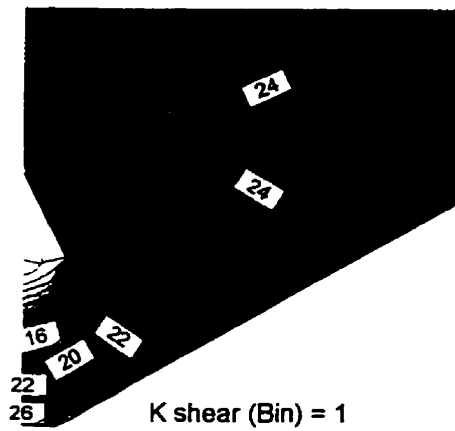
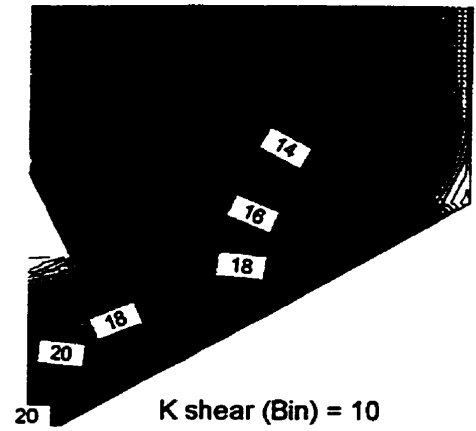
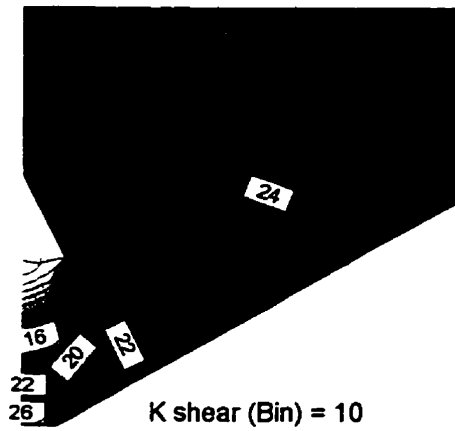


Figure 5.9.(a)

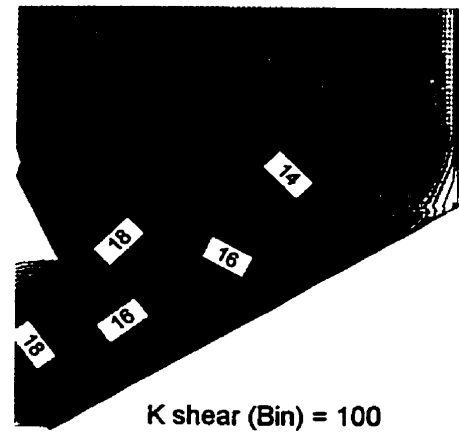
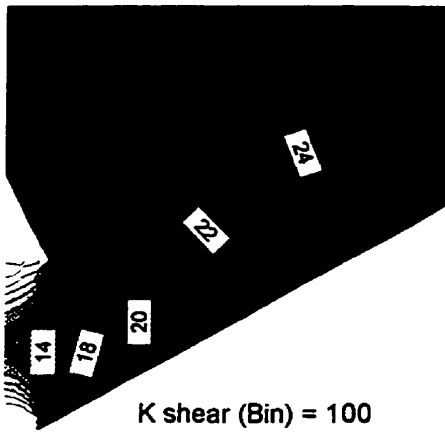
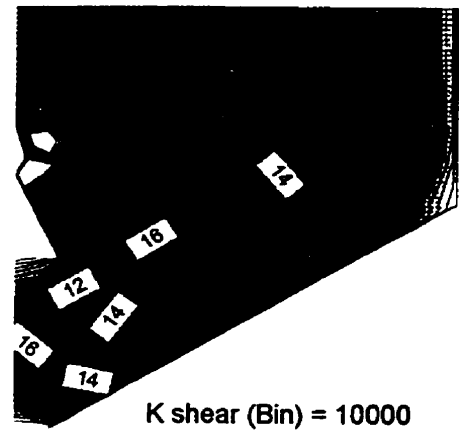
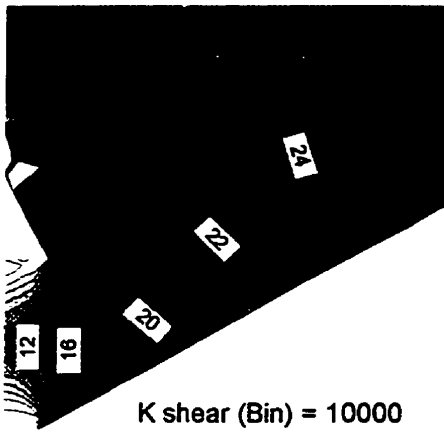
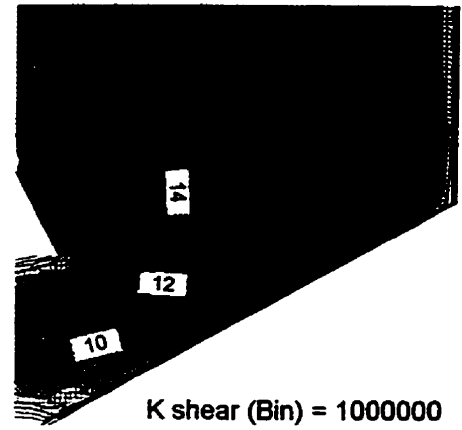
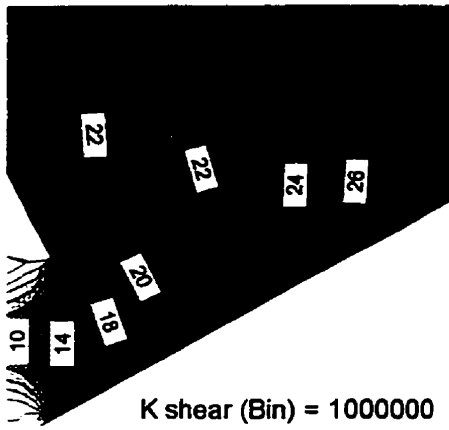
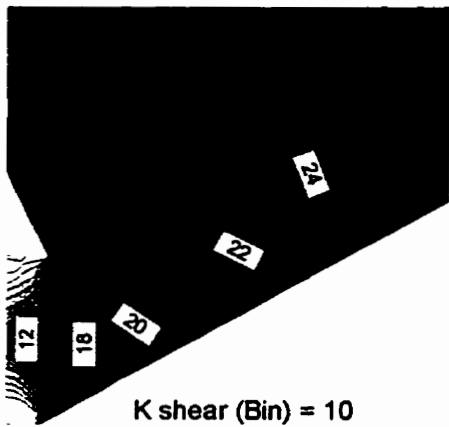
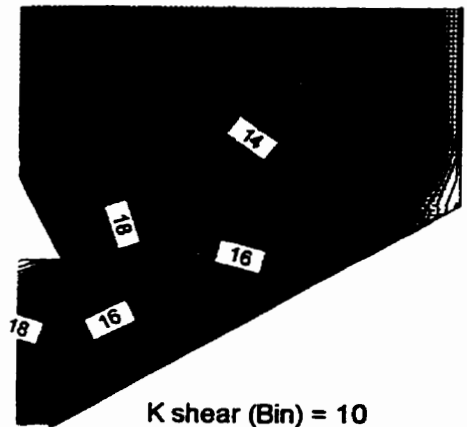


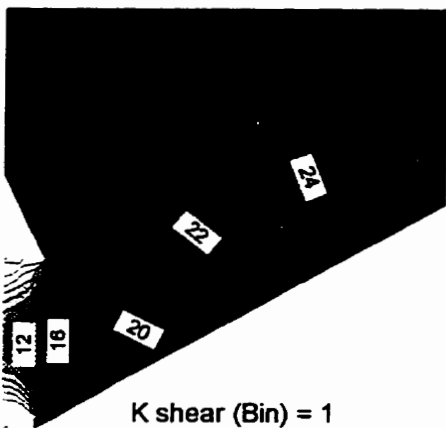
Figure 5.9.(b) Effect of bin wall friction on stress distribution in *farm bin* after draw down initiation. Y-total stress (left column) and x-total stress (right column)



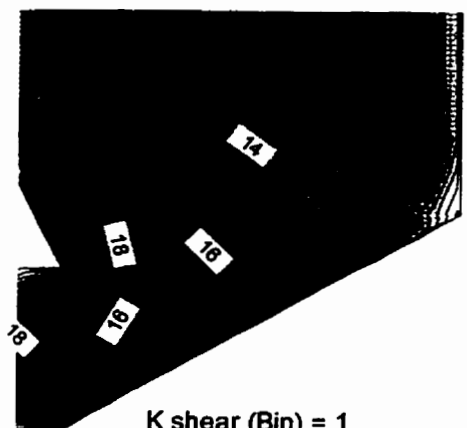
K shear (Bin) = 10



K shear (Bin) = 10



K shear (Bin) = 1



K shear (Bin) = 1

Figure 5.9.(b)

6. CONCLUSIONS

The following conclusions can be drawn from this study:

1. Modified Cam-clay model can be applied to describe the constitutive behaviour of ground feed.
2. Placing an insert inside a storage bin changes the horizontal and vertical stress distribution under the at-rest condition and at the draw-down initiation.
3. Stress distribution in stored material changes with the change in parameter such as insert location, insert size, insert friction, hopper outlet size, hopper slope, and bin wall friction.
4. It was concluded from the simulations for different conditions that:
 - i. Placing an insert at 175 mm ($R/W = 0.18$) from the hopper bottom in *Half bin* results in maximum flowability.
 - ii. Chances of arch formation in a bin decrease when an asymmetric hinged insert is used instead of a symmetric fixed/hinged insert.
 - iii. In *Farm bin*, maximum flowability can be attained by placing insert between 300 ($R/W = 0.18$) and 400mm ($R/W = 0.15$) from the hopper bottom.
 - iv. Flowability increases as insert size is increased to 300mm ($R/W = 0.24$).
 - v. Insert with low surface friction may be used to improve flow behaviour.
 - vi. Flowability increases with increase in size of hopper outlet.
 - vii. As the hopper slope decreases, chances of arch formation increase.
 - viii. Flowability increases with decrease in wall friction.
7. The results of simulation are in concurrence with the experimental results of previous research done by Hao (1998) for a model bin of 2.4 m x 1.0 m. Results of simulation

indicate a similar trend of increase in flowability as the mounting location of insert is moved from 85 to 260 mm from the hopper bottom. Mounting the insert higher up does not improve the flowability. The simulations also indicate that when an asymmetric hinged insert is used in a bin, the chances of arch formation are the least when compared to other mounting methods.

7. RECOMMENDATIONS FOR FUTURE WORK

The study was undertaken with the objective of demonstrating the applicability of modified Cam-clay model to ground feed stored in bins. The study also dealt with determining stress distribution in ground feed when it is stored in a bin and stress distribution at incipient flow condition. Since the results of simulation are in agreement to earlier experiments carried out by Hao (1998), the study has great potential to be extended to problems in storage bins of varying shapes and sizes. The results can also be extended to problems related to structural design of bins. To have a better understanding of bulk material handling and storage, the following studies are recommended:

1. Modified Cam-clay model should be applied to other cohesive powders and results should be compared to actual experiments.
2. Results from simulations need to be substantiated with experimental evidence for frictional parameters.
3. The effect of moisture content on material properties, modified Cam-clay model parameters, and stress distribution needs to be studied to understand stress distribution under varying storage conditions.
4. Asymmetric results in symmetric conditions for mounting method of insert in *Full bin* need to be reinvestigated using other programs/software by carrying out more simulations.
5. The simulations carried out in this study were quasi-static in nature. To simulate stress distribution during flow and to determine flow behaviour after draw-down initiation, the dynamic component needs to be incorporated into the model.
6. More simulations and experiments need to be carried out to get a better understanding of the analogy between stress distribution and flow behaviour.

8. REFERENCES

- Akai, K. and T. Yano. 1985. A contribution to constitutive relation of cohesive soil based on elasto-plastic theory. *Memoirs of the Faculty of Engineering, Kyoto University*, 47(1):58-68.
- ASAE. 1993. ASAE Standards EP 433: Loads Exerted by Free-Flowing Grains on Bins. St. Joseph, MI: ASAE.
- ASAE . 1993. ASAE Standards S352.2:Moisture measurement - Unground Grains and Seeds. St. Joseph, MI: ASAE.
- Ashton, M. D., D. C. H. Cheng, R. Farley, and F.H.H. Valentin. 1965. Some investigations into the strength and flow properties of powders. *Rheologica Acta*, BA and 4, Heft 3, 206-218.
- Askari, A. H. and A. E. Elwi. 1988. Numerical prediction of hopper-bin pressures. *Journal of Engineering Mechanics* 114(2):342-352.
- Atkinson, J. H. and Bransby, P. L. 1978. *The Mechanics of Soils: An Introduction to Critical State Soil Mechanics*, Berkshire, England: McGraw-Hill.
- Bathe, K. J. 1982. *Finite Element Procedures in Engineering Analysis*, New Jersey, NJ: Prentice-Hall.
- Bernache, P. L. 1969. Flow of dry bulk solids on bin walls. *Transactions of the ASME* 91(2):489-496.
- Bin, H. 1998. Effect of insert on velocity profile in a grain bin. Unpublished M.Sc. thesis. Department of Biosystems Engineering, University of Manitoba, Winnipeg, MB.
- Bock, R. G. 1989. Viscoelastic load response of wheat en masse. Unpublished M.S. thesis. The Pennsylvania State University, University Park, PA.
- Bock, R. G., V. M. Puri, and H.B. Manbeck. 1989. Modelling stress relaxation response of wheat en masse using the triaxial test. *Transactions of the ASAE* 32(5):1701-1708.
- Britto, A. M. and M. J. Gunn. 1987. *Critical-state Soil Mechanics via Finite Elements*, West Sussex, England: Ellis Horwood Limited.
- Brown, R. L. and J. C. Richards. 1970. *Principles of Powder Mechanics*. Headington Hill Hall, Oxford: Pergamon Press Ltd.

- Brown, S. B. and G. G. Weber. 1988. A constitutive model for the compaction of metal powders. In *Proceedings of the 1988 International Powder Metal Conference* 18:465-476.
- Bucklin, R. A., S. A. Thompson, and I. J. Ross. 1991. Flow patterns in model flat bottom grain bins. *Transactions of the ASAE* 34(2): 577-585.
- Carson, J. W. and J. Marinelli. 1994. To ensure smooth flow. *Chemical Engineering* 78-90.
- Carter, J. P., J. R. Booker, and C.P. Wroth. 1982. Acritical state soil model for cyclic loading. In *Soil Mechanics-transient and Cyclic Loads*, ed. G.N. Pande and O.C. Zienkewicz, 219-252. New York, NY: John Wiley & Sons.
- Desai, C. S. and H. J. Siriwardane, 1984. *Constitutive Laws for Engineering Materials with Emphasis on Geological Materials*. Englewood Cliffs, NJ: Prentice-Hall Inc.
- Doraively, S. M., H. L. Gegel, J. S. Gunasekera, J. C. Malas, and J. T. Morgan. 1984. A new yield function for compressible P/M materials. *International Journal of Mechanical Science* 26(9/10):527-535.
- Drucker, D.C., and Prager, W. 1952. Soil mechanics and plastic analysis or limit design. *Quart Applied Mathematics* 10(2):157-165.
- Ersov, L. V., and A. A. Lisin. 1964. Methods to improve operations of bunker plants. *Teploenergetika* 11:44-47.
- Gaylord, Edwin H. Jr. and Charles N. Gaylord. 1984. *Design of Steel Bins for Storage of Bulk Solids*. Englewood Cliffs, NJ: Prentice-Hall Inc.
- Giunta, J. S. 1969. Flow patterns of granular materials in flat-bottom bins. *Transactions of the ASME* B91:406-413.
- Hausler, U. and J. Eibl. 1984. Numerical investigations on discharging silos. *Journal of Engineering Mechanics* 110(6):957-971.
- Hirai, H. 1989. A combined hardening model for anisotropically consolidated clays. *Soils and Foundations* 29(3):14-24.
- Hvorslev, M. J. 1969. Physical Properties of Remoulded Cohesive Soils. U. S. Army Corps of Engineers Waterways Express Station., Vicksburg.
- Jenike, A. W. 1964. Storage and flow of bulk solids. Bulletin No. 123. Utah Engineering Experiment Station, University of Utah, Salt Lake City, Utah.

- Jenike, A. W. 1965. Gravity flow of frictional-cohesive solids-convergence to radial stress field. *Transactions of the ASME* March 1965 :205-207.
- Jenike, A. W. and J.R. Johanson. 1969. On the theory of bin loads. *Transactions of the ASME* 91(2):339-344.
- Jenike, A. W. and T. Leser. 1964. A flow no-flow criterion in gravity flow of powders in converging channels. In *Proceedings of the Fourth Congress on Rheology*, 125-141. Brown University.
- Johanson, J. R. 1964. Stress and velocity fields in the gravity flow of bulk solids. *Journal of Applied Mechanics* 13(3):499-506.
- Johanson, J. R. 1966. The use of flow-corrective inserts in bins. *Transactions of the Society of Mining Engineers* 224-230.
- Kvapil, R. and T. Tanaka. 1965. Bins and bunkers with shield inserts. *Aufber Techn* 6:45-49
- Lade, P. V. 1977. Elastic-plastic stress-strain theory for cohesionless soils with curved yield surfaces. *Journal of Soils and Structures* 13:1019-1035.
- Laforge, M. R. and B. K. Boruff. 1964. Profiling flow of particles through hopper openings. *Industrial and Engineering Chemistry* 56(2):42-46.
- Lee, C. A. 1964. Solid feeders. *Chemical Engineering* 71:119-134.
- Li, Y. 1989. Modelling thermally induced cyclic loads in grain bins using elasto-viscoplastic theory for stored granular material. Unpublished Ph.D. thesis, The Pennsylvania State University, University Park, PA.
- Li, Y., V. M. Puri, and H. B. Menbeck. 1990. Elastic-viscoplastic cyclic constitutive model parameter determination and evaluation for wheat en masse. *Transactions of the ASAE* 33(6):1984-1995.
- Li, Y., V. M. Puri, and H. B. Menbeck. 1991. Finite element model prediction of cyclic thermally induced loads in a scaled bin using elasto-viscoplastic constitutive equation. *Transactions of the ASAE* 34(5):2207-2215.
- Link, R. A. and A. E. Elwi. 1990. Incipient flow in silo-hopper configurations. *Journal of Engineering Mechanics* 116(1):172-188.
- Linton, P. F., M. C. McVay, and D. Bloomquist. 1988. Measurement of deformations in the standard triaxial environment with a comparison of local versus global measurements on a fine, fully drained sand. In *Advanced Triaxial Testing of Soil and Rock*, ed. R. T. Donaghe, R. C. Chaney, and M. L. Silver, 202-215. Philadelphia, PA: ASTM.

- Messing, G. L., C. J. Markhoff, and L. G. McCoy. 1982. Characterization of ceramic powder compaction. *American Ceramic Society Bulletin* 61(8):857-860.
- Molerus, O. 1975. Theory of yield of cohesive powders. *Powder Technology* 12(1975):259-275.
- Molerus, O. 1975. Effect of interparticle cohesive forces on the flow behaviour of powders. *Powder Technology* 20(1978):161-175.
- Moriyama, R. 1983. The effect of filling method on the flow pattern in a bin. In *Proceedings of the Second International Conference on Design of Silos for Strength and Flow*, 1:317-331.
- Nagoa, T., Y. Hatamura, H. Matsui, and T. Mikami. 1988. Stress analysis on the compaction of granular materials by FEM. In *Micromechanics of Granular Materials*, ed. M. Satake and J. T. Jenkins, 215-224. Netherland: Elsevier Science Publishers.
- Nova, R. 1981. Mathematical modelling of cyclic behaviour of soils. In *Symposium on Geotechnical Aspects of Coastal and Offshore Structures*, 47-59. Bangkok.
- Nova, R. and D. M. Wood. 1979. A constitutive model for sand in triaxial compression. *International Journal for Numerical and Analytical Methods in Geomechanics* 3:255-278.
- O'Callaghan, J. R. 1960. Internal flow in moving beds of granular material. *Journal of Agricultural Engineering Research* 5:200-217.
- Ooms, M. and A. W. Roberts. 1985. Significant influence of wall friction in the gravity flow silos. *Bulk Solids Handling* 5(6):1271-1277.
- Pariseau, W. G. 1969. Gravity flow of ideally plastic materials through slots. *Transactions of the ASME* 91(2):414-422.
- Pariseau, W. G. and D. E. Nicholson. 1979. Elastic-plastic finite element analysis of hopper filling and flow initiation. In *The Joint ASME-CSME Applied Mechanics, Fluids Engineering and Bioengineering Conference*, ed. S. C. Cowin, 61-77. Niagara Falls, New York.
- Peschl, I. A. S. Z. 1969. Theory of the formation of arches in bins. *Transactions of the ASME* 91(2):423-433.
- Rankine, W. J. M. 1857. On the stability of loose earth. *Philosophical Transactions of the Royal Society*.

- Rappen, A. and H. Wright. 1983. In *Proceedings of the 2nd International Conference on Design of Silos for Strength of Flow* 423-434. Powder Advisory Centre, London.
- Rendulic, L. 1936. Pore-Index and Pore Water Pressure. *Bauingenieur* 17(559).
- Roberts A. W. 1991. Bulk solids handling recent developments and future directions. *Bulk Solids Handling* 11(1):17-35.
- Roscoe, K. H., A. N. Schofield, and A. Thurairajah. 1963. Yielding of clays in states wetter than critical. *Geotechnique* 13(1):211-240.
- Roscoe, K. H., A. N. Schofield, and C. P. Wroth. 1958. On the yielding of soils. *Geotechnique* 8:22-53.
- Schwab, C. V., I. J. Ross, G. M. White, and D. G. Colliver. 1989. Investigation of the grain pressure phenomenon in a full-scale bin, part I: Grain loads and flow characteristics. ASAE Paper No. 89-4007. St. Joseph, MI: ASAE.
- Schweds, Jörg. 1983. Evaluation of bulk solids technology since 1974. *Bulk Solids Handling* 3(1):1-3.
- Shamlou, P. A. 1988. *Handling of Bulk Solids: Theory and Practice*. Essex, England: Butterworth & Co. Ltd.
- Stainforth, P. T. and R. C. Ashley. 1973. An analytical hopper design method for cohesive powders. *Powder Technology* 7(1973):215-243.
- Thompson, R. A. 1981. Mechanics of powder pressing: 1, Model for powder densification; 2, Finite-element analysis of end-capping in pressed green powders; and 3, Model for the green strength of pressed powders. *Ceramic Bulletin* 60(2):237-251.
- Trasorras, J., T. M. Krauss, and B. L. Ferguson. 1989. Modelling of powder compaction using the finite element method. In *Advances in Powder Metallurgy*, ed. T. G. Gasbarre and W. F. Jandeska, 1:85-104. American Powder Metallurgy Institute, Princeton, NJ.
- Tripodi, M. A. 1994. Constitutive models and parameter determination for cohesive dry powders with application to powder compaction. Unpublished Ph.D. thesis. The Pennsylvania State University, University Park, PA.
- Tripodi, M. A., V. M. Puri, H. B. Manbeck, and G. L. Messing. 1994. Triaxial testing of dry, cohesive powder and it's application to a modified Cam-clay constitutive model. *Powder Technology* 80:35-43.

- Tripodi, M. A., V. M. Puri, H. B. Manbeck, and G. L. Messing. 1995. Elastoplastic finite element model for low pressure uniaxial compaction of dry cohesive powders. *Powder Technology* 85:241-251.
- Tüzün, U. and R. M. Nedderman. 1983. Gravity flow of granular materials around obstacles. In *Silos, Hoppers Bins & Bunkers for Storing Bulk Materials*, ed. Reinhard H. Wohlbiel, 117-127. Germany: Trans Tech Publications.
- Weber, G. G. and S. B. Brown. 1989. Simulation of the compaction of powder components. In *Advances in Powder Metallurgy*, ed. T. G. Gasbarre and W. F. Jandeska, 1:105-118. American Powder Metallurgy Institute, Princeton, NJ.
- Williams, J. C., J. M. Head, and J. J. Ahumada. 1983. In *Proceedings of the 2nd International Conference on Design of Silos for Strength of Flow* 401-423. Powder Advisory Centre, London.
- Youngs, R. R. 1982. A three-dimensional effective stress model for cyclic loaded granular soils. Unpublished Ph.D. thesis. The University of California, Berkeley, CA.
- Zhang, Q., V. M. Puri, H. B. Manbeck, and M. C. Wang. 1987. A finite element model for predicting static and thermally induced bin wall pressures. *Transactions of the ASAE* 30(6):1797-1806.5.

APPENDIX A - Formulation in SIGMA/W

A.1. Finite Element Equations

The finite element equation used in the SIGMA/W formulation for a given time increment is,

$$\int_v [B]^T [C] [B] dv \{a\} = b \int_v \langle N \rangle^T dv + p \int_A \langle N \rangle^T dA + \{F_n\} \quad (A.1)$$

where:

$[B]$ = strain-displacement matrix

$[C]$ = constitutive matrix

$\{a\}$ = column vector of nodal incremental x- and y-displacements

A = area along the boundary of an element

v = volume of an element

b = unit body force intensity

$\langle N \rangle$ = row vector of interpolating functions

p = incremental surface pressure

$\{F_n\}$ = concentrated incremental nodal loads

Summation of this equation over all elements is implied. It should be noted the SIGMA/W is formulated for incremental analysis. For each time step, incremental displacements are calculated for the incremental applied load. These incremental values are then added to the values from the previous time step. The accumulated values are reported

in the output files. Using this incremental approach, the unit body force is only applied when an element is included for the first time during an analysis.

For a two-dimensional plane strain analysis, SIGMA/W considers all elements to be of unit thickness. For constant element thickness, t , Equation A.1 can be written as:

$$t \int_A [B]^T [C] [B] dA \{a\} = bt \int_A \langle N \rangle^T dA + pt \int_L \langle N \rangle^T dL \quad (A.2)$$

However, in an axisymmetric analysis, the equivalent element thickness is the circumferential distance about the axis of symmetry. Although the complete circumferential distance is 2π radians times the radial distance, R , SIGMA/W is formulated for one radian (unity). Consequently, the equivalent thickness is R and the finite element equation for the axisymmetric case becomes,

$$\int_A ([B]^T [C] [B] R) dA \{a\} = b \int_A (R \langle N \rangle^T) dA + p \int_L (R \langle N \rangle^T) dL + \{F_n\} \quad (A.3)$$

Unlike the thickness, t , in a two-dimensional analysis, this radial distance, R , is not a constant within an element. Consequently, R needs to be evaluated inside the integral.

In an abbreviated form, the finite element equation is,

$$[K]\{a\} = \{F\} = \{F_b\} + \{F_s\} + \{F_n\} \quad (A.4)$$

where: $[K]$ = element characteristic (or stiffness) matrix

$$= t \int_A ([B]^T [C] [B]) dA \text{ (for plane strain), or}$$

$$= \int_A ([B]^T [C] [B] R) dA \text{ (for axisymmetric)}$$

$\{a\}$ = nodal incremental displacements

$\{F\}$ = applied nodal incremental force which is made up of the following:

$\{F_b\}$ = incremental body forces

$\{F_s\}$ = force due to surface boundary incremental pressures

$$= pt \int_L (< N >^T) dL \quad (\text{plane strain}), \text{ or}$$

$$= p \int_L (R < N >^T) dL \quad (\text{axisymmetric})$$

$\{F_n\}$ = concentrated nodal incremental forces

SIGMA/W solves this finite element equation for each time step to obtain incremental displacements and calculates the resultant incremental stresses and strains. It then sums all these increments since the first time step and reports the summed values in the output files.

A.2. Strain-Displacement Matrix

SIGMA/W uses engineering shear strain in defining the strain vector

$$\{\varepsilon\} = \begin{Bmatrix} \varepsilon_x \\ \varepsilon_y \\ \varepsilon_z \\ \gamma_{xy} \end{Bmatrix} \quad (\text{A.5})$$

The field variable of a stress/deformation problem is displacement which is related to the strain vector through:

$$\{\varepsilon\} = [B] \begin{Bmatrix} u \\ v \end{Bmatrix} \quad (\text{A.6})$$

where:

$[B]$ = strain matrix,

u, v = nodal displacement in x - and y -directions, respectively.

SIGMA/W is restricted to performing infinitesimal strain analyses. For a two-dimensional plane strain problem, ε_z is zero and the strain matrix is defined as:

$$[B] = \begin{bmatrix} \frac{\partial N_1}{\partial x} & 0 & \dots & \frac{\partial N_8}{\partial x} & 0 \\ 0 & \frac{\partial N_1}{\partial y} & \dots & 0 & \frac{\partial N_8}{\partial y} \\ 0 & 0 & \dots & 0 & 0 \\ \frac{\partial N_1}{\partial y} & \frac{\partial N_1}{\partial x} & \dots & \frac{\partial N_8}{\partial y} & \frac{\partial N_8}{\partial x} \end{bmatrix} \quad (\text{A.7})$$

For an axisymmetric problem, the strain matrix can be written as:

$$\{\epsilon\} = \begin{Bmatrix} \epsilon_x \\ \epsilon_y \\ \epsilon_z \\ \gamma_{xy} \end{Bmatrix} = \begin{Bmatrix} \frac{\partial u}{\partial x} \\ \frac{\partial v}{\partial y} \\ \frac{u}{r} \\ \frac{\partial u}{\partial y} + \frac{\partial v}{\partial x} \end{Bmatrix} \quad (\text{A.8})$$

The associated strain matrix $[B]$ is then:

$$[B] = \begin{bmatrix} \frac{\partial N_1}{\partial x} & 0 & \dots & \frac{\partial N_8}{\partial x} & 0 \\ 0 & \frac{\partial N_1}{\partial y} & \dots & 0 & \frac{\partial N_8}{\partial y} \\ \frac{N_1}{R} & 0 & \dots & \frac{N_8}{R} & 0 \\ \frac{\partial N_1}{\partial x} & \frac{\partial N_1}{\partial y} & \dots & \frac{\partial N_8}{\partial x} & \frac{\partial N_8}{\partial y} \end{bmatrix} \quad (\text{A.9})$$

A.3. Elastic Constitutive Relationship

Stresses are related to strains as follows, within the theory of elasticity,

$$\{\sigma\} = [C]\{\epsilon\} \quad (\text{A.10})$$

where $[C]$ is the constitutive (element property) matrix and is given by:

$$[C] = \frac{E}{(1+\nu)(1-2\nu)} \begin{bmatrix} 1-\nu & \nu & \nu & 0 \\ \nu & 1-\nu & \nu & 0 \\ \nu & \nu & 1-\nu & 0 \\ 0 & 0 & 0 & \frac{1-2\nu}{2} \end{bmatrix} \quad (\text{A.11})$$

where:

E = Young's modulus

ν = Poisson's ratio

The $[C]$ matrix is the same for both the two-dimensional plane strain and the axisymmetric cases.

A.4. Body Forces

SIGMA/W can model body forces applied in both the vertical and the horizontal directions. These forces are applied to all elements when they first become active. The body force in the vertical direction, b_v , is due to gravity acting on an element. For a given material, the unit body force intensity in the vertical direction is given by its unit weight, γ_s , which is in turn related to its mass density, ρ :

$$\gamma_s = \rho g \quad (\text{A.12})$$

where g is the gravitational constant. When the unit weight γ_s is non-zero, SIGMA/W

evaluates the integral $\gamma_s \int_v (\langle N \rangle^T) dv$ by numerical integration and applies a vertically downward (negative) force at each node of the element.

Similarly, when the unit body force intensity in the horizontal direction, b_h , is nonzero,

nodal forces in the horizontal direction are computed using $b_h \int_v (\langle N \rangle^T) dv$.

A.5. Numerical Integration

SIGMA/W uses Gauss-Legendre numerical integration (also termed quadrature) to form the element characteristic (or stiffness) matrix $[K]$. The variables are first evaluated at specific points within an element. These points are called integration points or Gauss points. These values are then summed for all the Gauss points within an element. This mathematical procedure is as described in the following.

To carry out numerical integration, SIGMA/W replaces the following integral from Equation A.2,

$$\int_A [B]^T [C] [B] dA$$

with the following equation:

$$\sum_{j=1}^n [B_j]^T [C_j] [B_j] \det |J_j| W_j \quad (A.13)$$

where:

j = integration point

n = total number of integration points or integration order

$\det |J_j|$ = determinant of the Jacobian matrix

W_{1j}, W_{2j} = weighting factors

Tables A.1. to A.4. show the numbering scheme and location of integration points used in SIGMA/W for various element types.

Table A.1. Sample point locations and weightings for four point quadrilateral element

Point	r	s	w ₁	w ₂
1	+0.57735	+0.57735	1.0	1.0
2	-0.57735	+0.57735	1.0	1.0
3	-0.57735	-0.57735	1.0	1.0
4	+0.57735	-0.57735	1.0	1.0

Table A.2. Sample point locations and weightings for nine point quadrilateral element

Point	r	s	w ₁	w ₂
1	+0.77459	+0.77459	5/9	5/9
2	-0.77459	+0.77459	5/9	5/9
3	-0.77459	-0.77459	5/9	5/9
4	+0.77459	-0.77459	5/9	5/9
5	0.00000	+0.77459	8/9	5/9
6	-0.77459	0.00000	5/9	8/9
7	0.00000	-0.77459	8/9	5/9
8	+0.77459	0.00000	5/9	8/9
9	0.00000	0.00000	8/9	8/9

Table A.3. Sample point location and weighting for one point triangular element

Point	r	s	w ₁	w ₂
1	0.33333	0.33333	1.0	0.5

Table A.4. Sample point locations and weightings for three point triangular element

Point	r	s	w ₁	w ₂
1	0.16666	0.16666	1/3	1/2
2	0.66666	0.16666	1/3	1/2
3	0.16666	0.66666	1/3	1/2

The appropriate integration order is dependent on the number of secondary nodes. When secondary nodes are present, the interpolating functions are non-linear and consequently a higher integration order is required. Table A.5. gives the acceptable integration order for various element types.

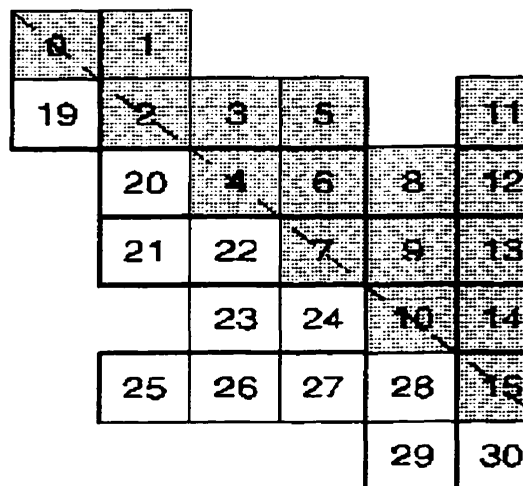
Table A.5. Acceptable element integration orders

Element Type	Secondary Nodes	Integration
		Order
Quadrilateral	no	4
Quadrilateral	yes	9
Triangular	no	1
Triangular	yes	3

A.6. Assemblage of Global Equations

SIGMA/W SOLVE assembles and stores the global finite element equations in a one-dimensional array. Figure A.1. illustrates this storage scheme. The numbers in each box represent the position of the coefficients in the one-dimensional array. Since coefficients above the skyline are zeroes, only the coefficients below the skyline need to be stored.

Figure A.1. Storage scheme for global characteristic matrix



In most cases, the global characteristic (stiffness) matrix is symmetrical, and only the upper-half of the matrix, including the diagonal elements, needs to be stored.

A.7. Equation Solver

SIGMA/W uses Gauss elimination techniques to solve the finite element equations. This involves reducing the coefficient matrix to an upper triangular matrix. The unknown field variables are then calculated by back-substitution. The field variables in SIGMA/W are the nodal displacements in the x - and y -directions. SIGMA/W has two equation solvers: one for symmetric global matrices and one for non-symmetric global matrices. The appropriate solver is chosen automatically according to analysis type and material parameters. Both equation solvers can accommodate missing elements in the global characteristic matrix. This feature makes it possible to add and delete elements from a finite element mesh without renumbering the nodes and elements. In this way, it is possible to simulate fill placement.

A.8. Element Stresses

SIGMA/W computes the stresses and strains at each integration point within each element once the nodal displacements have been obtained. Strains are computed from nodal displacements using Equation A.6. Stresses are computed at each Gauss point using the constitutive matrix $[C]$ in the following manner:

$$\begin{Bmatrix} \sigma_x \\ \sigma_y \\ \sigma_z \\ \tau_{xy} \end{Bmatrix} = [C] \begin{Bmatrix} \epsilon_x \\ \epsilon_y \\ \epsilon_z \\ \gamma_{xy} \end{Bmatrix} \quad (\text{A.14})$$

A.9. Nonlinear Analysis

SIGMA/W is capable of performing analysis involving nonlinear material properties. The finite element equilibrium Equation A.4 is derived for a linear static case. For nonlinear material properties, the global stiff matrix, $[K]$, is no longer linear and iterations are required to achieve an acceptable solution. Additional information on the procedure for nonlinear analysis can be found in finite element text-books such as Bathe (1982), and Zienkiewicz and Taylor (1991).

In general, the basic problem in a nonlinear analysis is to find the state of equilibrium of a body corresponding to the externally applied loads. If these loads are a function of time, at time t the nonlinear equilibrium problem can be formulated as a solution of the following equation:

$$\{ {}^t\Psi \} = \{ {}^tR(a) \} - \{ {}^tF \} = 0 \quad (\text{A.15})$$

where:

Ψ = nodal unbalanced loads,

F = externally applied nodal loads,

R = nodal loads due to element stresses, and,

a = nodal displacements.

It is assumed that the solution will start from an equilibrium (or, at least, near equilibrium)

state such that $\{ \Psi^{-1} \}$ is approximately zero. The vector $\{ R \} = \int [B] \{ \sigma \} dv$ is calculated

based on the internal element stresses as described previously in this chapter. In SIGMA/W, external applied loads are described using continuous spline functions, which describe the total load being applied on the system versus time. Therefore, for a particular time increment t , $\{^t F\}$ is an incremental load obtained by the difference between the value of the load functions evaluated at time t and at time $t-1$. SIGMA/W solves Equation A.15 iteratively using the Newton-Raphson technique which approximates this equation as:

$$\{\Psi^{i+1}\} = \{\Psi^i\} + \left[\frac{\partial \Psi^i}{\partial \alpha} \right] \{\delta \alpha^i\} \quad (\text{A.16})$$

where i is the iteration counter and the superscript t has been omitted for clarity. To start the iteration process for time step t , displacements at the end of the previous time step (i.e., time $t-1$) are used as the initial estimate:

$${}^t a^1 = {}^{t-1} a \quad (\text{A.17})$$

If the derivative term in Equation A.16 is written as:

$$\left[\frac{\partial \Psi}{\partial \alpha} \right] = \left[\frac{\partial R}{\partial \alpha} \right] = [K_T] \quad (\text{A.18})$$

where:

$[K_T]$ = the tangential stiffness matrix.

The iterative correction applied to the nodal displacements can be calculated as:

$$[K_T^i] \{\delta a^i\} = -\{\Psi^i\} \quad (\text{A.19})$$

or

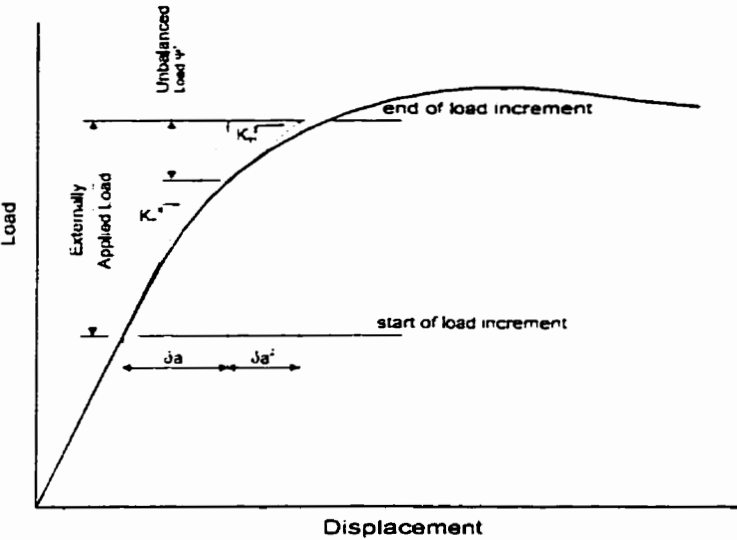
$$\{\delta a^i\} = -[K_T^i]^{-1} \{\Psi^i\} \quad (\text{A.20})$$

A series of successive iterations gives the following result:

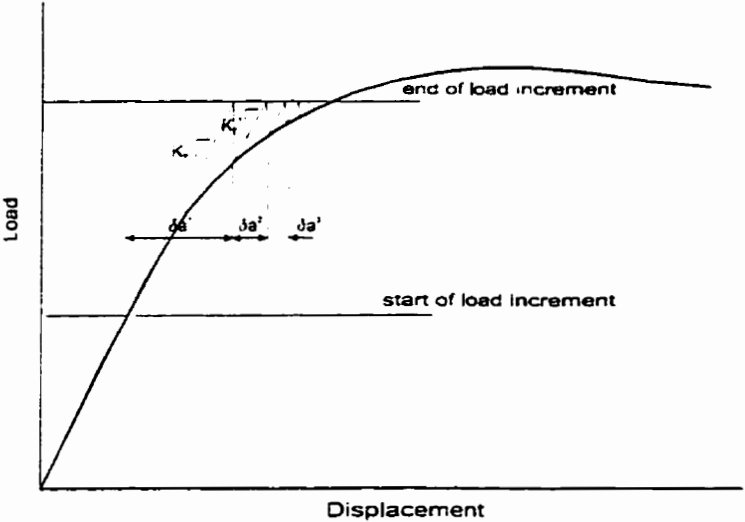
$$\{^t a^{i+1}\} = \{^t a^i\} + \sum_{k=1}^i \{\delta a^k\} \quad (\text{A.21})$$

In the Newton-Raphson method, the stiffness matrix is tangential to the load-displacement curve and is updated every iteration. This process is illustrated in Figure A.2(a). For an analysis involving strain-softening materials, this process is modified such that the stiffness matrix is not updated but the stiffness matrix used in the first iteration is retained throughout the time step, as illustrated in Figure A.2(b). In order to achieve stability in SIGMA/W, the initial modulus is always calculated based on elastic behaviour.

Figure A.2. Iteration schemes for non-linear analysis



a) Iteration Scheme Using Tangential Modulus



b) Iteration Scheme Using Constant (Initial) Modulus

It should be noted that the load term is the externally applied load for the first iteration in a load step; and the load term is the unbalanced load for subsequent iterations.

Incremental displacements resulting from increment load $\{^tF\}$ at time t are obtained

upon solving Equation A.15. These incremental displacements are added to the displacements at the beginning of the time increment. In the displacement output files, SIGMA/W reports the total displacements at each node since the beginning of an analysis at Time Step 1.

A.10. Convergence Criteria

Two convergence criteria, the displacement convergence criterion and the unbalanced load criterion, can be used in SIGMA/W to control the iteration process. When a convergence criterion is satisfied, the analysis is considered to have converged (or achieved convergence) and SIGMA/W will stop the iteration process and go to the next time step.

Both criteria are expressed as the Euclidean norm of a vector quantity. The (Euclidean) norm of a vector is a measure of its magnitude and is defined as:

$$\|d\| = \left(\sum_{i=1}^n d^2 \right)^{1/2} \quad (\text{A.22})$$

where:

$\|d\|$ = the norm of a vector quantity d

d = a vector quantity, for example, incremental nodal displacement for a particular iteration

n = the size of that vector.

For example, the norm of nodal displacements, $\|\delta a\|$, is given by:

$$\|\delta \mathbf{a}\| = \sqrt{\sum_{n=1}^N (\delta a_{xn}^2 + \delta a_{yn}^2)} \quad (\text{A.23})$$

where:

N = total number of nodes

δa_{xn} = incremental x -displacement at node n

δa_{yn} = incremental y -displacement at node n

The displacement convergence criterion compares the norm of incremental displacements in an iteration to the norm of the accumulated incremental displacements in a time step. This criterion is expressed as a ratio in percentages, for the i -th iteration, it can be expressed as:

$$\frac{\|\delta \mathbf{a}'\|}{\|\mathbf{a}\|} \times 100\% \leq \varepsilon_d \quad (\text{A.24})$$

where:

ε_d = a user-defined tolerance number

\mathbf{a} = accumulated nodal displacements in the load step = $\sum_{k=1}^{i-1} \delta \mathbf{a}^k$

$\delta \mathbf{a}$ = the vector of nodal increment displacements for the i -th iteration

The unbalanced load convergence criterion compares the norm of unbalanced load in an iteration to the norm of the externally applied load in a time step. This criterion is also expressed as a ratio in percentages, for the i -th iteration, it can be expressed as:

$$\frac{\|\Psi^i\|}{\|F\|} \times 100\% \leq \varepsilon_f \quad (\text{A.25})$$

where:

ε_f = a user-defined tolerance number

Ψ^i = nodal unbalanced load for the i -th iteration

F = applied increment load for the load step

A.11. Evaluation of the Plastic Matrix, Cam-clay Model

To evaluate the plastic matrix, $[C_p]$, for the Cam-clay model, it is necessary

to compute the elastic matrix $[C_e]$, the vector of derivatives of the yield function, $\left\{ \frac{\partial F}{\partial \sigma'} \right\}$,

the derivative terms $\frac{\partial F}{\partial \hat{\phi}'_x}$, $\frac{\partial \hat{\phi}'_x}{\partial v^p}$ and F_m , and the initial specific volume, v_0 . For given values

of the effective stress Young's modulus, E' , and Poisson's ratio, ν' , the elastic matrix,

$[C_e]$, is the same as that for a linear elastic model. The Poisson's ratio, ν' , is a constant value

input by the user, while the modulus, E , is calculated from the slope of the overconsolidation line, κ .

The slope of the overconsolidation line, κ , can be written as:

$$\kappa = -\frac{dv}{d \ln p'} = -p' \frac{dv}{dp'} \quad (\text{A.26})$$

A change in volumetric strain is related to a change in specific volume through the following equation.

$$d\varepsilon_v = -\frac{dV}{V} = -\frac{de}{1+e} = -\frac{dv}{v} \quad (\text{A.27})$$

where:

V = total volume

e = void ratio of the soil

Combining Equations A.26 and A.27, the following expression for the incremental volumetric strain is obtained.

$$d\varepsilon_v = \left(\frac{\kappa}{vp'}\right) dp' \quad (\text{A.28})$$

By definition, the effective bulk modulus, K' , is given by

$$K' = \frac{dp'}{d\varepsilon_v} \quad (\text{A.29})$$

The bulk modulus, K' , can also be expressed in terms of K .

$$K' = \frac{\nu p'}{\kappa} = \frac{(1+e)p'}{\kappa} \quad (\text{A.30})$$

In turn, the following expression is obtained for the effective stress modulus E' .

$$E' = 3K'(1-2\nu) = \frac{3p'}{\kappa}(1+e)(1-2\nu) \quad (\text{A.31})$$

The vector of derivatives of yield function with respect to stresses is:

$$\left\{ \frac{\partial F}{\partial \sigma'} \right\} = \left\langle \frac{\partial F}{\partial \sigma'_x} \quad \frac{\partial F}{\partial \sigma'_y} \quad \frac{\partial F}{\partial \sigma'_z} \quad \frac{\partial F}{\partial \tau'_{xy}} \right\rangle^T \quad (\text{A.32})$$

These derivatives can be expressed as derivatives with respect to stress invariants I_1' and J_2 using the chain rule of differentiation.

$$\begin{aligned}\frac{\partial F}{\partial \sigma'_i} &= \frac{\partial F}{\partial p'} \frac{\partial p'}{\partial \sigma'_i} + \frac{\partial F}{\partial q} \frac{\partial q}{\partial \sigma'_i} \\ &= \frac{\partial F}{\partial p'} \frac{\partial p'}{\partial \sigma'_i} + \sqrt{3} \frac{\partial F}{\partial q} \frac{\partial J_2}{\partial \sigma'_i}\end{aligned}\tag{A.33}$$

where:

i = stress components x, y, z and xy

By definition, $q = \sqrt{3J_2}$. The derivatives of the yield function F with respect to the stress invariants are expressed as follows:

$$\begin{aligned}\frac{\partial F}{\partial p'} &= -\frac{q}{Mp'^2} + \frac{1}{p'} \\ \frac{\partial F}{\partial q} &= \frac{1}{Mp'}\end{aligned}\tag{A.34}$$

The remaining terms in the plastic matrix $[C_p]$, $\frac{\partial F}{\partial p'_x}$, $\frac{\partial p'_x}{\partial v^p}$, v_0 , and F_m , are described in the following equations.

$$\frac{\partial F}{\partial p'_x} = -\frac{1}{p'_x}\tag{A.35}$$

$$\frac{\hat{\phi}'_x}{\hat{\alpha}^p} = \frac{p'_x}{\lambda - \kappa} \quad (\text{A.36})$$

$$\begin{aligned} F_m &= \frac{\partial \mathcal{F}}{\partial \sigma'_x} + \frac{\partial \mathcal{F}}{\partial \sigma'_y} + \frac{\partial \mathcal{F}}{\partial \sigma'_z} \\ &= \frac{\partial \mathcal{F}}{\partial p'} \left(\frac{\hat{\phi}'_x}{\hat{\alpha} \sigma'_x} + \frac{\hat{\phi}'_y}{\hat{\alpha} \sigma'_y} + \frac{\hat{\phi}'_z}{\hat{\alpha} \sigma'_z} \right) + \frac{\partial \mathcal{F}}{\partial q} \left(\frac{\hat{\alpha} q}{\hat{\alpha} \sigma'_x} + \frac{\hat{\alpha} q}{\hat{\alpha} \sigma'_y} + \frac{\hat{\alpha} q}{\hat{\alpha} \sigma'_z} \right) \\ &= \frac{\partial \mathcal{F}}{\partial p'} (1) + \frac{\partial \mathcal{F}}{\partial q} (0) \\ &= -\frac{q}{M p'^2} + \frac{1}{p'} \end{aligned} \quad (\text{A.37})$$

A.12. Slip Surface Element

SIGMA/W can simulate a slip surface using four-noded quadrilateral elements with Slip Surface as its soil model. Using the Slip Surface material model, a user can specify stiffness in two orthogonal directions. These directions are parallel and perpendicular to the long side of the element. Figure A.3. shows a typical slip surface element with its long (x') axis inclined at angle β from the global x -axis with nodes numbered as 1, 2, 3 and 4. SIGMA/W treats a slip surface element as a combination of four bar elements. For example, for the element illustrated in Figure A.3., there are two bar elements with stiffness, K_n , in the local normal y' -direction, 1-4 and 2-3; and two bar elements in the local tangential x' -direction, 1-2 and 4-3, with stiffness K_t . K_t and K_n are the user-specified tangential and normal stiffness for the element.

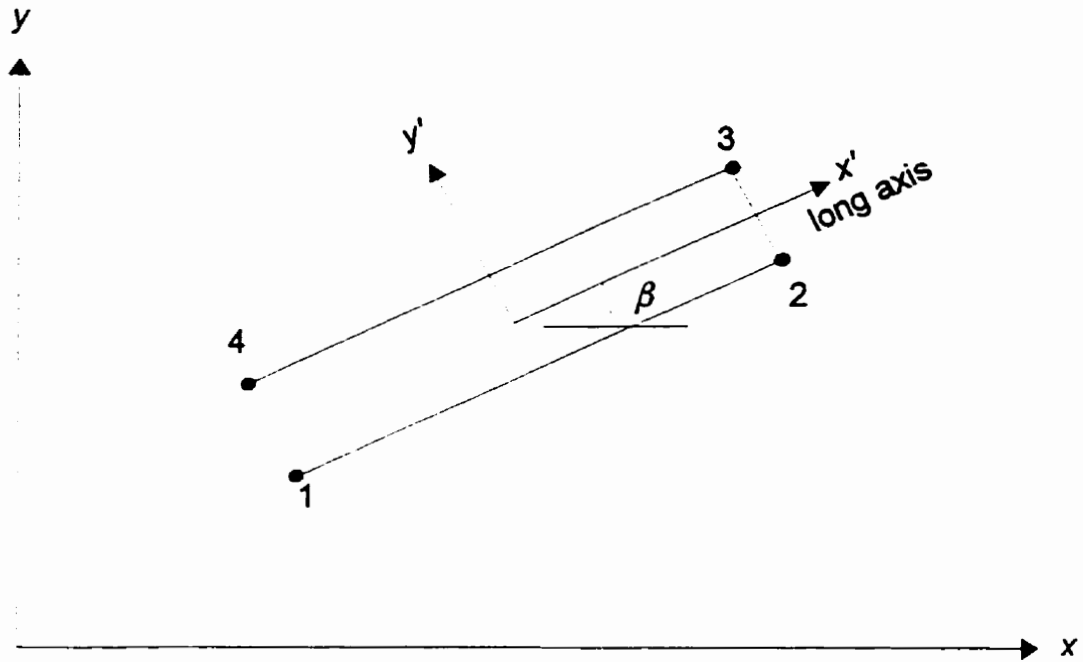


Figure A.3. A typical slip surface element

When formulating the element stiffness matrix $[K]$, instead of evaluating the integral

$\int [B]^T [C] [B] dv$, SIGMA/W first forms the local stiffness matrix $[K']$ by assigning stiffness

values K_t or K_n directly to the appropriate location in the matrix. For the element illustrated

in Figure A.3., its local stiffness matrix, $[K']$, in the local $(x'-y')$ coordinate system is:

$$\begin{bmatrix} K_t & 0 & -K_t & 0 & 0 & 0 & 0 & 0 \\ 0 & K_n & 0 & 0 & 0 & 0 & 0 & -K_n \\ -K_t & 0 & K_t & 0 & 0 & 0 & 0 & 0 \\ 0 & 0 & 0 & K_n & 0 & -K_n & 0 & 0 \\ 0 & 0 & 0 & 0 & K_t & 0 & -K_t & 0 \\ 0 & 0 & 0 & -K_n & 0 & K_n & 0 & 0 \\ 0 & 0 & 0 & 0 & -K_t & 0 & K_t & 0 \\ 0 & -K_n & 0 & 0 & 0 & 0 & 0 & K_n \end{bmatrix}$$

$[K']$ is then rotated to the global coordinate system to obtain $[K]$ using the following transformation:

$$[K] = [T][K'][T]^T \quad (\text{A.39})$$

where:

$$[T] = \begin{bmatrix} \cos^2 \beta & \sin^2 \beta & 0 & -2\sin\beta\cos\beta \\ \sin^2 \beta & \cos^2 \beta & 0 & 2\sin\beta\cos\beta \\ 0 & 0 & 1 & 0 \\ \sin\beta\cos\beta & -\sin\beta\cos\beta & 0 & \cos^2 \beta - \sin^2 \beta \end{bmatrix}$$

When the normal stress on a slip is zero or tensile (negative), the stiffness values are reduced by a factor of 0.001.

APPENDIX B - Results of experiments

B.1. Triaxial Tests

B.1.1. Drained Tests

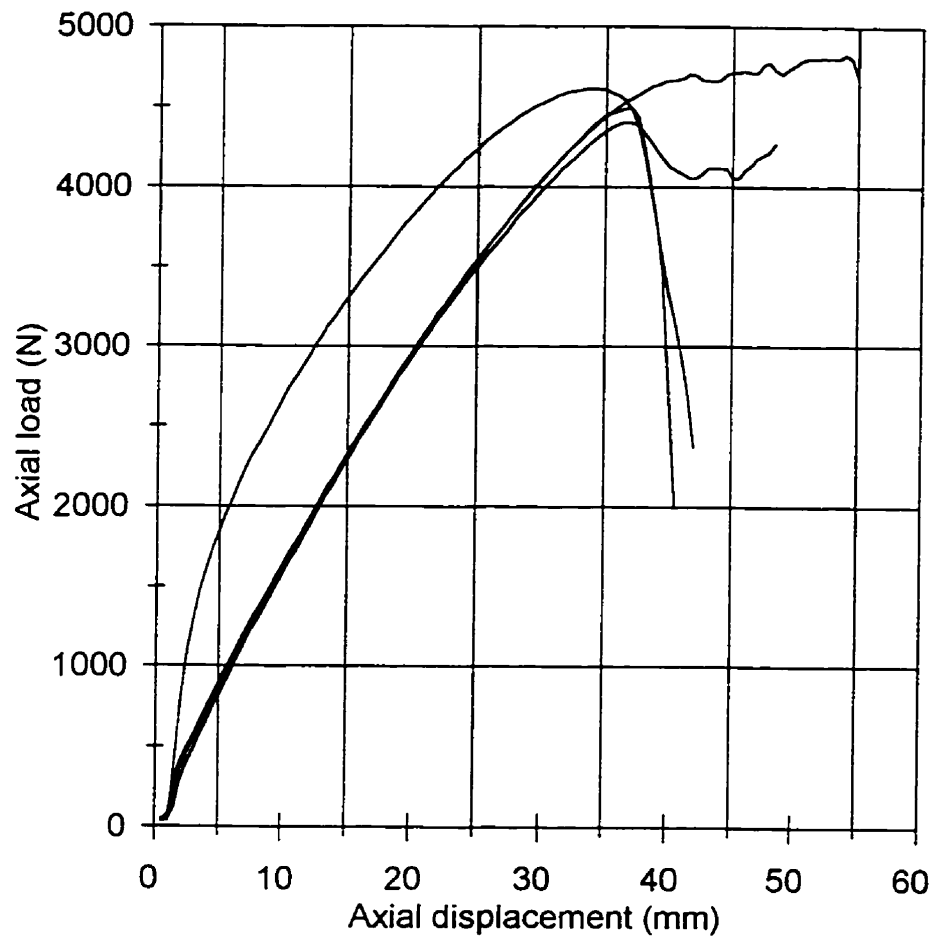


Figure B.1.(a) Drained tests at 100 kPa

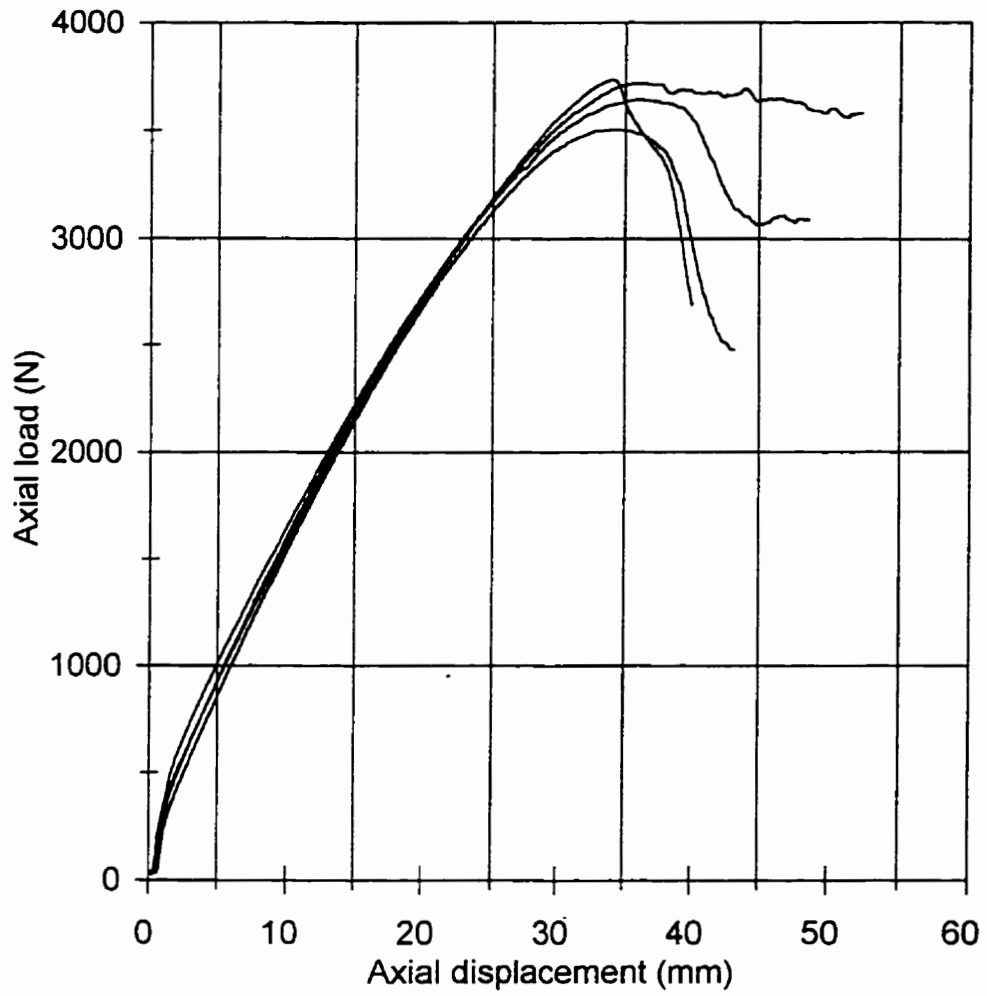


Figure B.1.(b) Drained tests at 75 kPa

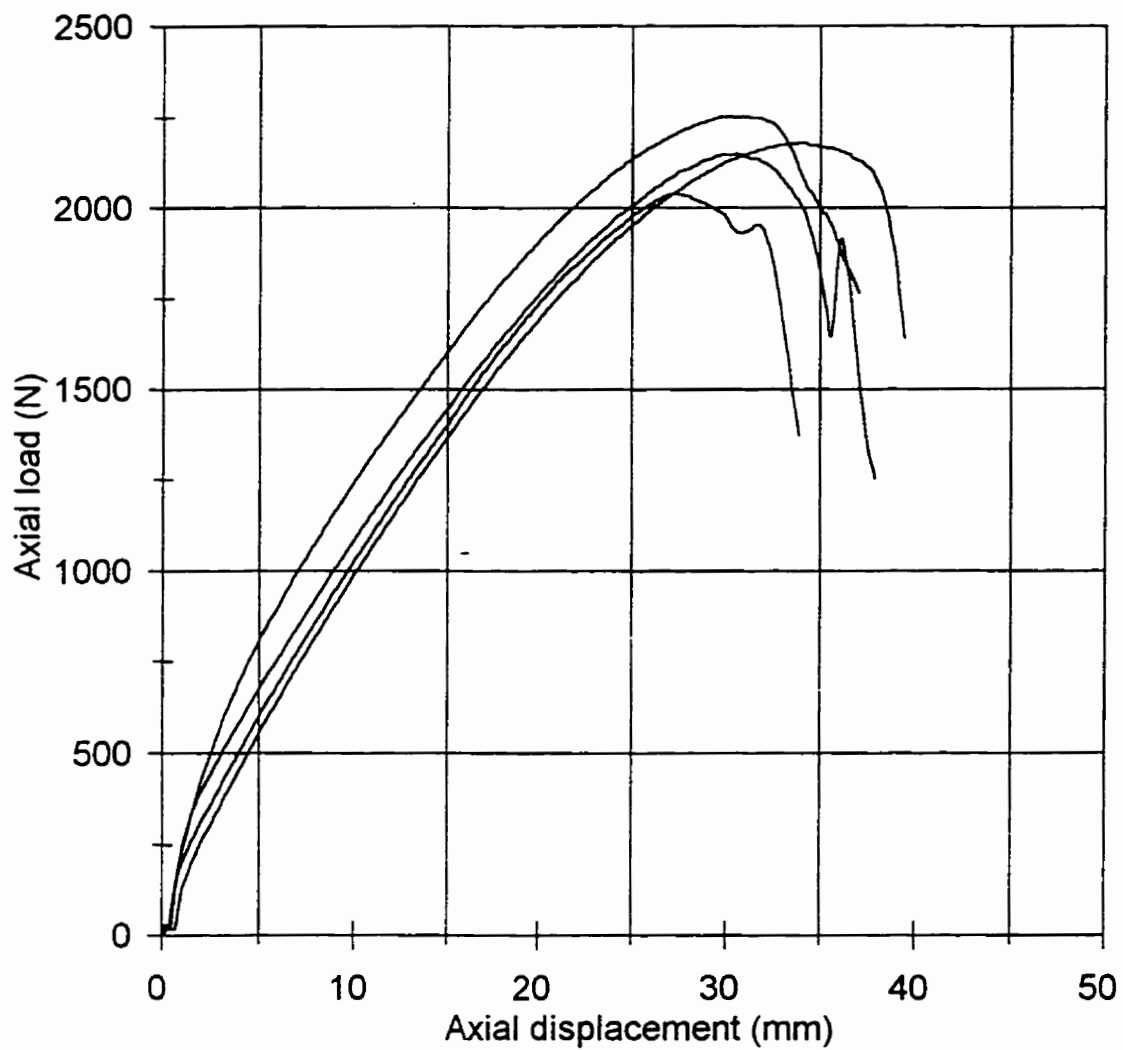


Figure B.1.(c) Drained tests at 40 kPa

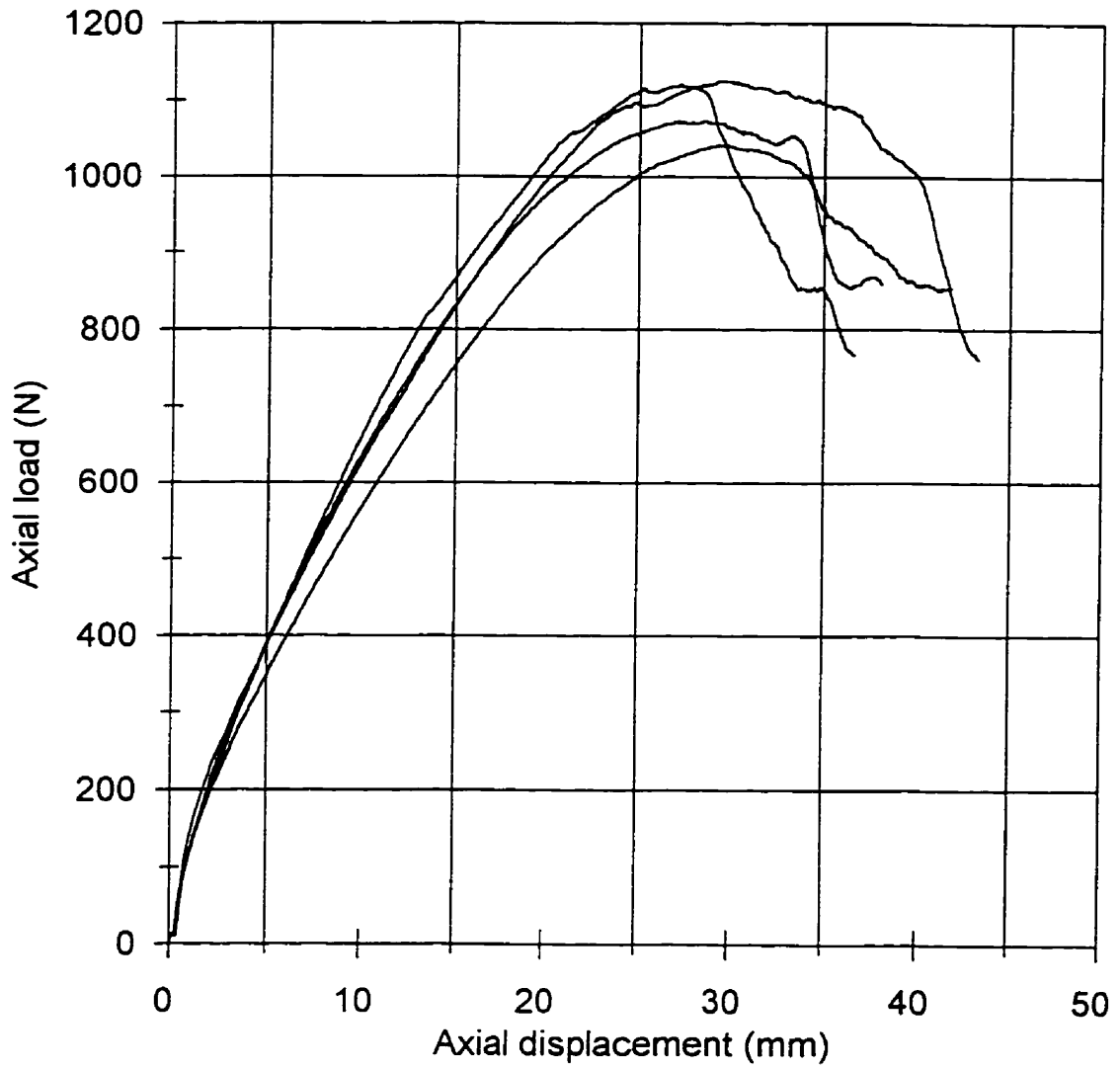


Figure B.1.(d) Drained tests at 20 kPa

B.1.2. Undrained Tests

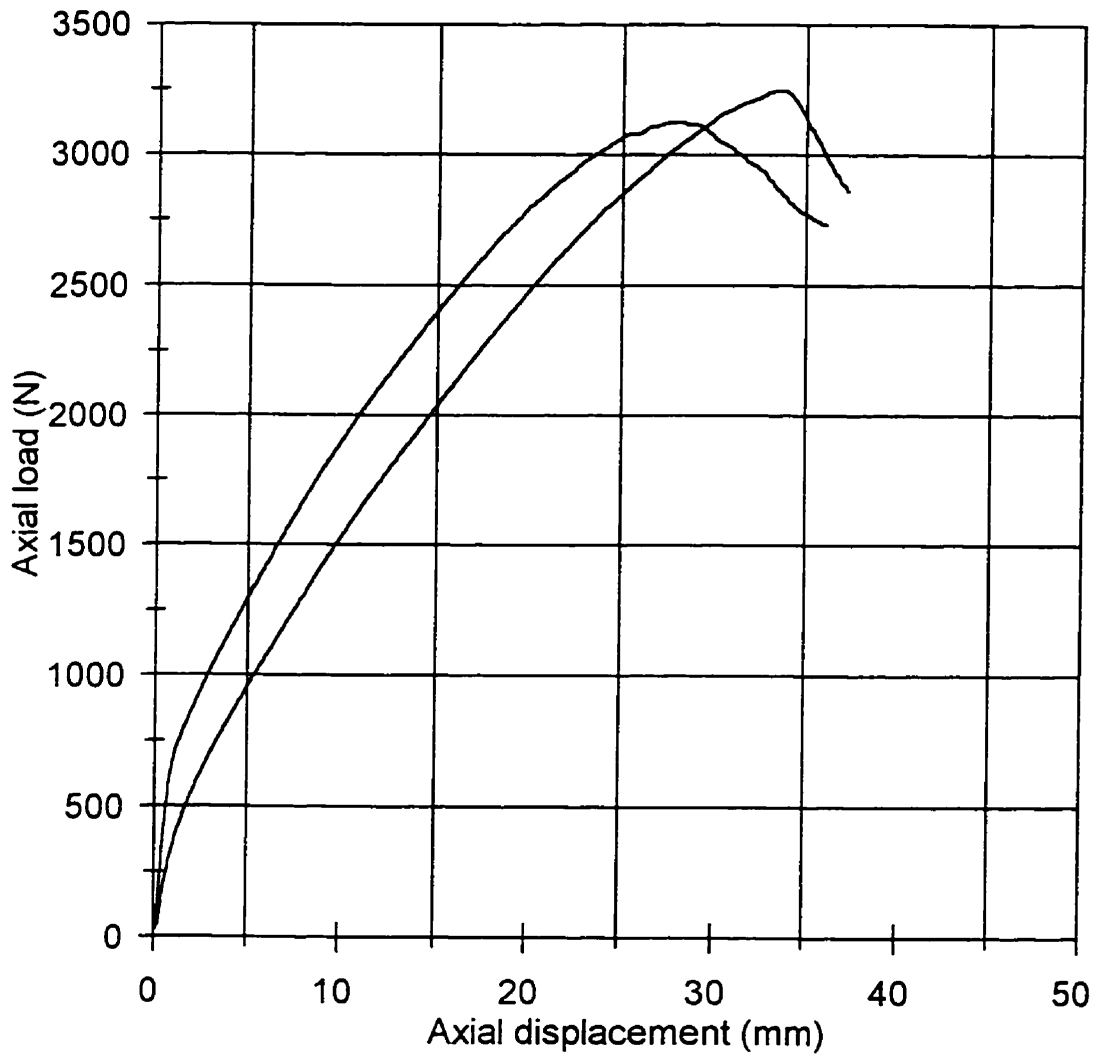


Figure B.2.(a) Undrained tests at 100 kPa

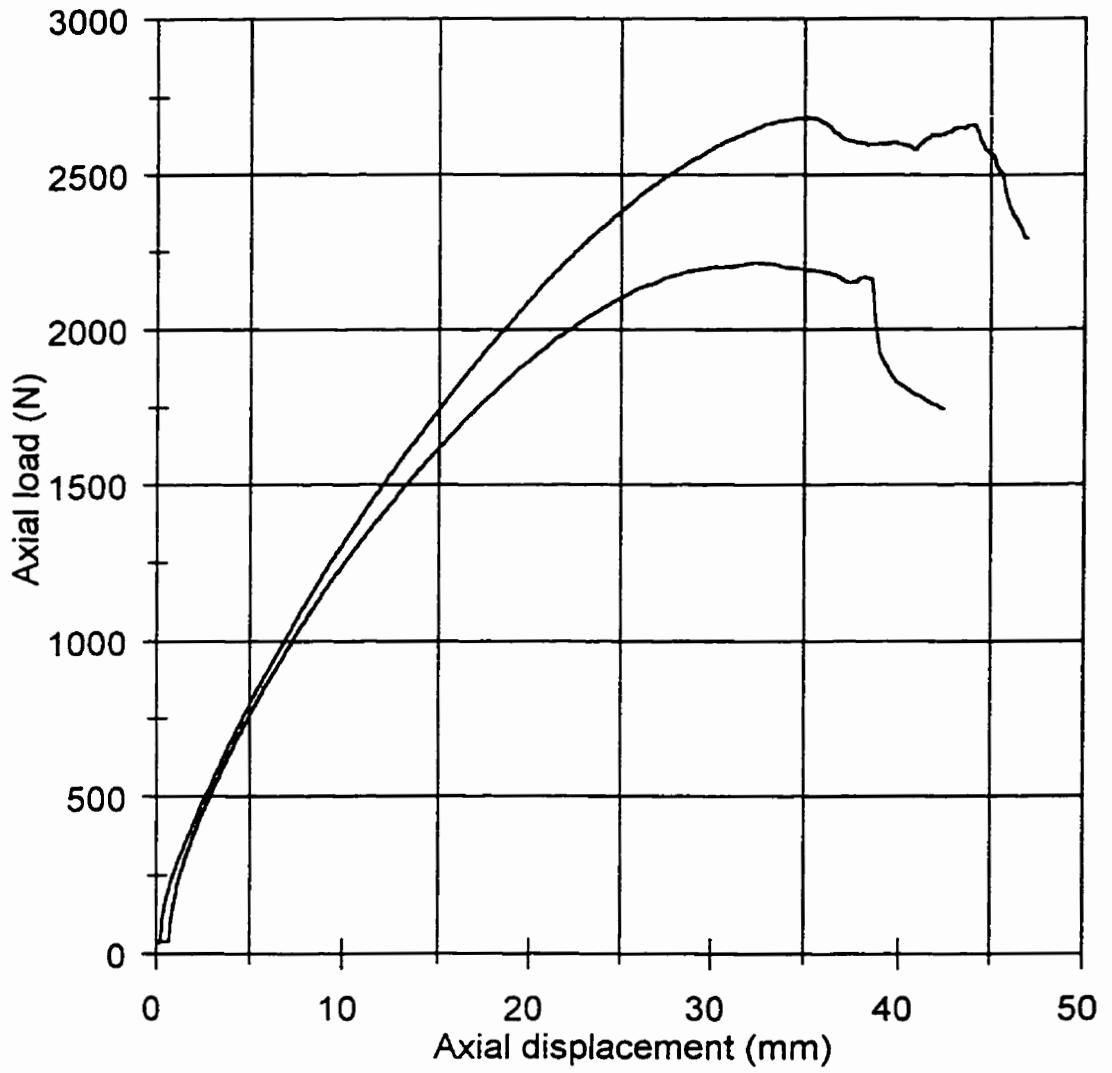


Figure B.2.(b) Undrained tests at 75 kPa

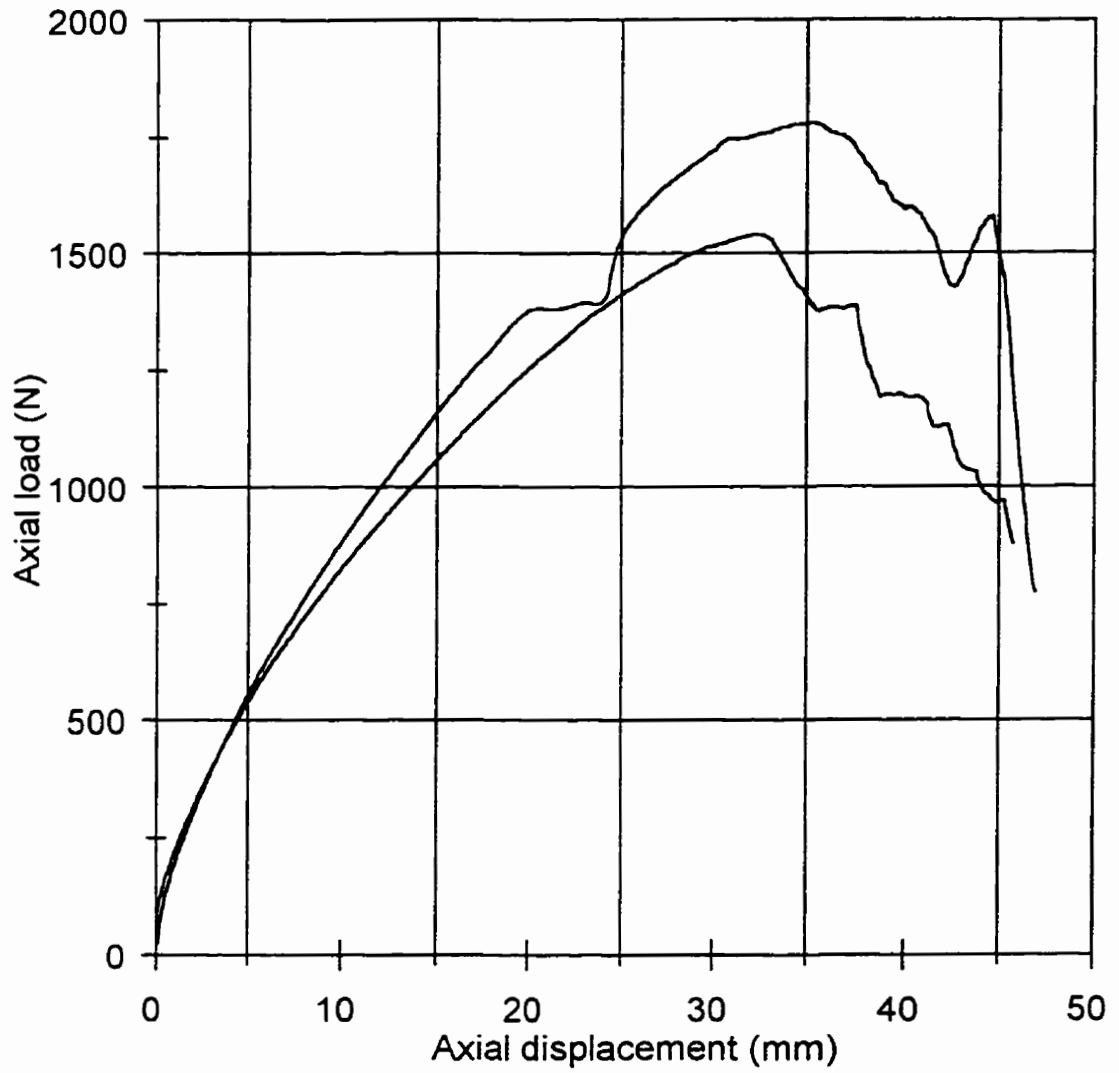


Figure B.2.(c) Undrained tests at 40 kPa

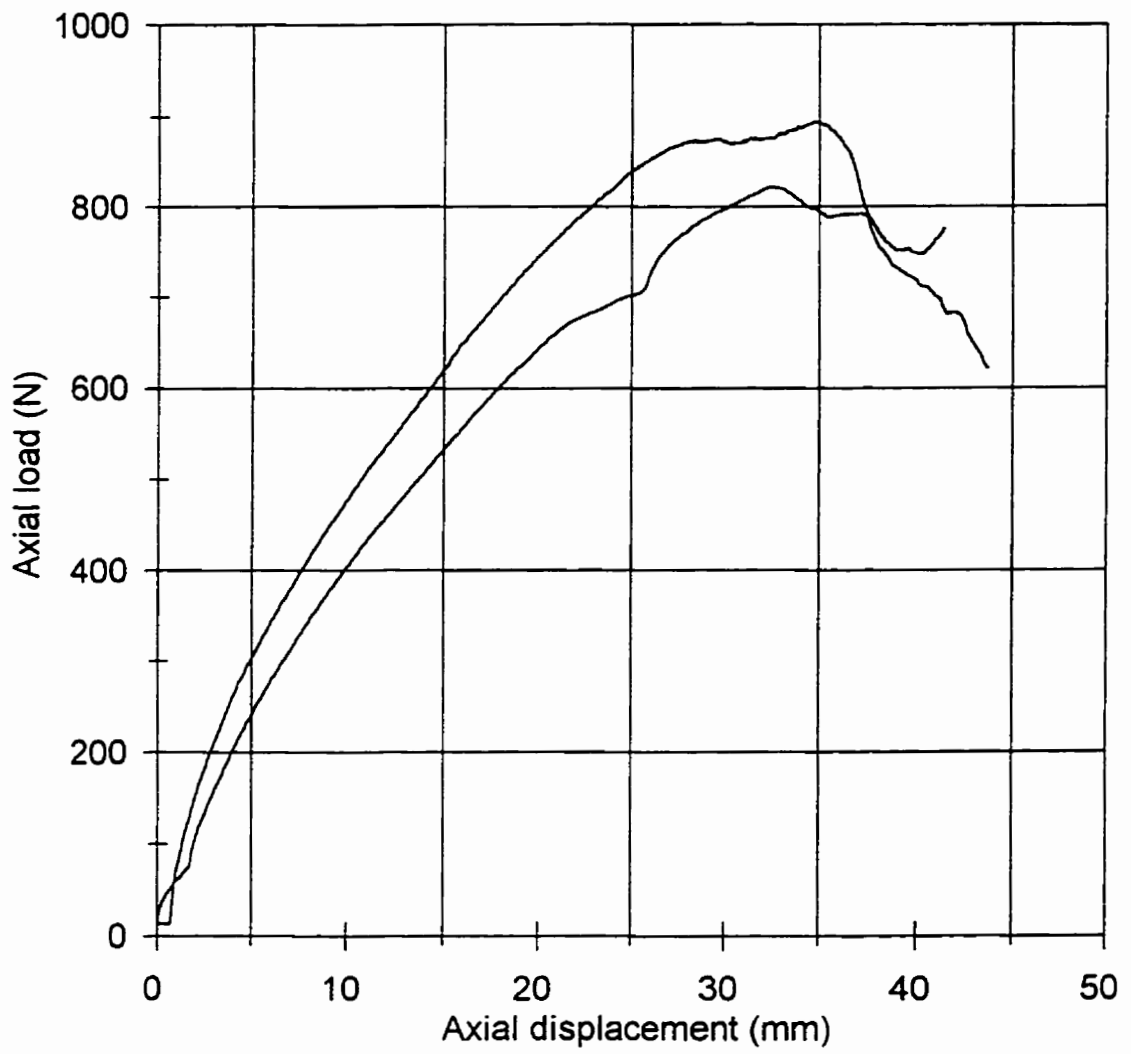


Figure B.2.(d) Undrained tests at 20 kPa

B.1.3. Isotropic Tests

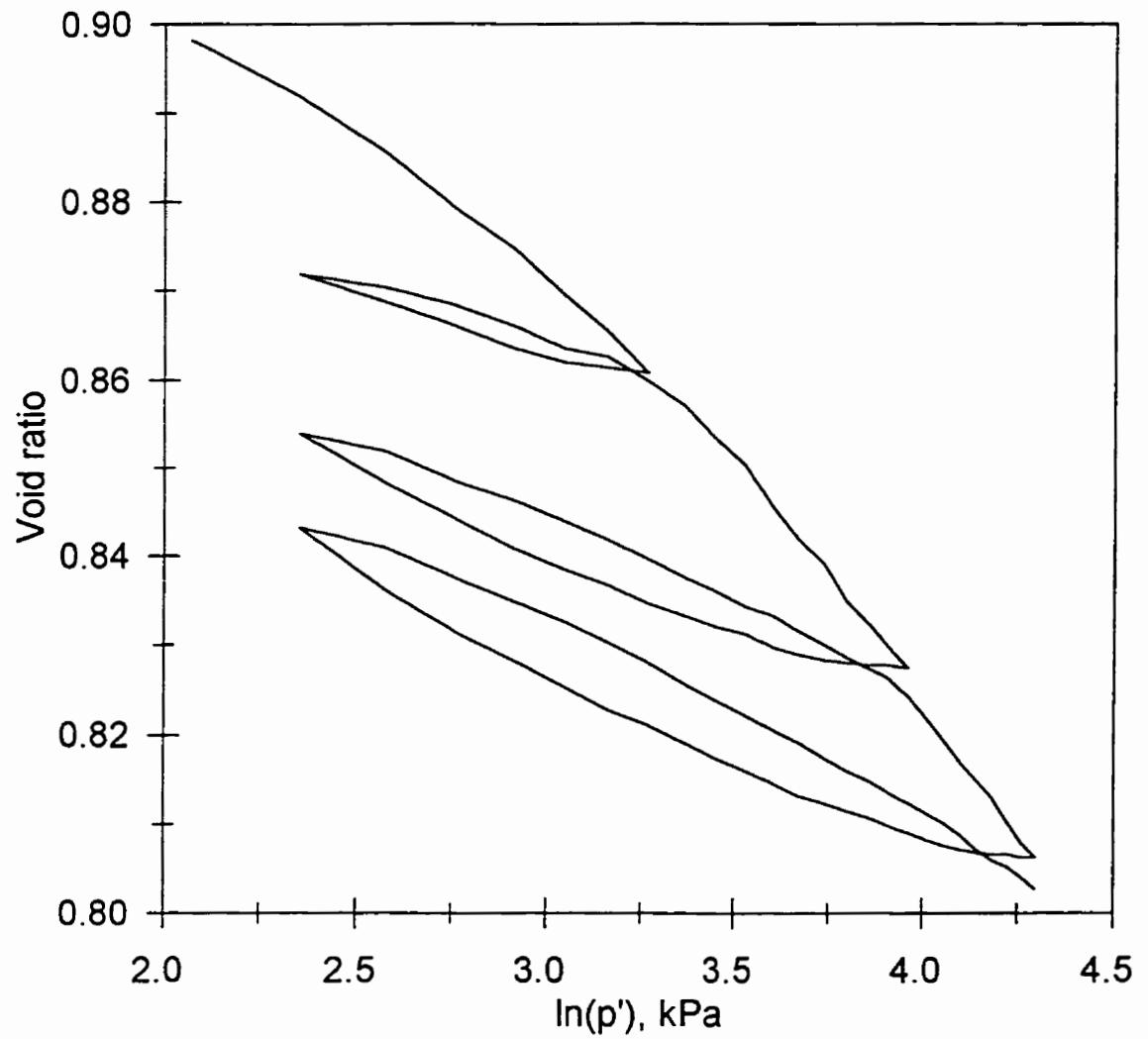


Figure B.3.(a) Three cycle isotropic test

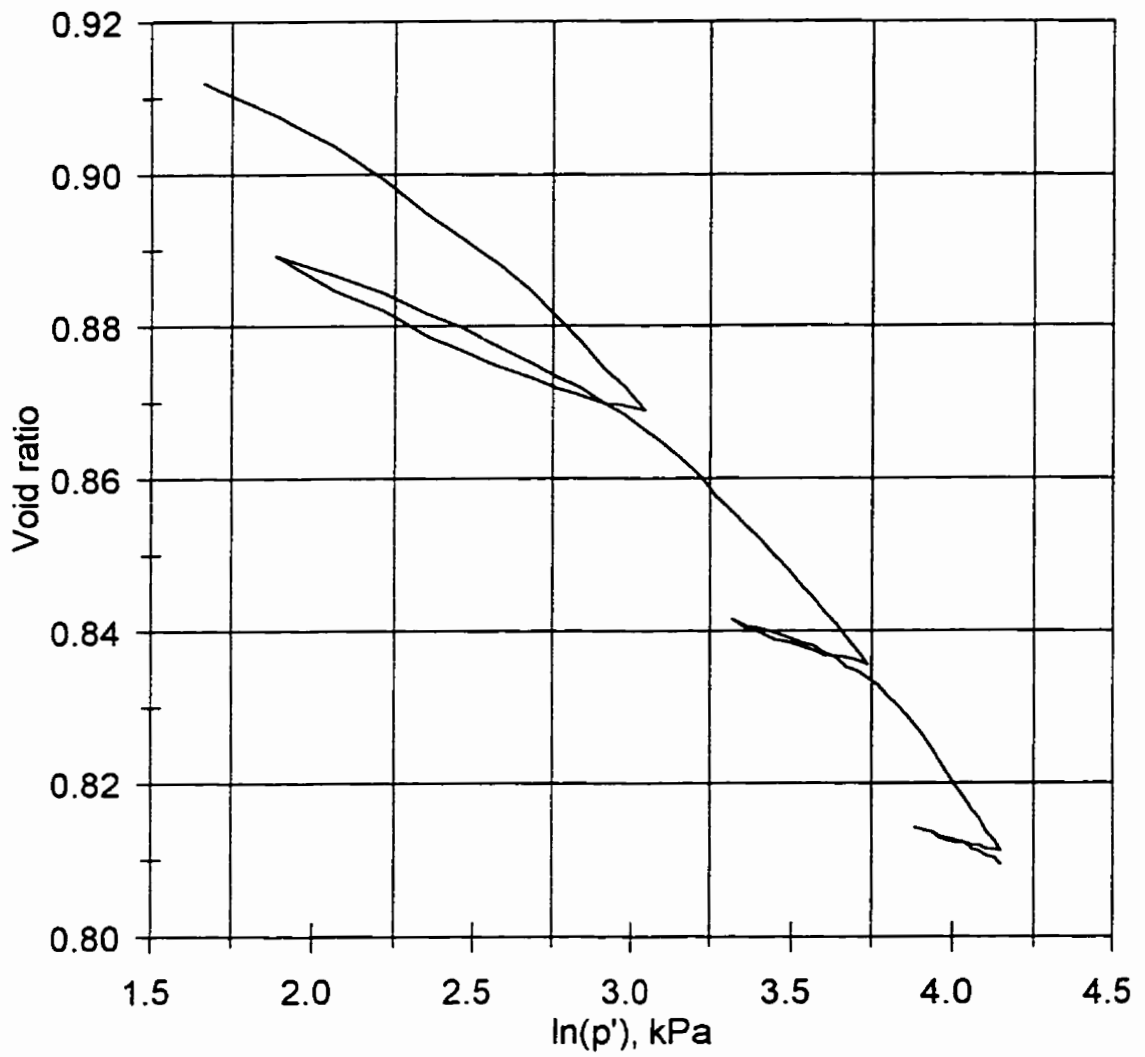


Figure B.3.(b) Three cycle isotropic test

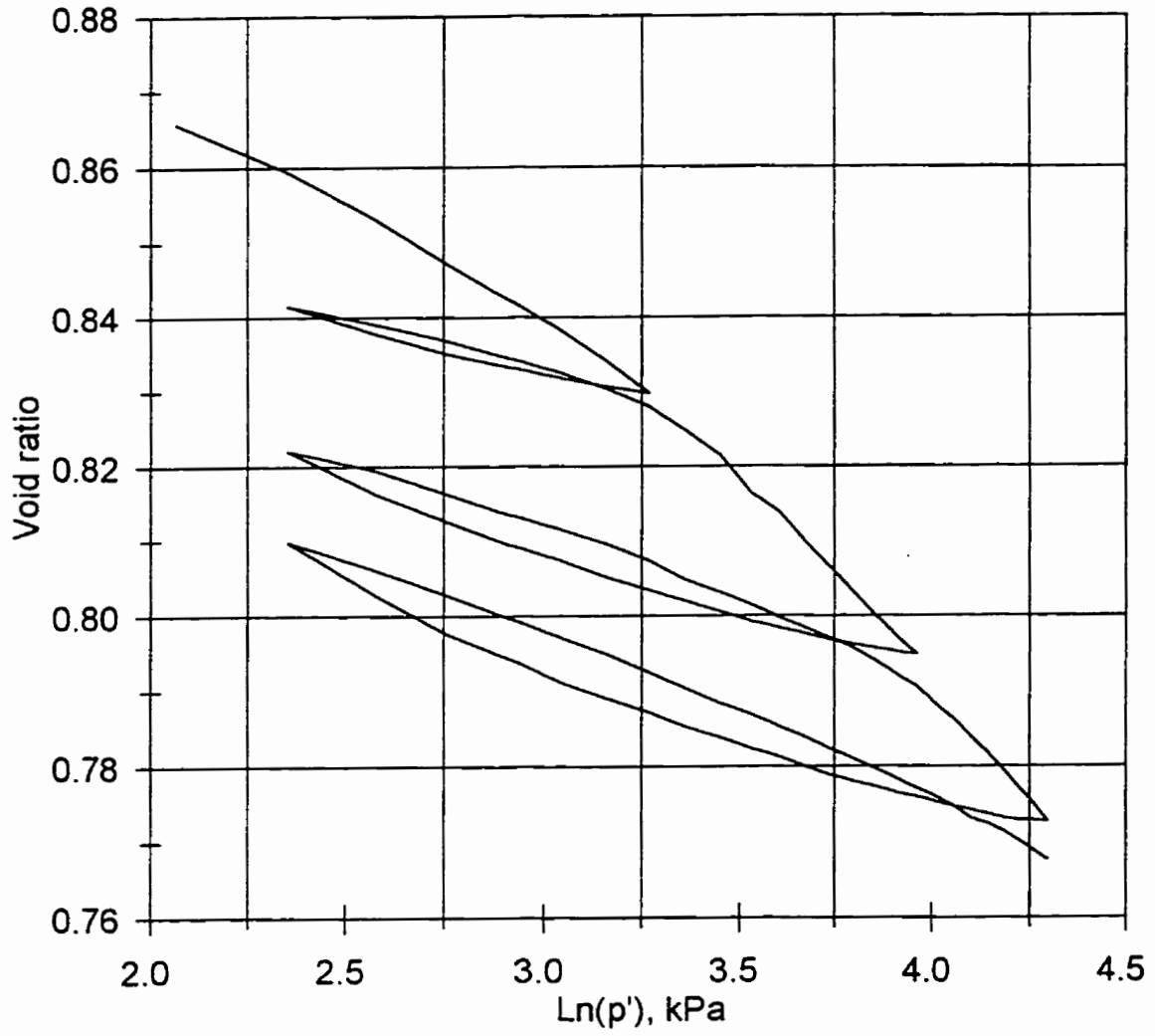


Figure B.3.(c) Three cycle isotropic test

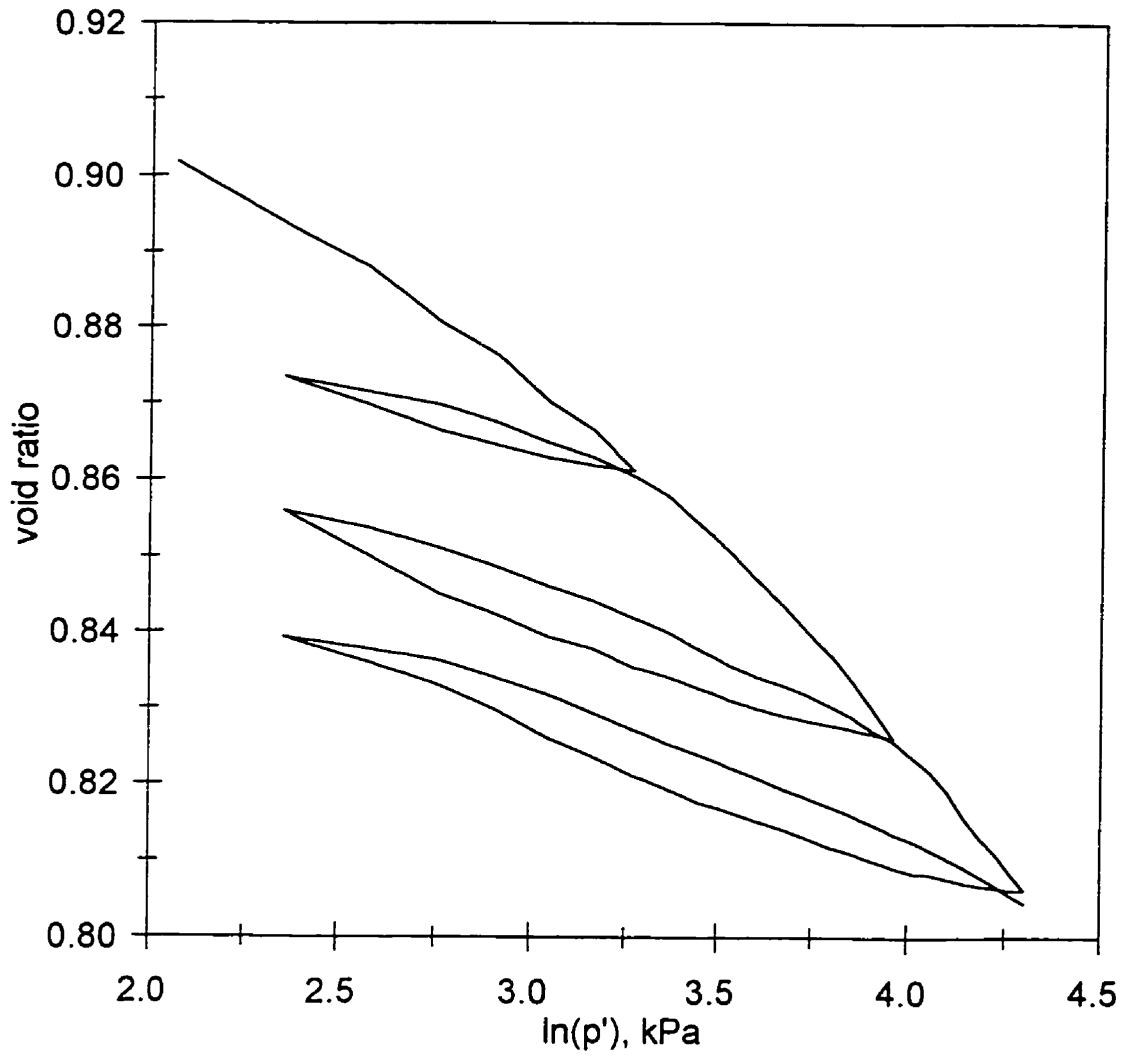


Figure B.3.(d) Three cycle isotropic test

APPENDIX C -Other Tests

Table C.1. Tests to determine particle density of ground feed

Void Ratio: Zero Error of pycnometer = -0.09

Volume of Container = 50

Wt. of Container = 102.357

All volumes in cc

All weights in gram

Sample No.	Void Ratio			Bulk Density g/cc
	Reading of Counter	Volume of Ground Feed	Void Ratio	
1	23.37	23.46	1.1313	0.7455
2	22.93	23.02	1.1720	0.7507
3	23.19	23.28	1.1478	0.7468
4	23.37	23.46	1.1313	0.7494
5	23.05	23.14	1.1608	0.7414
6	22.81	22.90	1.1834	0.7444
7	22.93	23.02	1.1720	0.7523
8	22.84	22.93	1.1805	0.7516
9	23.58	23.67	1.1124	0.7421
10	23.16	23.25	1.1505	0.7434
Mean				0.7468
SD				0.2242
From void ratio and bulk density of the sample, Particle Density = 1.6087				

Table C.2. Tests to determine moisture content of ground feed

All weights in grams

Sample No.	Moisture Content			
	Wt. of dish & moist sample	Wt. of dish & dry sample	Wt. of dish	Moisture Content
1	19.724	18.624	6.572	9.1271
2	19.378	18.251	6.535	9.6193
3	19.766	18.604	6.117	9.3057
4	19.989	18.783	6.394	9.7344
5	20.416	19.227	6.861	9.6151
6	19.070	17.945	6.054	9.4609
7	20.438	19.228	6.291	9.3530
8	20.919	19.855	8.606	9.4586
9	19.357	18.237	6.405	9.4659
10	19.919	18.741	6.551	9.6637
	Mean			9.4804
	SD			0.1756

Table C.3. Tests to determine poisson's ratio for ground feed

Height to diameter ratio of samples = 1:1

Poisson's ratio = (change in diameter/diameter)/(axial compression/height)
= change in diameter/axial compression

Sample No.	Poisson's Ratio		
	Axial compression (mm)	Change in diameter of sample (mm)	Poisson's Ratio
1	30	10	0.3333
2	28	10	0.3571
3	27	10	0.3704
4	29	10	0.3448
5	30	10	0.3333
6	29	10	0.3448
7	29	10	0.3448
8	30	10	0.3333
9	27	10	0.3704
10	28	10	0.3571
	Mean		0.3490
	SD		0.0135

APPENDIX D - Verification of modified Cam-clay model

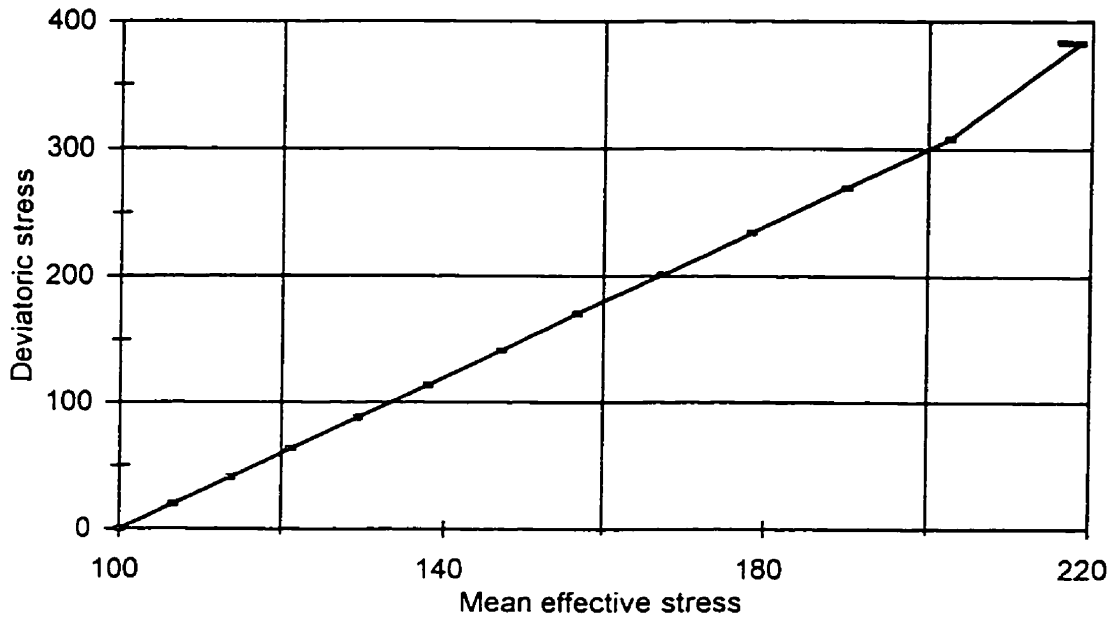


Figure D.1. Typical effective stress path during triaxial simulation (at confining pressure = 100 kPa)

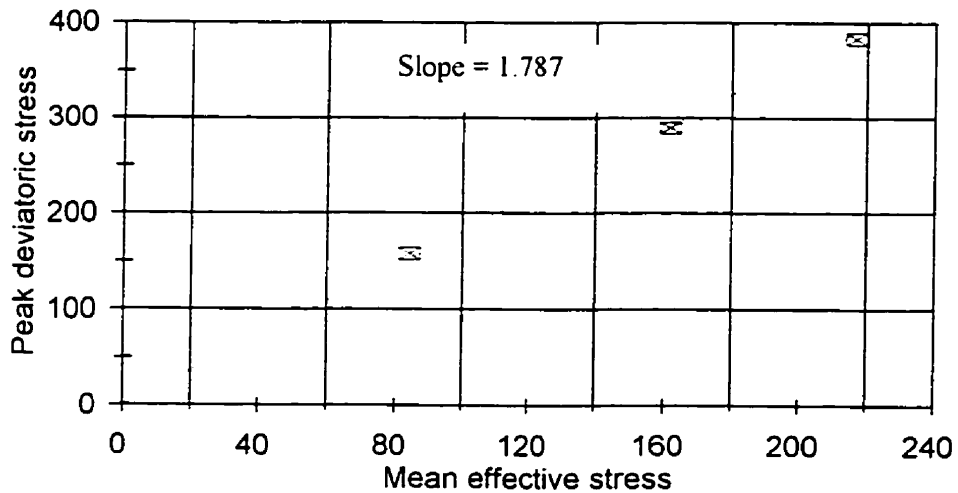


Figure D.2. Critical state line (Slope = M) determined by triaxial simulation

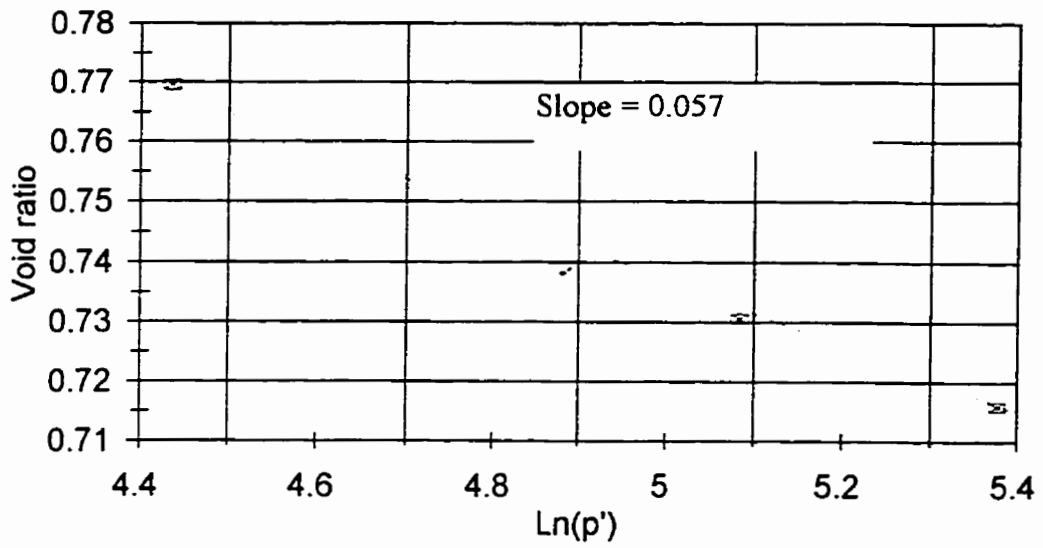


Figure D.3. Critical state line in $e-\ln(p')$ plot to determine the parameter λ and Γ by triaxial test simulation

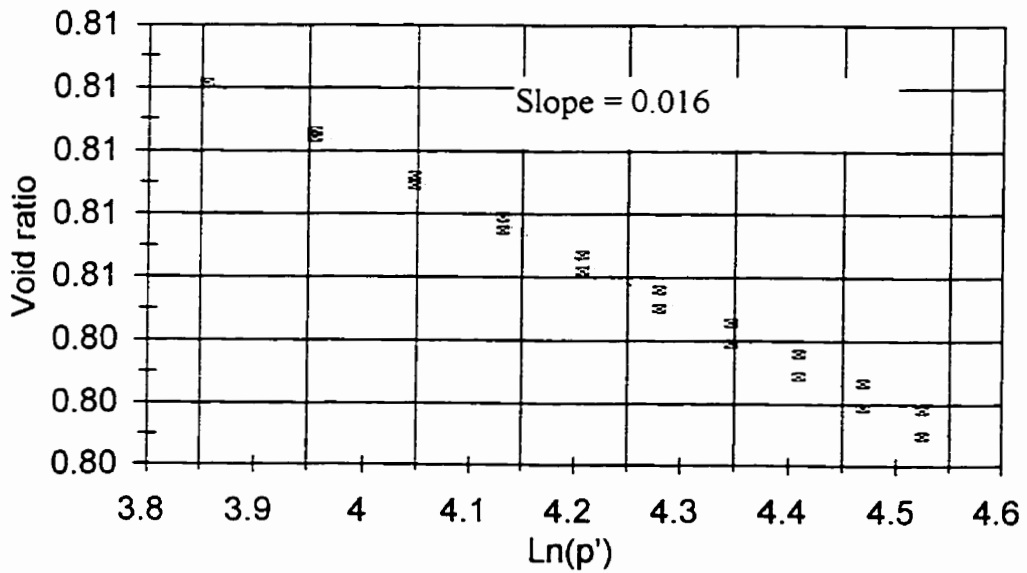


Figure D.4. Unloading-reloading cycle in triaxial test simulation to determine the parameter κ

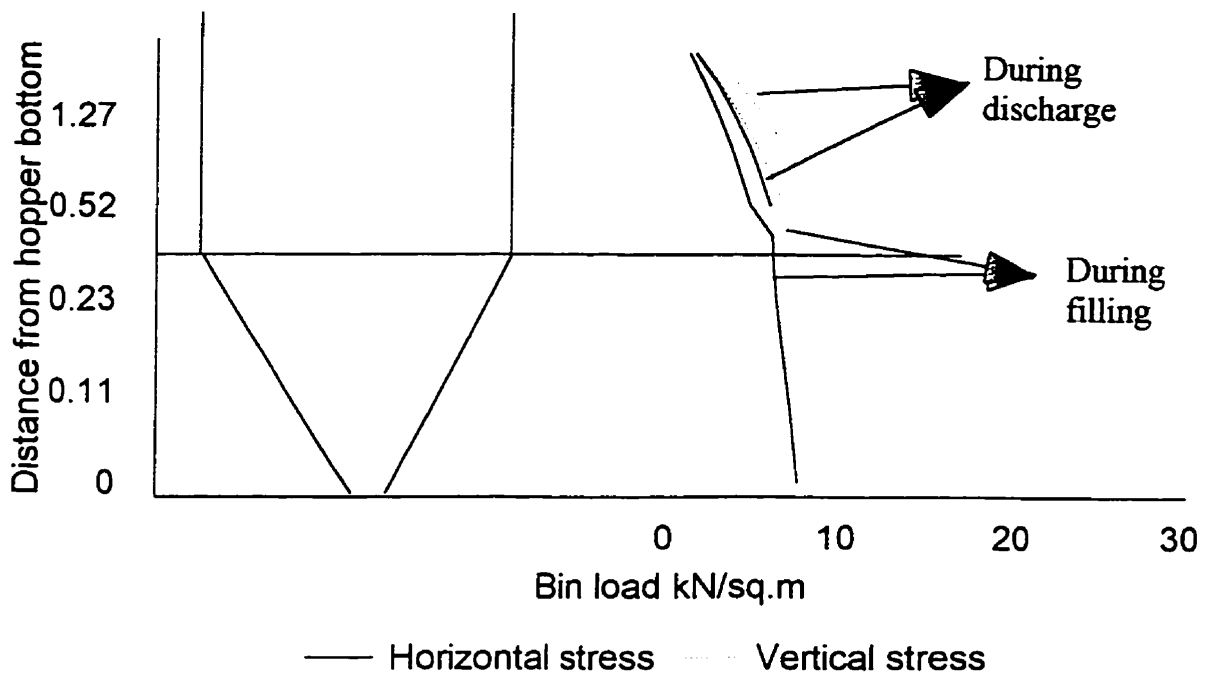


Figure D.5. Stress conditions at bin-hopper wall calculated by Janssen's equations

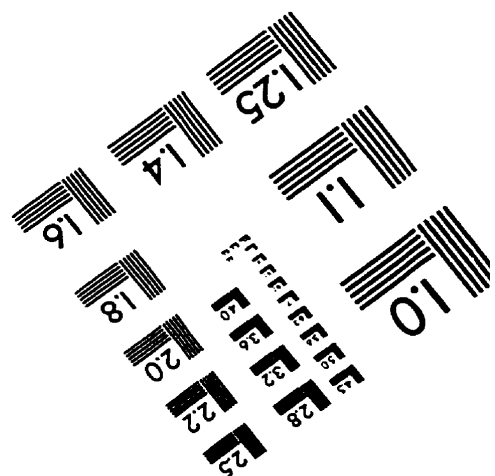
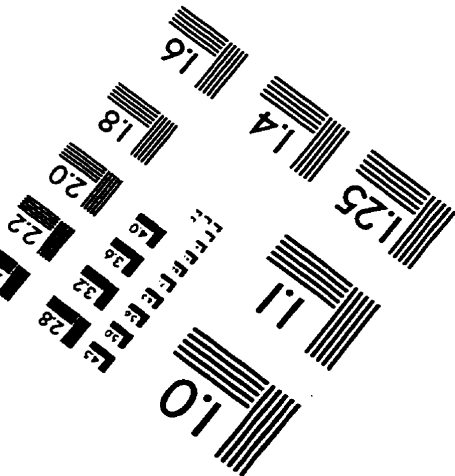
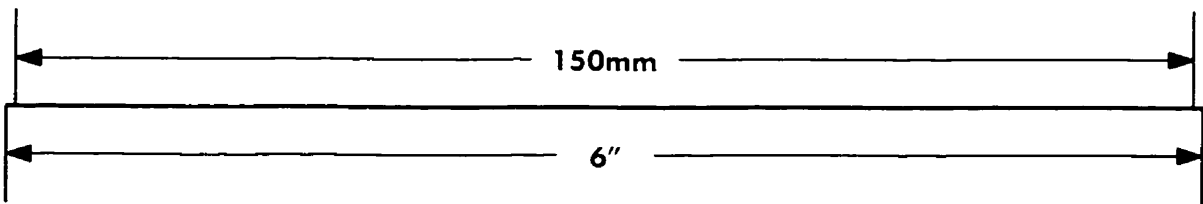
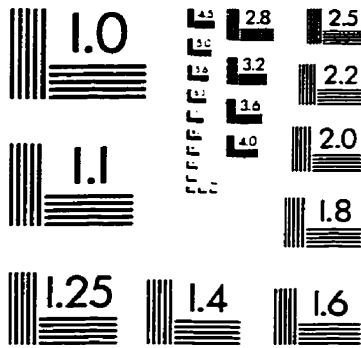
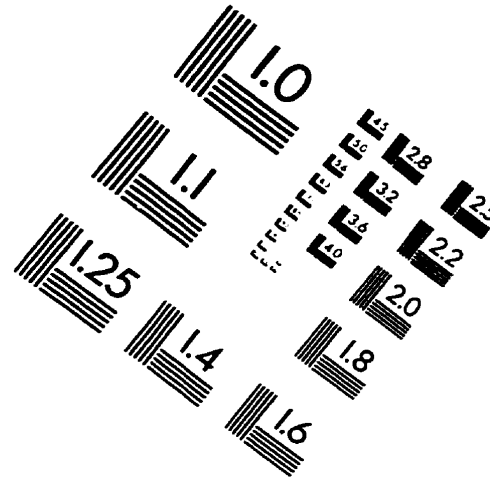
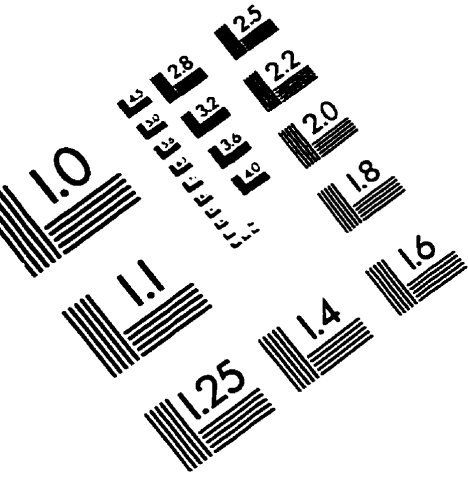
Table D.1. Comparison of bin-hopper stresses during discharge

Distance from hopper bottom (m)	Stresses calculated by Janssen's equations		Stresses calculated by SIGMA/W	
	Horizontal	Vertical	Horizontal	Vertical
1.52	1.43	2.07	0.9	1.61
1.27	2.62	3.81	1.89	3.53
1.02	3.62	5.25	2.65	4.94
0.77	4.46	6.46	3.57	6.74
0.52	5.16	7.47	4.25	8.51
0.27	5.74	8.32	5.11	10.06

Table D.2. Comparison of bin-hopper stresses after filling

Distance from hopper bottom (m)	Stresses calculated by Janssen's equations (kPa)		Stresses calculated by SIGMA/W (kPa)	
	Horizontal	Vertical	Horizontal	Vertical
1.52	1.01	1.47	0.91	1.73
1.27	1.90	2.76	1.93	3.62
1.02	2.69	3.90	2.64	5.00
0.77	3.38	4.90	3.64	6.82
0.52	3.99	5.79	4.29	8.47
0.27	4.53	6.56	4.42	8.31
0.23	6.13	6.81	6.39	9.00
0.19	6.36	7.06	7.07	8.82
0.15	6.58	7.32	7.51	8.75
0.11	6.81	7.57	8.09	8.92
0.07	7.03	7.82	8.57	9.08
0.03	7.26	8.07	8.91	9.17
0.00	7.43	8.26	6.27	10.51

IMAGE EVALUATION TEST TARGET (QA-3)



APPLIED IMAGE, Inc
1653 East Main Street
Rochester, NY 14609 USA
Phone: 716/482-0300
Fax: 716/288-5989

© 1993, Applied Image, Inc., All Rights Reserved